“EFFECT OF LIPID COMPOSITION AND CALCIUM IONS ON THE STRUCTURE AND FUNCTION OF SARS-CoV-2 FUSION PEPTIDES”

“EFEITO DA COMPOSIÇÃO LIPÍDICA E DE ÍONS CÁLCIO NA ESTRUTURA E FUNÇÃO DOS PEPTÍDEOS DE FUSÃO DO SARS-CoV-2”

MIGUEL EDUARDO SALAZAR AURICH

STATE UNIVERSITY OF NORTHERN RIO DE JANEIRO DARCY RIBEIRO

UNIVERSIDADE ESTADUAL DO NORTE FLUMINENSE DARCY RIBEIRO

CAMPOS DOS GOYTACAZES - RJ

FEBRUARY, 2025

“EFFECT OF LIPID COMPOSITION AND CALCIUM IONS ON THE STRUCTURE AND FUNCTION OF SARS-CoV-2 FUSION PEPTIDES”

“EFEITO DA COMPOSIÇÃO LIPÍDICA E DE ÍONS CÁLCIO NA ESTRUTURA E FUNÇÃO DOS PEPTÍDEOS DE FUSÃO DO SARS-CoV-2”

MIGUEL EDUARDO SALAZAR AURICH

Thesis presented to the Center for Biosciences and Biotechnology at the State University of Northern Rio de Janeiro Darcy Ribeiro, as part of the requirements for obtaining the title of Master in Biosciences and Biotechnology.

ADVISOR: Prof. Dr. Luís Guilherme Mansor Basso

STATE UNIVERSITY OF NORTHERN RIO DE JANEIRO DARCY RIBEIRO

UNIVERSIDADE ESTADUAL DO NORTE FLUMINENSE DARCY RIBEIRO

CAMPOS DOS GOYTACAZES - RJ

FEBRUARY, 2025

FICHA CATALOGRÁFICA
UENF - Bibliotecas
Elaborada com os dados fornecidos pelo autor.

A928 Aurich, Miguel Eduardo Salazar.

Efeito da composição lipídica e de íons cálcio na estrutura e função dos peptídeos de fusão do SARS-CoV-2. / Miguel Eduardo Salazar Aurich. - Campos dos Goytacazes, RJ, 2025.

88 f. : il.
Bibliografia: 56 - 63.

Dissertação (Mestrado em Biociências e Biotecnologia) - Universidade Estadual do Norte Fluminense Darcy Ribeiro, Centro de Biociências e Biotecnologia, 2025.
Orientador: Luís Guilherme Mansor Basso.

1. SARS-CoV-2. 2. Fusion peptides. 3. Membrane fusion. 4. Lipid composition. 5. Calcium. I. Universidade Estadual do Norte Fluminense Darcy Ribeiro. II. Título.

CDD - 570

“EFFECT OF LIPID COMPOSITION AND CALCIUM IONS ON THE STRUCTURE AND FUNCTION OF SARS-CoV-2 FUSION PEPTIDES.”

MIGUEL EDUARDO SALAZAR AURICH

Thesis presented to the Center for Biosciences and Biotechnology at the State University of Northern Rio de Janeiro Darcy Ribeiro, as part of the requirements for obtaining the title of Master in Biosciences and Biotechnology.

Approved on February 26, 2025.

Examination Committee:

gov.br Documento assinado digitalmente
ANDRE DE OLIVEIRA CARVALHO
Data: 28/02/2025 10:28:47-0300
Verifique em https://validar.iti.gov.br

Prof. Dr. André de Oliveira Carvalho
(Ph.D. in Biosciences and Biotechnology) - LFBM/UENF

gov.br Documento assinado digitalmente
LUIS FELIPE SANTOS MENDES
Data: 28/02/2025 08:50:09-0300
Verifique em https://validar.iti.gov.br

Prof. Dr. Luis Felipe Santos Mendes
(Ph.D. in Applied Physics to Medicine and Biology) - IFSC/USP

gov.br Documento assinado digitalmente
ITALO AUGUSTO CAVINI
Data: 28/02/2025 08:09:47-0300
Verifique em https://validar.iti.gov.br

Prof. Dr. Italo Augusto Cavini
(Ph.D. in Biomolecular Applied Physics) - FCFRP-USP

gov.br Documento assinado digitalmente
LUIS GUILHERME MANSOR BASSO
Data: 26/02/2025 23:58:02-0300
Verifique em https://validar.iti.gov.br

Prof. Dr. Luís Guilherme Mansor Basso
(Ph.D. in Physics) - LCFIS/UENF

Dedicatory

I dedicate this work to my parents, Miguel and Mari, to my siblings, Bruno and Greta, and to my grandmother Carmen.

Acknowledgments

I would like to acknowledge my family for their unconditional support in my development, both as a person and as a professional.

To Professor Dr. Luis Basso for his invaluable guidance and support throughout the development of this work, helping me to expand both my theoretical and critical knowledge to become a good researcher, and also for being not only my advisor but also a friend.

To my friends, both those I already had and those I made during the course of this work, especially Ana Flavia and Eduarda, for their sincere friendship and great support during these two years of my master's degree.

To Fadi and Gustavo, for always being willing to help me with the experiments involved in this work and for sharing their knowledge of physics, an area in which I lacked expertise, without which the development of this research would have been much more difficult.

I would also like to thank Professor Dr. Ana Eliza Zeraik for her support and for always being willing to answer my questions regarding the biological aspects of this work. Additionally, I am grateful to all members of the Molecular Biochemistry and Biophysics group at UENF, composed of the research groups led by Professors Ana Eliza and Luis.

To the professors of the Centro de Biociências e Biotecnologia (CBB) at UENF, especially those who are part of the Laboratorio de Química e Função de Proteínas e Peptídeos (LQFPP) and Laboratorio de Fisiologia e Bioquímica de Microorganismos (LFBM), for contributing to my training as a researcher and for always providing fundamental knowledge in their respective fields of study. I also appreciate the technical staff of these laboratories for their assistance.

To the administrative staff and faculty members of the Programa de Pós-Graduação em Biociências e Biotecnologia for their support and for always being willing to help whenever needed.

Finally, I would like to express my gratitude to the Universidade Estadual do Norte Fluminense Darcy Ribeiro - UENF for the opportunity given to me. *This study was financed in part by the Coordenação de Aperfeiçoamento de Pessoal de Nível Superior – Brasil (CAPES) – Finance Code 001.*

TABLE OF CONTENTS

ABBREVIATIONS

Abrev.	Meaning/Description
%Δ	Percentage change of the parameter
$\Delta\bar{x}$	Standard error of the mean
1FP1	SARS-CoV fusion peptide 1
1FP1H7	SARS-CoV fusion peptide 1 with poly-lysine tag
crac1FP1H7	SARS-CoV fusion peptide 1 with CRAC motif and poly-lysine tag
1FP2ext	Extended version of FP2 from SARS-CoV
$2A_{max}$	Outer hyperfine splitting
$2A_{min}$	Inner hyperfine splitting
2FP1H7	SARS-CoV-2 fusion peptide 1 with poly-lysine tag
crac2FP1H7	SARS-CoV-2 fusion peptide 1 with CRAC motif and poly-lysine tag
2FP2ext	Extended version of FP2 from SARS-CoV-2
5-PCSL	1-palmitoyl-2-stearoyl-(5-doxyl)-sn-glycero-3-phosphocholine
ACE2	Angiotensin-converting enzyme 2
BMP	bis(monoacylglycero)phosphate
CD	Connector domain
CD	Circular dichroism
CD147	Cluster of differentiation 147
CH	Centra helix
Chol	Cholesterol
COVID-19	Coronavirus disease 2019
CRAC	Cholesterol recognition/interaction amino acid consensus
CARC	Inverted counterpart of CRAC
CT	Cytoplasmic tail
CTD1	C-Terminal domain 1 of S1 subunit
CTD2	C-Terminal domain 2 of S1 subunit
DLS	Dynamic light scattering
DMPC	1,2-dimyristoyl-sn-glycero-3-phosphocholine
DOPC	1,2-dioleoyl-sn-glycero-3-phosphocholine
DOPE	1,2-dioleoyl-sn-glycero-3-phosphoethanolamine
DOPS	1,2-dioleoyl-sn-glycero-3-phospho-L-serine
DOTAP	1,2-dioleoyl-3-trimethylammonium-propane
DPC	Dodecyl phosphocholine
DPPG	1,2-dipalmitoyl-sn-glycero-3-phospho-(1'-rac-glycerol)
DPPS	1,2-dipalmitoyl-sn-glycero-3-phospho-L-serine
DPPTC	1,2-dipalmitoyl-sn-glycero-3-phospho (tempo)choline
EPR	Electron paramagnetic resonance
F_0	Fluorescence intensities of mixed labeled/unlabeled liposomes before peptide addition
F_{100}	fluorescence intensities of mixed labeled/unlabeled liposomes after the addition of 1% (v/v) of Triton X-100
FP	Fusion peptide
FP1	Fusion peptide 1
FP2	Fusion peptide 2
FP2ext	Extended version of FP2
FP2H7	Fusion peptide 2 with poly-lysine tag

FRET	Förster Resonance Energy Transfer
GAGs	Glycosaminoglycans
h_{+1}	Low-field spectral line
h_0	Central-field spectral lines
H7	Poly-lysine tag
H7-C	Poly-lysine tag (with a cysteine as the second amino acid residue)
HIVFPH7	Human immunodeficiency virus fusion peptide with poly-lysine tag
HR1	Heptad repeat sequence 1
HR2	Heptad repeat sequence 2
IFP	Internal fusion peptide
IFPH7	Internal fusion peptide with poly-lysine tag
LPC	1-palmitoyl-2-hydroxy-sn-glycero-3-phosphocholine
LPG	1-palmitoyl-2-hydroxy-sn-glycero-3-phospho-(1'-rac-glycerol)
MD	Molecular dynamics
MLV	Multilamellar vesicle
NBD-PE	1,2-dioleoyl-sn-glycero-3-phosphoethanolamine-N-(7-nitro-2-1,3-benzoxadiazol-4-yl)
NMR	Nuclear magnetic resonance
NTD	N-terminal domain
ORFs	Open Reading Frames
PC	Phosphatidylcholine
PE	Phosphatidylethanolamines
PG	Phosphatidylglycerol
PI	Phosphatidylinositol
POPC	1-palmitoyl-2-oleoyl-sn-glycero-3-phosphocholine
POPE	1-palmitoyl-2-oleoyl-sn-glycero-3-phosphoethanolamine
POPG	1-palmitoyl-2-oleoyl-sn-glycero-3-phospho-(1'-rac-glycerol)
POPS	1-palmitoyl-2-oleoyl-sn-glycero-3-phospho-L-serine
PS	Phosphatidylserine
RBD	Receptor-binding domain
Rhod-PE	1,2-dipalmitoyl-sn-glycero-3-phosphoethanolamine-N-(lissamine rhodamine B sulfonyl)
RNA	Ribonucleic acid
S protein	Spike protein
S1	Spike's S1 subunit
S1/S2	Cleavage site between S1 and S2 subunit
S2	Spike's S2 subunit
S2'	Cleavage site inside S2 subunit
SARS-CoV	Severe acute respiratory syndrome coronavirus
SARS-CoV-2	Severe acute respiratory syndrome coronavirus 2
SM	Sphingomyelin
SUV	Small unilamellar vesicle
S_{zz}	Effective order parameter
TM	Transmembrane domain
TMPRSS2	Transmembrane serine protease 2
WHO	World Health Organization
ζ-potential	zeta potential
σ	Standard deviation
$\bar{x}$	Average

LIST OF FIGURES

ratio was 20:1, corresponding to a peptide concentration of 3.75 μM. Peptides were added at 50 seconds, and the experiment duration varied based on the time required for the peptide to stabilize its activity. Finally, 1% (v/v) Triton X-100 was added to simulate 100% fusion. Buffer: 10 mM HEPES/MES, 150 mM NaCl, pH 5.0.

Fig. 6. Representative kinetic data of lipid-mixing experiments in SUVs containing POPS at different pH values. The fusogenic activity was recorded at 37 °C using SUVs composed of POPC/POPS/Chol 60/20/20 (molar ratio) at pH 5.0 (**A**) and pH 7.4 (**B**). The H7 tag showed no lipid-mixing activity at both pH values. The lipid-to-peptide molar ratio was 20:1, peptides were added at 50 seconds, and 1% (v/v) Triton X-100 was added at the end of the experiments to simulate 100% fusion. Buffers: 10 mM HEPES/MES, 150 mM NaCl, pH 5.0 or 7.4. 20

Fig. 7. CD spectra of all fusion peptides in solution at pH 5.0. Representative spectra of 1FP1H7, 2FP1H7, FP2H7, IFPH7, and HIVFP in 10 mM MES, 150 mM NaF, pH 5.0, at 37 °C. Concentration of peptides are indicated. 22

Fig. 8. Representative CD spectra of FP2H7 in the presence of membranes with different lipid compositions. FP2H7 (40 μM) was analyzed in solution and in the presence of SUVs at 200 μM and 800 μM, containing 20 mol% of DOTAP (**A**), POPC (**B**), POPG (**C**), and POPS (**E**) at pH 5.0. Additionally, POPS-containing SUVs were tested at the same concentrations at pH 7.4 (**F**). Micelles composed of LPG were also tested at a concentration of 20 mM at pH 5.0 (**D**). Spectra were recorded at 37 °C. The buffers used were 10 mM HEPES/MES, 150 mM NaF pH 5.0, and 10 mM Tris, 150 mM NaF, pH 7.4. 23

Fig. 9. Secondary structure content of fusion peptides in solution and in the presence model membranes at pH 5.0 and 7.4. Percentages of secondary structural elements for 1FP1H7 (**A**), 2FP1H7 (**B**), FP2H7 (**C**), and IFPH7 (**D**) in solution and in the presence of LPG micelles at pH 5.0, as well in the presence of POPC/Chol (60/20) SUVs containing 20 mol% of DOTAP, POPC, POPG, and POPS at pH 5.0, and POPS at pH 7.4. Spectral deconvolution was carried out with the samples exhibiting the highest lipid-to-peptide molar ratio (20:1). 24

Fig. 10. **Illustrative EPR spectra for spin-labeled vesicles in the absence and presence of 1FP1H7.** Lipid structures of the spin labels 5-PCSL (**A**) and DPPTC (**B**). EPR spectra of 5-PCSL (**C**) and DPPTC (**D**) embedded in 5 mg/mL SUVs composed of POPC/POPS/Chol at a 60/20/20 molar ratio in the absence (black) and presence (red) of 1FP1H7. The figure highlights the definitions of $2A_{max}$ and $2A_{min}$ in the 5-PCSL spectra, and h_{+1} and h_0 in the DPPTC spectra. The residual (gray line), obtained by subtracting the peptide-containing spectrum from the vesicle-only one, is included to facilitate the identification of spectral changes. 1FP1H7 was added at a lipid-to-peptide ratio of 20:1. Buffer: 10 mM HEPES/MES, 150 mM NaCl, pH 5.0 26

LIST OF TABLES

LIST OF ANNEXES

ABSTRACT

The fusion of viral and host cell membranes, mediated by fusion peptides (FPs) within the Spike (S) protein, is a critical step in the entry of coronaviruses such as SARS-CoV and SARS-CoV-2. These peptides modulate membrane dynamics, enabling the virus to overcome energetic barriers and successfully merge its envelope with host cell membranes. This study investigates how lipid composition, pH, cholesterol, and calcium ions affect the structure and function of four fusion peptides – 1FP1H7, 2FP1H7, FP2H7, and IFPH7 – using fluorescence spectroscopy, circular dichroism, and electron paramagnetic resonance. The results revealed that the fusogenic activity and membrane-ordering effects were significantly enhanced in negatively charged membranes containing phosphatidylserine (POPS) and phosphatidylglycerol, with the highest activity generally observed under acidic conditions. However, IFPH7 displayed a pH-dependent behavior, achieving its highest activity at neutral pH (7.4). Secondary structure analyses revealed that peptides largely retained a disordered conformation upon membrane binding, with only minor but functionally relevant *β*-strand formation in anionic membranes. Micelles, however, promoted α-helical conformations, particularly in IFPH7. Cholesterol modulated peptide activity in a sequence-dependent manner. 1FP1H7 exhibited linear increase in fusogenicity with rising cholesterol, while FP2H7 displayed reduced activity at elevated cholesterol levels, suggesting that excessive membrane rigidity can inhibit certain peptides. Cholesterol also enhanced membrane ordering, especially at the headgroup level, with peptide-specific effects on fusion efficiency. Calcium ions consistently inhibited the fusogenic activity of all peptides, with the strongest inhibition in POPS-containing membranes at neutral pH. While calcium had minimal impact on the peptides' secondary structures, it modestly enhanced lipid ordering at the headgroup level and reduced membrane surface charge, limiting peptide-membrane interactions. This study highlights the complex interplay between fusion peptides and membrane components, emphasizing how lipid composition, pH, cholesterol, and calcium ions can collectively regulate membrane fusion. These insights deepen our understanding of coronavirus entry mechanisms and may guide future therapeutic strategies targeting key factors involved in viral membrane fusion processes.

RESUMO

A fusão de membranas de células virais e hospedeiras, mediada por peptídeos de fusão (FPs) da proteína Spike (S), é uma etapa crítica na entrada de coronavírus como SARS-CoV e SARS-CoV-2. Esses peptídeos modulam a dinâmica da membrana, permitindo que o vírus supere barreiras energéticas e promova a fusão de seu envelope com as membranas de células hospedeiras. Este estudo investiga como a composição lipídica, pH, colesterol e íons de cálcio afetam a estrutura e a função de quatro peptídeos de fusão – 1FP1H7, 2FP1H7, FP2H7 e IFPH7 – usando espectroscopia de fluorescência, dicroísmo circular e ressonância paramagnética eletrônica. Os resultados revelaram que as atividades fusogênica e de ordenamento lipídico foram significativamente aumentados em membranas carregadas negativamente contendo fosfatidilserina (POPS) e fosfatidilglicerol, com a maior atividade geralmente observada em condições ácidas. Contudo, IFPH7 exibiu um comportamento dependente de pH, atingindo sua maior atividade em pH neutro (7,4). Análises de estrutura secundária revelaram que os peptídeos mantiveram uma conformação desordenada após a ligação à membrana, com a formação de pouco, mas funcionalmente relevante, conteúdo de fitas-β em membranas aniônicas. Micelas, no entanto, promoveram α-hélices, principalmente no IFPH7. O colesterol modulou a atividade do peptídeo de maneira dependente da sequência. 1FP1H7 exibiu aumento linear na fusogenicidade com o aumento do colesterol, enquanto FP2H7 exibiu atividade reduzida em níveis elevados de colesterol, sugerindo que a rigidez excessiva da membrana pode inibir certos peptídeos. O colesterol também aumentou o empacotamento lipídico, principalmente na cabeça polar, com efeitos específicos do peptídeo na eficiência da fusão. Íons de cálcio inibiram consistentemente a atividade fusogênica de todos os peptídeos, com a inibição mais forte em membranas contendo POPS em pH neutro. Embora o cálcio tenha tido impacto mínimo nas estruturas secundárias dos peptídeos, ele aumentou modestamente a ordenação lipídica na cabeça polar e reduziu a carga superficial da membrana, limitando as interações peptídeo-membrana. Este estudo destaca a interação complexa entre FPs e componentes da membrana, enfatizando como a composição lipídica, pH, colesterol e íons de cálcio podem regular coletivamente a fusão da membrana. Esses insights aprofundam nossa compreensão dos mecanismos de entrada do coronavírus e

podem orientar futuras estratégias terapêuticas visando fatores-chave envolvidos nos processos de fusão da membrana viral.

1. INTRODUCTION

1.1. Context – Problem reality

The coronavirus disease 2019 (COVID-19) pandemic, caused by the severe acute respiratory syndrome coronavirus 2 (SARS-CoV-2), has spurred the scientific community into action to elucidate the biology and structure of the virus, its interaction with human cells, and its mechanism of infection and replication, all with the aim of developing effective therapies for treating the disease[1,2]. According to World Health Organization (WHO), in its last COVID-19 epidemiological updates from January 17 of 2025, there have been over 777 million confirmed cases and more than 7 million deaths reported globally. In the Americas, the numbers of infected individuals and deaths account for 25% (193 million) and 43% (3 million) of the total, with Brazil being among the countries hardest hit by the pandemic, reporting 39 million cases and 714 thousand deaths[3–5]. As specified on the Brazil Ministry of Health's website, the Rio de Janeiro State has reported 2.9 million accumulated cases and 77 thousand deaths, with the city of Campos dos Goytacazes alone recording 58,700 cases and 2,480 deaths up until the end of January 2025[6].

1.2. Background

SARS-CoV-2 is an enveloped, positive-sense, single-strand RNA virus that has a spherical or elliptical shape, with diameters ranging from nearly 60 to 140 nm[7,8]. It belongs to the Betacoronavirus lineage B, within the *Coronaviridae* family, suborder *Cornidovirineae*, order *Nidovirales*[9]. This virus is capable of infecting vertebrates, with bats and pangolins identified as their intermediate hosts and humans as the final hosts[10]. It causes the disease known as Covid-19, which is transmitted person to person through close contact and droplets[8].

The SARS-CoV-2 RNA genome is 29,903 nucleotides length (GenBank accession number MN908947), with an organization similar to other betacoronaviruses. It shares sequence identities of 79% with SARS-CoV and 50% with MERS-CoV[1,11,12]. The genome structure includes the following Open Reading Frames (ORFs), in 5’ to 3’ sense order: replicase *ORF1ab* (ORF1a/ORF1ab), *spike* (*S*), *envelope* (*E*), *membrane* (*M*) and *nucleocapsid* (*N*). The ORF1ab encodes for 16 non-structural proteins, while the S, E, M, and N genes encode structural proteins with homonymous name[1]. In general, most genes of SARS-CoV-2 are similar in length to

their homologues in SARS-CoV, with structural proteins showing an amino acid identity of 90%. However, the S gene is highly divergent from those in other coronaviruses[13].

The infection process is similar to that of other enveloped viruses: the virus enters cells through the fusion of its viral membrane with the host cell membrane[14]. The process is mediated by the Spike glycoprotein (S) located on viral envelope, which binds to the angiotensin-converting enzyme 2 (ACE2) receptor found on host cells (respiratory epithelial cells, pneumocytes, and cells of the heart, kidneys, and gastrointestinal tract)[13,15]. In addition, some other molecules have been suggested as alternative receptors or attachment factors for the virus, such as lectins, CD147, and glycosaminoglycans (GAGs), including heparan sulfate and heparin[16,17].

Spike is a transmembrane homo-trimeric class I viral fusion glycoprotein, present in coronaviruses and giving them their characteristic crown-like appearance when observed under an electron microscope[18]. SARS-CoV-2's Spike glycoprotein monomers are composed of 1,273 amino acid residues (UniProtKB accession number P0DTC2) and are divided into two subunits: the S1 subunit, responsible for receptor's recognition and binding, and the S2 subunit, which mediates membrane fusion and anchors the protein in the viral membrane[1,19]. The two subunits are separated by the presence of a cleavage site at their interface, with a second cleavage site located within the S2 subunit[18]. The S1 subunit, the N-terminal part of Spike protein, is comprised of the N-terminal domain (NTD), the receptor-binding domain (RBD), and the C-terminal domains (CTD1 and CTD2)[20]. The S2 subunit includes functionally essential segments for infection, among them the fusion peptides (FP1 and FP2), the internal fusion peptide (IFP), two heptads repeat sequences that are highly conserved (HR1 and HR2), the transmembrane domain (TM), and the cytoplasmic domain or tail (CT)[20] (**Fig. 1**). Other additional segments inside S2 subunit are the central helix (CH) and the connector domain (CD), placed between the HR1 and HR2 regions. The S1 subunit, containing the RBD is the most variable part of the coronavirus genome, while S2 subunit is most conserved[21].

Fusion peptides (FP1, FP2 and IFP) are located in the N-terminal region of the fusion subunit (S2) and are relatively hydrophobic short segments, usually rich in glycine and alanine. These peptides have a high affinity for binding to host cell membranes and altering their properties to facilitate the fusion process[22]. Fusion peptides promote significant changes in the structure, fluidity, curvature, and hydration of the lipid bilayer of host cells[23,24]. The irreversible insertion of FPs into the lipid bilayer

of the target cells bridges the viral and cellular membranes through interactions between the TM and the fusion peptide domains (FP or IFP)[25]. Although there is no consensus on the nomenclature for the fusion peptides of SARS-CoV-2, we established the designation and extension of FP1, FP2, and IFP based on previous studies[26–29]. These studies, in turn, are based on sequence conservation and similarity across the *Coronaviridae* family and the lineage B betacoronaviruses, particularly with SARS-CoV, as well as their position within the Spike glycoprotein sequence (e.g., the FP1 peptide is located before the FP2 peptide). Additionally, in this study, a numerical suffix was added to indicate the peptide's origin: for example, 1FP1 refers to the FP1 of SARS-CoV, while 2FP1 refers to the corresponding peptide in SARS-CoV-2.

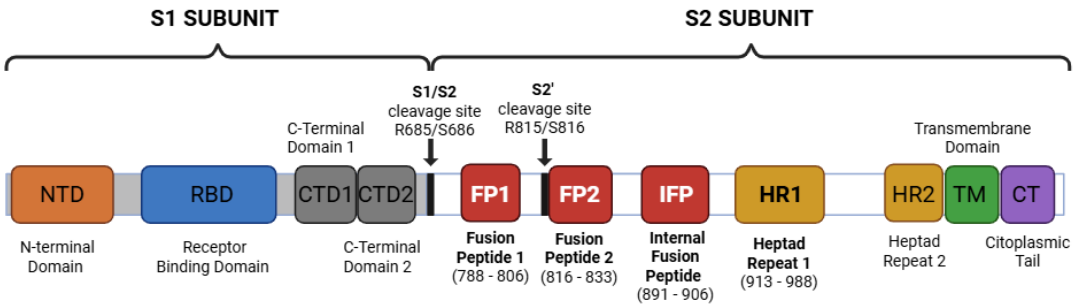

Fig. 1. Schematic representation of the SARS-CoV-2 spike glycoprotein. The functional domains of S1 and S2 subunits of the Spike protein are represented. NTD: N-terminal domain; RBD: Receptor-binding domain; CTD1: C-Terminal domain 1 of S1 subunit; CTD2: C-Terminal domain 2 of S1 subunit; FP1: Fusion peptide 1; FP2: Fusion peptide 2; IFP: Internal fusion peptide; HR1: Heptad repeat sequence 1; HR2: Heptad repeat sequence 2; TM: Transmembrane domain; CT: Cytoplasmic tail. The two cleavage sites S1/S2 and S2' are also shown.

The Spike protein exists in a metastable pre-fusion conformation that undergoes several structural rearrangements to mediate the fusion process, resulting in a stable post-fusion conformation (**Fig. 2**)[14]. These rearrangements are triggered by a series of events such as the binding of the S protein to its receptor, priming and cleavage by host proteases, FP exposure and interaction with target membranes, and refolding of the S protein forming the post-fusion state. These events provide the free energy needed to overcome the high kinetic barrier posed by the repulsive hydration forces of the water molecules tightly bound onto the viral and cell membrane surfaces[30].

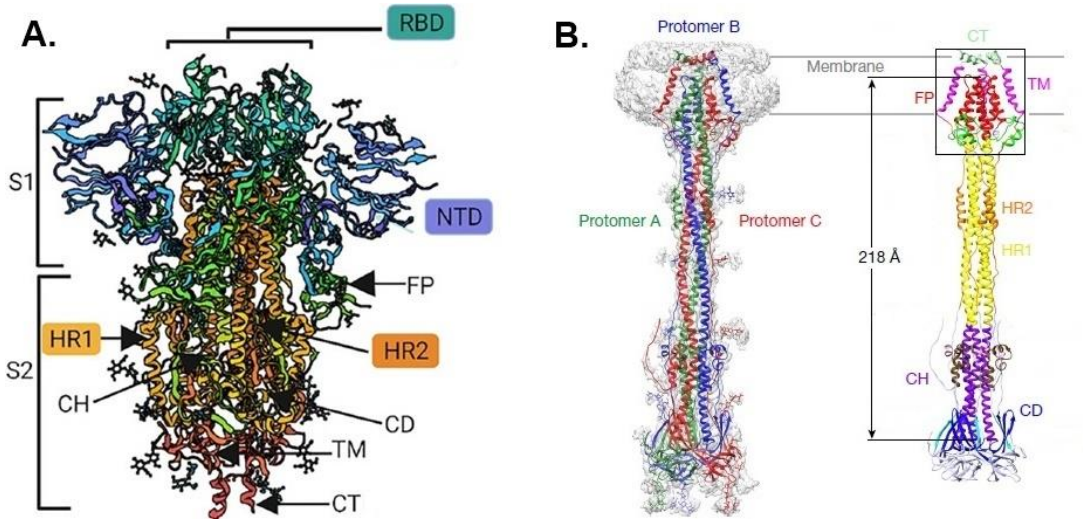

Fig. 2. Conformational states of the SARS-CoV-2 Spike protein [17,25]. **A.** Pre-fusion conformation of the trimeric assembly of the S protein, illustrating its domains as identified in Fig. 1; figure taken from (15). **B.** Post-fusion conformation of the trimeric structure of the Spike protein S2 subunit; figure adapted from (23). S1: S1 subunit; S2: S2 subunit; RBD: receptor-binding domain; NTD: N-terminal domain; FP: fusion peptide; HR1: Heptad repeat sequence 1; HR2: Heptad repeat sequence 2; CH: central helix; CD: connector domain; TM: transmembrane domain; CT: cytoplasmic tail.

Upon binding to the host ACE2 receptor, the protein conformational transitions begin with priming/triggering (**Fig. 3.i)** and cleavage by host proteases at two sites: the first cleavage at the S1/S2 boundary (R685/S686) by a furin protease on the host cell membrane, and the second at the S2' site (R815/S816) by either the transmembrane serine protease 2 (TMPRSS2) (on the cell membrane surface) or cathepsin L (in endolysosomes)[16,31]. The presence of TMPRSS2 dictates the virus entry pathway: the cell surface pathway at a physiological pH (pH7.4), or the endosomal pathway at a lower pH (pH 5.0) in cells lacking TMPRSS2[32] (**Fig. 4**). This second cleavage at the S2´site exposes the fusion peptides, allowing them to insert into the host lipid bilayer (**Fig. 3.ii**), bridging the two membranes together [31] (**Fig. 3.iii**). In this step, the Spike glycoprotein acquires an extended prehairpin structure. As the fusion process progresses, a hemifusion intermediate forms (**Fig. 3.iv**), where the HR1 and HR2 domains interact with each other, forming a six-helix bundle structure. This protein refolding brings the viral and cell membranes in such a close proximity that the outer leaflets of the membranes merge, but not the inner ones[30]. Finally, a fusion pore is formed (**Fig. 3.v**), merging completely both inner monolayers of the viral and host cell membranes, thus facilitating the exchange of the internal contents between the virus

and the host, and allowing the virus to use the host replication machinery to form new virions[17].

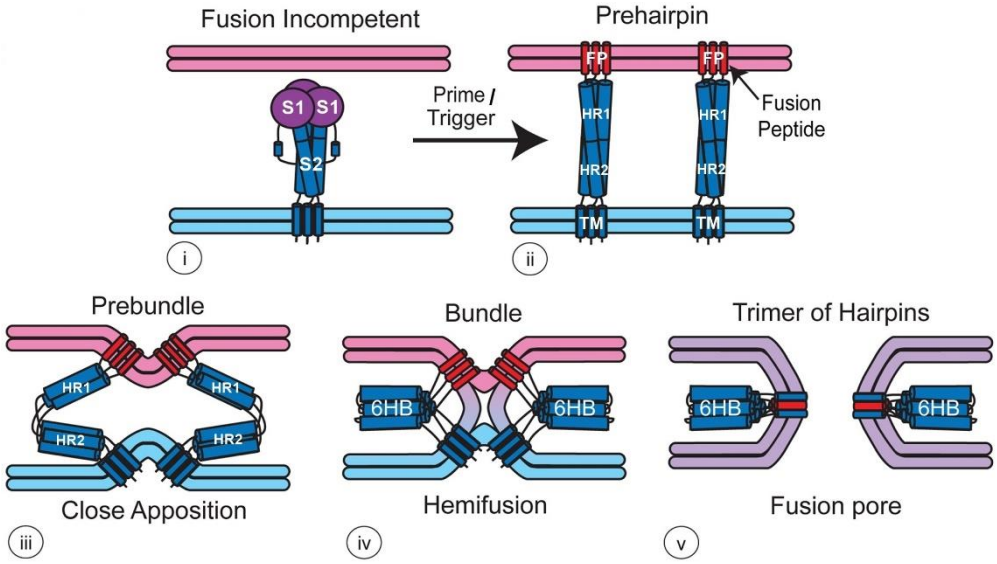

Fig. 3. Model for Spike glycoprotein fusion process[31]**.** Following priming/triggering (i), and cleavage events, the S2 subunit of the Spike protein becomes exposed, enabling FPs to interact with the host cell membrane (pink) and form a pre-hairpin structure (ii). Subsequently, the protein undergoes conformational changes, folding back the HR1 and HR2 domains to assemble a six-helix bundle (6HB). This structural rearrangement brings the host cell membrane and the viral membrane (light blue) into close proximity (iii), progressing through hemifusion (iv) and ultimately leading to fusion pore formation (v). S1: S1 subunit; S2: S2 subunit; FP: fusion peptide; TM: transmembrane domain; HR1: Heptad repeat sequence 1; HR2: Heptad repeat sequence 2; 6HB: six-helix bundle. Adapted from (31).

1.3. Previous works

Previous works have shown that the lipid composition is essential for the fusogenic activity of viral fusion peptides. It not only changes the membrane physical properties, such as curvature, fluidity, packing, and charge, allowing modulation of the membrane fusion process, but also alters the structure of the FPs[33]. It has been shown that all three fusion peptides sequences from SARS-CoV (FP1, FP2, and IFP) induce membrane ordering on lipid headgroups and on the acyl chain region at different extents[29,34,35]. This effect leads to membrane dehydration, which is a critical step for viral membrane fusion because it reduces the repulsive hydration forces between the viral and host membranes[34,35]. Additionally, despite their sequence similarity, it has been shown that an extended version of FP2 (2FP2ext), comprising an additional 22 amino acid residues in the C-terminal part (residues 816-855), from SARS-CoV-2 induces greater membrane ordering than the corresponding domain from SARS-CoV

(1FP2ext, residues 798-857) both in the headgroup region and in the shallow hydrophobic region of bilayers[36]. Increasing headgroup ordering by altering lipid composition may affect membrane fusion by enhancing dipolar interactions and lowering electrostatic energy, which may provide an energy source for membrane fusion[37].

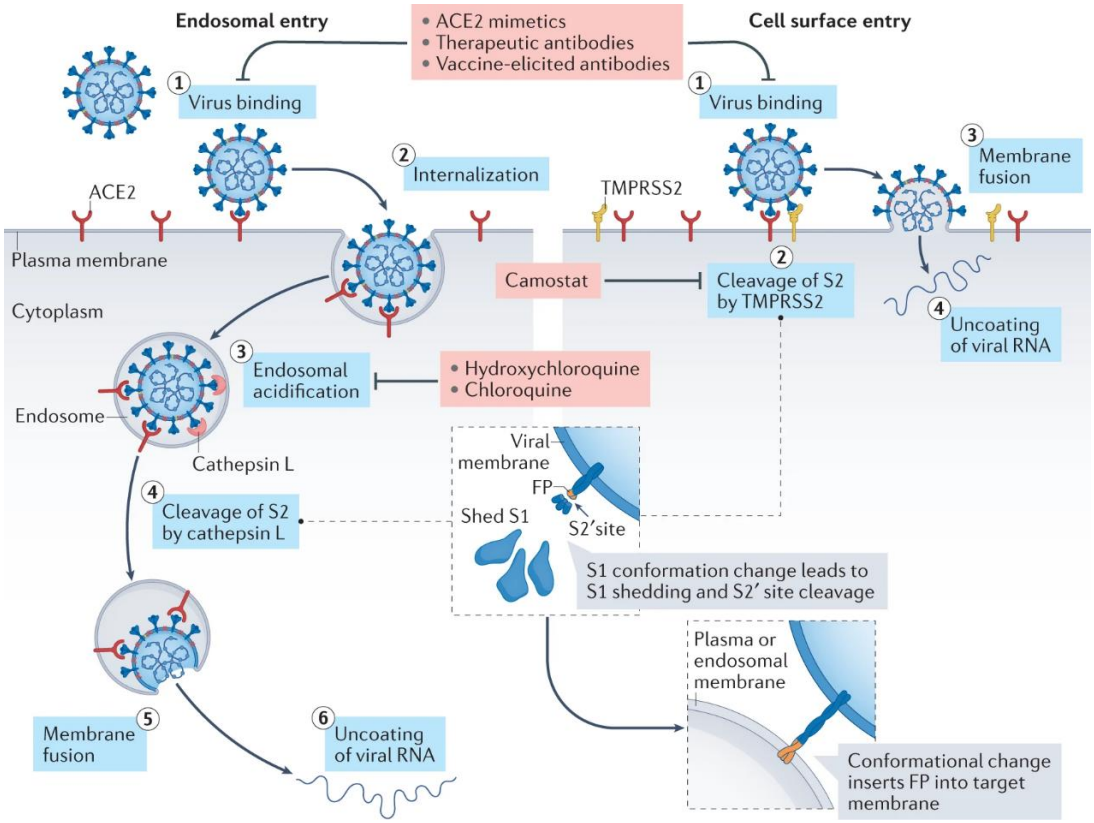

Fig. 4. Entry pathways of SARS-CoV-2 into cells[16]**.** Left: Cell surface entry pathway. Right: Endosomal entry pathway. Key aspects for each process are outlined and highlighted in blue. Some agents and drugs that interrupt the infection at different parts of the process are highlighted in red. ACE2: angiotensin-converting enzyme 2; TMPRSS2: transmembrane serine protease 2; FP: fusion peptide. Figure taken from (16).

Previous studies have demonstrated that the membrane fusion activity of the SARS-CoV and SARS-CoV-2 fusion peptides is also cholesterol-dependent. The IFP has been shown to promote hemifusion that increases with the increasing cholesterol content in membranes, an effect even more pronounced than that observed for the N-terminal FP1[38]. Cholesterol can modulate the peptide structure, its depth of penetration into the membrane, and the physical properties of the bilayers. Additionally, the presence of cholesterol and ceramide lipids facilitates the fusion process carried out by the Spike protein, whereas cholesterol depletion leads to a significant reduction in

membrane fusion[39]. Cholesterol-enriched lipid domains, also known as lipid rafts, on host cell membranes serve as a platform for viral entry by recruiting key host receptors like ACE2 and TMPRSS2. Furthermore, SARS-CoV and SARS-CoV-2 fusion peptides contain cholesterol-recognition motifs, including CRAC (*cholesterol recognition/interaction amino acid consensus*: [L/V]−[X]$_{(1-5)}$−[Y]−[X]$_{(1-5)}$−[R/K], where [X]$_{(1-5)}$ represents between one and five residues of any amino acid) and CARC (its inverted counterpart: [R/K] −[X]$_{(1-5)}$− [Y/F/W] −[X]$_{(1-5)}$−[L/V]), which may contribute to their interaction with cholesterol-rich membranes[40].

The membrane fusion mediated by fusion peptides may also be affected by calcium. The fusion peptide segment designated as FP2, a 17-residue sequence conserved in both SARS-CoV and SARS-CoV-2, contains a single Ca^{2+} binding site due to the presence of two aspartate and one glutamate residues in its primary structure. However, the extended variants of FP2 (1FP2ext and 2FP2ext), which are 22 residues longer than FP2 and differ by only three amino acid residues, possess three additional negatively charged residues, allowing the formation of an extra Ca^{2+} binding site. It has been shown that the SARS-CoV-2 FP2ext binds two Ca^{2+} ions in a more cooperativity manner than SARS-CoV FP2ext, potentially enhancing their membranotropic action[36]. The source of calcium ions depends on the subcellular localization of the membrane fusion event: at the plasma membrane, extracellular calcium (~2 mM) serves as the primary source, whereas in the endolysosomal compartment, calcium is supplied from luminal stores (~500 μM)[41–43]. The binding of Ca^{2+} ions drives deeper penetration of the peptide into the lipid bilayer[44], increasing membrane ordering effects,[34,36] which may enhance its fusogenicity. Experimental evidence indicates that the depletion of either extracellular or intracellular calcium significantly reduces the infectivity of SARS-CoV pseudovirions, suggesting that both the Spike protein and fusion peptides rely on calcium for their activity[34]. Neutron reflectometry and neutron scattering studies have demonstrated that calcium drives the FP2 to fully traverse the host plasma membrane, while calcium depletion reorients the peptide back toward the membrane's outer leaflet[44]. Additionally, an *in vitro* study on pseudovirus-liposome fusion reaction suggests that the SARS-CoV-2 Spike protein acts as a dynamic Ca^{2+} sensor, with its sensitivity enhanced by mutations found in viral variants. Notably, the fusion activity declines when calcium levels exceed physiological concentrations[42]. In SARS-CoV FP2ext, calcium ions interact with negatively charged residues (E801, D802, D812, E821, D825, and D830), with the preferred Ca^{2+} binding

pairs being E801/D802, E801/D830, and D812/E821, while D802 and D830 are essential for fusion activity[45]. However, conflicting findings suggest that calcium ions decrease lipid mixing activity – an indicator of the fusion activity – induced by SARS-CoV and SARS-CoV-2 FP2[29].

Despite these findings, the precise role of lipid composition and calcium ions in modulating the structure and function of SARS-CoV-2 fusion peptides remains inconclusive. Notably, no comparative studies have been conducted to evaluate how the lipid composition – including cholesterol content – and calcium ions influence the structure and function of all FP sequences in SARS-CoV and SARS-CoV-2. Such investigations are essential to elucidate the molecular mechanisms underlying viral membrane fusion and their potential implications for therapeutic strategies.

1.4. Problem

How do the lipid composition, including cholesterol, and calcium ions affect the conformation, and the fusogenic and membranotropic activities of SARS-CoV and SARS-CoV-2 fusion peptides?

1.5. Hypothesis

The differential action of fusion peptides on membranes is influenced by lipid composition, pH, and ions. These factors may affect not only the conformation and oligomerization state of the peptides within the membranes but also their depth of penetration into lipid bilayers, localization in lipid microdomains, and their ability to modify the physical properties of membranes. Specifically, our working hypothesis posits that the fusion peptides are largely inactive in membranes composed primarily of neutral lipids, such as phosphatidylcholine (PC), phosphatidylethanolamines (PE), and sphingomyelins (SM), but exhibit significant membrane and fusion activities in anionic membranes enriched with phosphatidylglycerol (PG) or phosphatidylserine (PS) lipids. Furthermore, we hypothesize that pH plays a crucial role in modulating peptide-membrane interactions, as it can influence both the net charge of the peptides and the surface charge density of the membranes, thereby altering their affinity and structural properties. Our second hypothesis proposes that cholesterol enhances the fusogenic and membrane ordering activity of peptides containing CRAC/CARC domains more effectively than those lacking such motifs or having incomplete CRAC/CARC motifs. This enhancement may also be influenced by the lipid

environment and the physicochemical properties of the membrane, including lipid packing and lateral organization. However, a detailed investigation of the relationship between membrane phase states (liquid ordered, liquid disordered, gel phase, solid phase, etc.) and phase coexistence (homogeneous single-phase *vs*. heterogeneous two-phase coexistence) with the peptide activity was not the primary focus of this study. Additionally, we hypothesize that calcium ions play a crucial role in reducing electrostatic repulsion between anionic membranes and fusion peptides, especially those with a net negative charge (such as FP2 constructs) at physiological pH values (ranging from 5.5 to 7.4). However, rather than direct calcium binding to the peptide being the primary determinant of membranotropic and fusion activities, we propose that calcium binding to the membrane itself may be the key factor in modulating these processes.

1.6. Justification

SARS-CoV-2, the causative agent of the Covid-19 disease, invades' human cells by fusing its viral membrane with the host cell membranes. This membrane fusion event is essential for viral entry, allowing the virus to introduce its genetic material into the cytoplasm, and exploit the host's replication machinery to generate new virions, thereby propagating the infection. A key player in this process is the fusion protein, named Spike, a membrane-anchored glycoprotein that undergoes significant conformational changes during the fusion process, which are crucial for merging the viral and host membranes. Within this protein, specific membranotropic segments known as fusion peptides (FP) play a pivotal role in initiating and stabilizing the fusion process. These peptides bind to the host cell membranes, modify their physical properties, and release the free energy required for driving the structural rearrangements of the whole Spike protein that facilitate membrane merger.

Despite advances in understanding the SARS-CoV-2 entry mechanism, the precise role of lipid composition in modulating FP activity remains underexplored. Since viral fusion occurs within the complex lipid environment of the host cell membrane, factors such as cholesterol content, lipid charge, phase behavior, and the presence of divalent cations (e.g., Ca^{2+}) may critically influence fusion efficiency. Previous studies have suggested that viral entry may depend on lipid rafts – cholesterol-enriched microdomains that recruit key host receptors, such as ACE2 and

TMPRSS2[46]. Additionally, alterations in lipid composition could modulate peptide conformation, membrane insertion depth, and fusogenic activity, impacting infectivity.

Understanding the interactions between the membranotropic domains of viral fusion proteins and the lipids present in the host cell membranes constitutes a significant step towards treating the disease. Specifically, alterations in the lipid composition of host membranes might influence the efficiency of viral entry and infection. Thus, investigating how the lipid composition affects the structure and function of the coronavirus fusion peptides may uncover the discovery of new therapeutic targets, as modulating the lipid environment or interfering with peptide-lipid interactions could serve as a strategy to inhibit viral entry. Therefore, the study of synthetic peptides derived from the SARS-CoV-2 Spike glycoprotein can provide valuable and detailed information on the structure and molecular dynamics of these segments with models of biological membranes. Ultimately, this research has the potential to contribute to the development of novel broad-spectrum antiviral compounds targeting membrane fusion, offering a strategic approach to combat not only SARS-CoV-2 but potentially other enveloped viruses that rely on similar fusion mechanisms as well.

2. OBJECTIVES

2.1. General objective

To determine the key factors influencing the membrane fusion process mediated by SARS-CoV-2 fusion peptides, focusing on the impact of membrane lipid composition and calcium ions on their structure and function.

2.2. Specific objectives

2.2.1. **Investigate the mechanism of action of FP1, FP2, and IFP fusion peptides using physiologically relevant membrane models.** This includes examining the structure, fusogenic activity, and capacity to alter the physical properties of vesicles mimicking plasma and endosomal membranes.

2.2.2. **Assess the role of cholesterol in modulating the secondary structure, fusogenic activity, and lipid packing capacity of FP1, FP2, and IFP in membrane models.** This involves varying the cholesterol concentration in

membrane models to study its impact on modulating peptide conformation and enhancing peptide-induced membrane fusion and lipid ordering.

2.2.3. **Evaluate how calcium ions affect the fusogenic and membranotropic activities of FP1, FP2 and IFP**. This includes assessing their structural changes and fusogenic and membrane-ordering activities in the absence and presence of calcium, as well as testing the effects of other monovalent and divalent cations.

3. METHODOLOGY

In this section, the materials and methods used in this work are described.

3.1. Materials

The peptides were commercially acquired from GenOne Biotechnologies (Rio de Janeiro, Brazil), acetylated at the N-terminus and amidated at the C-terminus. A -GGGKKKK tag (H7) was added to their C-terminus to enhance solubility and prevent aggregation[47]. This H7 tag was previously reported to not interfere with FP-membrane interactions. Peptide's sequences and characteristics are summarized in Table 1. An extended version of Table 1 is shown on Annex I. All parameters were calculated using Expasy Protparam tool (available at https://web.expasy.org/protparam/) and Prot pi Protein tool (available at https://www.protpi.ch/Calculator/ProteinTool).

Table 1. Peptide characteristics of all FPs used in this work. The name, position within the Spike protein, sequence, length, organism, theorical isoelectric point (pI), charge at pH 5.0 and 7.4, and molecular weight are specified. Positively charged amino acid residues are colored in red, negatively charged ones in blue, aromatic residues in green, and the lysine H7 tag in purple. CRAC domain residues are underlined. aa: amino acid residue; Ac-: acetylated; -Am: amidated; N/A: not applicable.

Peptide	Position (N° aa.)	Sequence	Origin	Theorical pI	Charge (pH 5.0)	Charge (pH 7.4)	Molecular Weight (g/mol)
1FP1H7	770-788	Ac-MWKTPTLKYFGGFNFSQILGGGKKKK-Am	SARS-CoV	10.40	+6.01	+5.25	2962.55
crac1FP1H7	767-788	Ac-VKQMWKTPTLKYFGGFNFSQILGGGKKKK-Am	SARS-CoV	10.48	+7.02	+6.50	3317.99
2FP1H7	788-806	Ac-IYKTPPIKDFGGFNFSQILGGGKKKK-Am	SARS-CoV-2	10.13	+5.13	+4.52	2869.40
crac2FP1H7	785-806	Ac-VKQIYKTPPIKDFGGFNFSQILGGGKKKK-Am	SARS-CoV-2	10.22	+6.12	+5.50	3224.84
FP2H7	798-815 / 816-833	Ac-SFIEDLLFNKVTLADAGFGGGKKKK-Am	SARS-CoV / SARS-CoV-2	9.40	+2.44	+1.21	2684.13
IFPH7	873-888 / 891-906	Ac-GAALQIPFAMQMAYRFGGGKKKK-Am	SARS-CoV / SARS-CoV-2	10.58	+5.02	+4.54	2499.03
HIVFPH7	512-534	Ac-AVGIGALFLGFLGAAGSTMGAASGGGKKKKK-Am	HIV	10.60	+5.02	+4.59	2851.40
H7-C	N/A	Ac-GCGKKKK-Am	synthetic	10.04	+4.02	+3.43	747.95
H7	N/A	Ac-GGGKKKK-Am	synthetic	10.48	+4.20	+3.54	701.87

Synthetic lipids such as the phospholipids 1-palmitoyl-2-oleoyl-sn-glycero-3-phosphocholine (16:0-18:1 PC or POPC), 1-palmitoyl-2-oleoyl-sn-glycero-3-phospho-(1'-rac-glycerol) (16:0-18:1 PG or POPG), 1-palmitoyl-2-oleoyl-sn-glycero-3-phospho-L-serine (16:0-18:1 PS or POPS), 1-palmitoyl-2-oleoyl-sn-glycero-3-phosphoethanolamine (16:0-18:1 PE or POPE), the lysophospholipid 1-palmitoyl-2-hydroxy-sn-glycero-3-phospho-(1'-rac-glycerol) (16:0-Lyso PG or LPG), brain sphingomyelin (SM), 1,2-dioleoyl-3-trimethylammonium-propane (18:1 TAP or DOTAP), the spin labels 1,2-dipalmitoyl-sn-glycero-3-phospho (tempo)choline (DPPTC) and 1-palmitoyl-2-stearoyl-(5-doxyl)-sn-glycero-3-phosphocholine (5-PCSL), cholesterol, and the fluorophores 1,2-dioleoyl-sn-glycero-3-phosphoethanolamine-N-(7-nitro-2-1,3-benzoxadiazol-4-yl) (18:1 NBD-PE) and 1,2-dipalmitoyl-sn-glycero-3-phosphoethanolamine-N-(lissamine rhodamine B sulfonyl) (16:0 Liss Rhod-PE) were purchased from Avanti Polar Lipids, Inc. (Alabaster, USA). Reagents such Triton X-100, 4-(2-hydroxyethyl)piperazine-1-ethanesulfonic acid (HEPES), 2-(N-morpholino)ethanesulfonic acid (MES), NaCl, NaF, $CaCl_2$, and Tris were purchased from Sigma-Aldrich (São Paulo, Brazil).

3.2. Methods

3.2.1. Preparation of peptides, liposomes, and micelles

Peptides were dissolved in Milli-Q millipore ultrapure water and their molar concentration was determined spectrophotometrically by using their theoretical molar extinction coefficients at 280 nm through Beer-Lambert law[48] $A = \varepsilon c l$, where A is the absorbance, ε is the molar absorption coefficient (cm^{-1}/M), c is the molar concentration (M), and l is the optical path length (cm). Absorbance measurements were performed using a Nanodrop One microvolume spectrophotometer. For peptides that do not contain tryptophan or tyrosine residues (FP2H7, HIVFP, and H7), the molar concentration was calculated directly from their molecular weight (*MW*) and the mass weighed (*m*) on the scale using the following equation: $M = \frac{m}{MW.V}$, where M is the molarity (*mol/l*) and V is the volume (*l*).

Micelles and liposomes, such as small unilamellar vesicles (SUVs), were prepared according to established protocols[29,35]. Briefly, to obtain SUVs, multilamellar vesicles (MLVs) were prepared by mixing in glass tubes adequate amounts of phospholipids, cholesterol, fluorophores, or spin labels, dissolved in chloroform. After drying under nitrogen gas, the resultant lipid films were placed under vacuum for about

2 hours in a desiccator to remove any remaining chloroform (or other organic solvents). Subsequently, these films were hydrated with the corresponding buffer and subjected to five freeze-thaw cycles, producing very homogeneous MLVs. SUVs were generated by sonicating the MLVs on ice using a probe-tip Sonics Vibra-Cell VCX 500 sonicator under the following conditions: total sonication time of 1 min, time on for 5 seconds, time off for 10 seconds, and amplitude of 25%. Titanium particles released from the tip were removed by centrifugation at 10,000 rpm for 10 min. SUVs with diameters below 50 nm were formed.

For lipid mixing and electron paramagnetic resonance (EPR) assays, labeled SUVs were prepared. A total of 1 mol% of the lipid fluorophores NBD-PE and Liss Rhod-PE for fluorescence or the spin-labeled lipids DPPTC or 5-PCSL for EPR, dissolved in chloroform, were mixed with the phospholipids, and MLVs were prepared as described above. The lipid films were hydrated either with 10 mM HEPES/MES, 150 mM NaCl, pH 5.0 or 7.4. Unlabeled SUVs for lipid mixing assays were prepared using the same procedure.

For circular dichroism (CD) experiments, micelles and unlabeled SUVs were prepared. SUVs were obtained by hydrating the films with 10 mM MES, 150 mM NaF, pH 5.0, or 10 mM Tris, 150 mM NaF, pH 7.4. NaF was used in place of NaCl to avoid the high absorbance of chloride ions in the wavelength region of the circular dichroism spectrum[49]. Micelles were prepared by weighing lysophospholipids and hydrating them with the corresponding buffer solution, followed by sonication in a bath-type sonicator (SPlabor ultrasonic bath SSBu 10 L) for 10 min and centrifugation.

The lipid compositions used throughout this work were the following (numbers in parentheses indicate the molar ratio): POPC/POPS/Chol 60/20/20, POPC/POPG/Chol 60/20/20, POPC/DOTAP/Chol 60/20/20, POPC/POPE/Chol 60/20/20, POPC/SM/Chol 60/20/20, POPC/Chol 80/20, POPC/POPG 80/20, POPC/POPG/Chol 70/20/10, and POPC/POPG/Chol 50/20/30.

3.2.2. Fluorescence membrane fusion experiments

Fluorescent-based lipid-mixing assays were performed to evaluate the fusogenic activity of the peptides. These experiments are based on the Förster Resonance Energy Transfer (FRET) and measure the extent of lipid intermixing between fluorescently labeled vesicles and unlabeled ones during membrane fusion[50].

In this assay, an unlabeled population of SUVs is mixed with a labeled population containing 1 mol % of fluorescent lipids 18:1 NBD-PE and 16:0 Liss Rhod-PE at a 9:1 unlabeled:labeled molar ratio with 75 μM of total lipid. In the absence of a membrane fusion inducer, the fluorescent lipids in the labeled vesicles are quenched due to their close distance. Excitation of the donor fluorophore (NBD-PE) transfers its energy to the acceptor molecule (Rhod-PE), that emits a photon[51,52]. Fusion of the two membranes (labeled and unlabeled) induced by the fusion peptides allows the two membranes to exchange their lipids, diluting the probes and decreasing FRET[53]. Thus, the kinetics of membrane fusion is then measured based on the increase of the emission intensity of the donor upon FPs addition.

The percentage of lipid mixing was calculated using the following equation:

$$\%fusion = \frac{F - F_0}{F_{100} - F_0} x\ 100$$

where F_0 and F_{100} are the fluorescence intensities of the mixed labeled/unlabeled liposomes before peptide addition and after the addition of 1% (v/v) of Triton X-100. The average of all related experiments was calculated along with the standard error of the mean ($\bar{x}\pm\Delta\bar{x}$). The standard error of the mean ($\Delta\bar{x}$) was calculated using the following equation:

$$\Delta\bar{x} = \frac{\sigma}{\sqrt{N}}$$

where σ is the standard deviation of the experiments and N is the number of replicates.

Fluorescence measurements were carried out in a SHIMADZU RF-5301 PC spectrofluorophotometer using a fluorescence quartz cuvette of 1 cm path length. The excitation and emission wavelengths were set to 467 nm and 530 nm, respectively, and the excitation and emission slit widths were adjusted, respectively, to 1.5 nm and 20 nm. Peptides were added into a 1 ml vesicle solution under constant stirring at 37 ºC. A 2 mM $CaCl_2$ solution was also added in some experiments to analyze the effect of calcium on the fusogenic activity of the peptides. Lipid-to-peptide molar ratio was established at 20:1 for these experiments.

3.2.3. Circular dichroism (CD) studies

CD studies were conducted to monitor changes in the secondary structure of the peptides influenced by lipid composition, pH, and ions[54,55]. The measurements were performed at 37 °C on a Jasco J-815 spectropolarimeter using a 1 mm path length quartz cell, under the following parameters: wavelength range from 270 nm to

190 nm, bandwidth of 2.0 nm, data pitch of 0.5 nm, scanning speed of 50 nm/min, and 6 to 10 consecutives scans.

Spectra were recorded for peptides (20 μM or 40 μM) in buffer solution (10 mM MES, with or without 150 mM NaF, pH 5.0, or 10 mM Tris, with 150 mM NaF, pH 7.4), in the presence of SUVs (100, 200, 400, and 800 μM) or LPG micelles (10 mM or 20 mM), and in the absence and presence of 2 mM calcium ($CaCl_2$). For SUVs, a final lipid-to-peptide molar ratio of 20:1 was maintained. Spectra of the control samples (buffer, SUVs, or micelles) were acquired under the same conditions, subtracted from the averaged peptide spectra, and converted to mean residue molar ellipticity using CDtoolX software[56]. The resulting data were analyze using the BeStSel web server to predict their secondary structure composition[57].

3.2.4. Electron paramagnetic resonance (EPR) assays

EPR spectroscopy was used to analyze peptide-induced changes in fluidity and packing of lipid bilayers[29]. Experiments were conducted at 25 °C on an X band (9.5 GHz) Bruker ELEXSYS E500 spectrometer. Lipid and lipid/peptide samples were transferred into glass capillaries, which were subsequently sealed. The final lipid concentration was 5 mg/ml, with a 20:1 lipid-to-peptide molar ratio. Spectra were recorded with a modulation amplitude of 1.0 G and a microwave power of 20 mW.

To estimate membrane packing and order, parameters such as the outer ($2A_{max}$) and inner ($2A_{min}$) hyperfine splittings and the intensities of the low (h_{+1}) and central (h_0) field lines were directly measured on the EPR spectra of 5-PCSL and DPPTC, respectively.[29] The order parameter S_{zz} for 5-PCSL was calculated from $2A_{max}$ and $2A_{min}$ as described elsewhere.[58] The percentage change of both h_{+1}/h_0 and S_{zz} parameters were estimated as follows:

$$Percentage\ change\ (\%\Delta) = \frac{(Final\ value - Initial\ value)}{Initial\ value}\ x\ 100$$

3.2.5. Dynamic light scattering (DLS) and zeta potential experiments

DLS and zeta potential (ζ-potential) measurements were performed at 25 °C using an Anton Paar Litesizer 500 to characterize the average size, homogeneity, and surface charge of the membranes and to assess the effect of calcium on the surface charge of vesicles. Measurements were conducted using disposable cuvettes for DLS and omega cuvettes for ζ-potential analysis.

4. RESULTS

This section is divided into four subsections. The first subsection details the characterization of SUVs prepared for subsequent experiments. The second subsection describes how the lipid composition in membrane models (SUVs and micelles) influences the fusogenic activity, secondary structure, and the membrane-ordering effects of the fusion peptides. The third and fourth subsections investigate the impact of cholesterol and calcium ions, respectively, on these parameters using the same analytical techniques.

4.1. Characterization of prepared SUVs

To evaluate the effects of lipid composition, pH, and calcium ions on the fusogenic activity and structure of fusion peptides, SUVs were prepared. These SUVs contained a standard molar concentration of POPC (60 mol%) and cholesterol (20 mol%), while the remaining 20 mol% was varied to incorporate different lipids (POPE, SM, DOTAP., POPG, and POPS), in order to confer distinct properties to the membranes, particularly the surface charge. POPC, POPE, and SM are zwitterionic lipids, POPG and POPS are negatively charged, while DOTAP is positively charged in the pH range used in this work[59]. The size and surface charge of these vesicles were characterized at a concentration of 100 μM in 10 mM HEPES/MES buffer (pH 5.0 or 7.4), both in the presence and absence of 150 mM NaCl. The results are shown in **Table 2**.

Although all experiments in this work were conducted in the presence of sodium ions at a physiological concentration (150 mM), size measurements were performed both with and without NaCl, whereas zeta potential measurements were carried out only in the absence of NaCl due to the conductivity limitations of the Litesizer (< 1 mS).

In the presence of NaCl, most SUVs had an average size ranging from 28 to 36 nm, except for vesicles containing DOTAP, which were significantly larger, measuring 72 nm. When NaCl was absent, SUVs generally increased in size, reaching values between 40 and 56 nm, except for DOTAP-containing vesicles, which instead decreased in size to 51 nm. This indicates that the addition of NaCl resulted in a size reduction of approximately 65% for most SUVs, except for those containing DOTAP, which instead exhibited a 41% increase in size.

Table 2. Characterization of SUVs size and surface charge. Vesicles were analyzed both in the presence and absence of NaCl. Size is reported based on number distribution, while ζ-potential serves as an indicator of vesicle surface charge. $\bar{x}$ and σ correspond to the mean value and the standard deviation, respectively.

Membrane	pH	Size (nm)				ζ-potential (mV)	
		With NaCl		Without NaCl		Without NaCl	
		$\bar{x}$	σ	$\bar{x}$	σ	$\bar{x}$	σ
POPC/Chol 80/20	5.0	32.7	5.9	55.0	10.3	-10.2	0.6
POPC/POPE/Chol 60/20/20	5.0	31.9	6.6	47.5	9.3	-11.2	0.9
POPC/SM/Chol 60/20/20	5.0	36.1	6.8	56.2	10.4	-6.8	0.7
POPC/DOTAP/Chol 60/20/20	5.0	72.3	13.2	51.2	9.8	14.9	1.0
POPC/POPG/Chol 60/20/20	5.0	33.1	6.0	47.2	8.2	-18.1	0.9
POPC/POPS/Chol 60/20/20	5.0	31.5	6.0	47.6	7.8	-15.1	1.0
POPC/POPS/Chol 60/20/20	7.4	27.9	4.7	39.5	7.5	-54.8	1.8

Zeta potential measurements confirmed charge variations among the different vesicle compositions. At pH 5.0, SUVs containing POPE, SM or only POPC were slightly negatively charged, while DOTAP-containing SUVs exhibited a positive charge. In contrast, SUVs containing POPS or POPG were more negatively charged, consistent with the presence of anionic lipids. At pH 7.4, SUVs containing POPS exhibited an even higher negative charge density compared to those at pH 5.0, reflecting a stronger electrostatic repulsion between lipid components at neutral pH.

The size reduction observed in the presence of NaCl in anionic membranes is likely due to the electrostatic screening effect of sodium ions (Na^+) and protons (H^+). In negatively charged membranes, these cations bind to negatively charged lipid headgroups, reducing the electrostatic repulsion between them, leading to vesicle compaction and a consequent decrease in SUV size. This same mechanism may also explain the increased negative ζ-potential of POPC/POPS/Chol SUVs at pH 7.4 compared to pH 5.0, as the lower proton concentration at higher pH results in less charge screening, leading to a more negative surface potential. Conversely, binding of Na^+ to the POPC phosphate group in DOTAP-containing membranes may increase the electrostatic repulsion among the lipids, thus increasing vesicle size in the presence of NaCl.

4.2. Effect of the lipid composition on FPs structure and function

4.2.1. SARS-CoV-2 fusion peptides are highly active on membranes containing negatively charged lipids

To assess the effect of lipid composition on SARS-CoV-2 fusion peptide activity, lipid-mixing assays were performed using SUVs with distinct lipid compositions (20 mol% POPE, SM, DOTAP, POPS, or POPG). These assays primarily probe membrane hemifusion, an intermediate step in the fusion process characterized by the mixing of lipids from the outer monolayers of two interacting membranes. Since hemifusion precedes pore formation, lipid-mixing assays are widely used to assess the fusogenic activity of viral fusion peptides[29,60–62].

The SARS-CoV-2 fusion peptides analyzed in these assays were 2FP1H7, FP2H7, and IFPH7. For comparative purposes, 1FP1H7 (SARS-CoV) and HIVFP were also tested. Additionally, the activity of H7 tag alone was probed to rule out potential effects unrelated to the fusion peptides themselves. The assays were primarily conducted at pH 5.0 (endosomal pH), as FP2H7, often described as the *bona fide* fusion peptide of SARS-CoV-2[25], had exhibited its highest fusogenic activity at acidic pH in previous studies[29]. All experiments were performed at 37 °C to mimic physiological conditions. Representative membrane fusion experiments are shown in **Fig. 5** and **Fig. 6**, which illustrate the kinetics of lipid mixing induced by the addition of 5 mol% of peptides in anionic membranes. A summary of the results is provided in **Table 3.**

At pH 5.0, the peptides exhibited minimal fusogenic activity (ranging from 0 to 5.6%) in vesicles containing zwitterionic or slightly negative lipids – such as POPE, SM, pure POPC – and the positively charged lipid DOTAP. In contrast, SUVs containing negatively charged lipids (POPS and POPG) demonstrated significantly higher peptide-induced lipid-mixing activity (**Table 3**). Taken together, these results suggest that SARS-CoV-2 FPs display a low activity in neutral or positively charged membranes, whereas anionic charge enhances peptide-induced fusion, indicating that electrostatic interactions play a crucial role in their fusogenic activity.

Interestingly, fusion peptides exhibited greater fusogenic activity in the more anionic POPG- than in POPS-containing membranes, except for IFPH7, whose activity remained nearly unchanged in these two membranes. Notably, FP2H7 was the most fusogenic peptide, at pH 5.0, achieving 87.4% activity in POPG membranes, whereas IFPH7 exhibited the lowest fusogenicity, with only about 7% in POPG SUVs.

Additionally, the fusogenicity of 2FP1H7 was consistently lower than that of 1FP1H7, indicating that sequence variations between these peptides influence their ability to promote lipid mixing. Furthermore, both 2FP1H7 and IFPH7 displayed lower activity than HIVFP under this acidic environment, suggesting that the HIV fusion peptide may have a more robust fusogenic mechanism or stronger membrane interactions in this environment, despite their similar effective charge (Table 1).

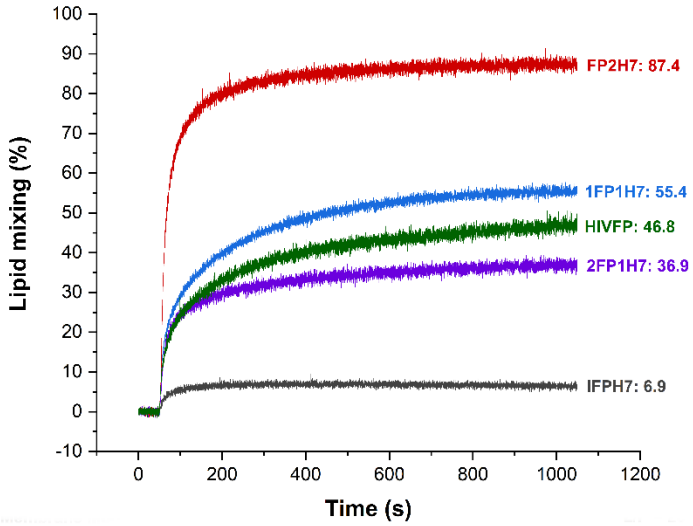

Fig. 5. **Representative kinetic data of lipid-mixing assays in SUVs containing POPG at pH 5.0**. The fusogenic activity was recorded at 37 °C using SUVs composed of POPC/POPG/Chol 60/20/20 (molar ratio). The total membrane concentration was 75 μM, with an unlabeled:labeled membrane molar ratio (UM/LM) of 9:1. The lipid-to-peptide molar ratio was 20:1, corresponding to a peptide concentration of 3.75 μM. Peptides were added at 50 seconds, and the experiment duration varied based on the time required for the peptide to stabilize its activity. Finally, 1% (v/v) Triton X-100 was added to simulate 100% fusion. Buffer: 10 mM HEPES/MES, 150 mM NaCl, pH 5.0.

To further explore the influence of pH, the peptides activity was investigated in POPS-containing vesicles at both pH 5.0 and pH 7.4 due to the physiological relevance of phosphatidylserine in cellular membranes[63]. At pH 7.4, 1FP1H7 and IFPH7 exhibited increased fusogenic activity compared to their performance in the acidic environment, with IFPH7 showing the most pronounced increase, rising from 7.2% at pH 5.0 to 55.7% at pH 7.4. This substantial enhancement suggests that IFPH7 might undergo pH-dependent conformational changes or membranotropic effect that enhance its fusogenicity at neutral pH. In contrast, FP2H7 displayed a slight decrease in activity at pH 7.4, dropping from 58.4% to 50.6%, while 2FP1H7 remained unchanged. This observation indicates that the fusogenic activity of FP2H7 may be optimized under

acidic conditions, potentially due to either protonation effects or membrane surface charge shielding that stabilize its membrane-bound conformation.

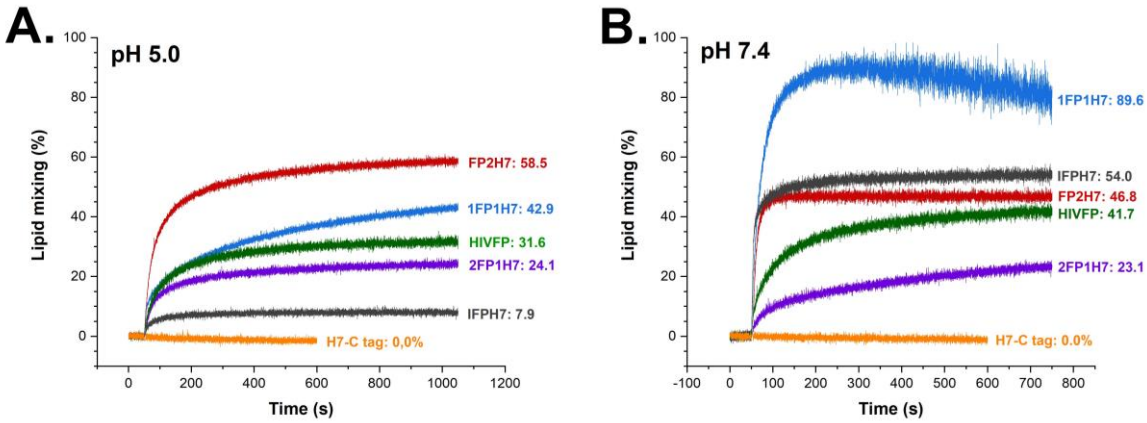

Fig. 6. Representative kinetic data of lipid-mixing experiments in SUVs containing POPS at different pH values. The fusogenic activity was recorded at 37 °C using SUVs composed of POPC/POPS/Chol 60/20/20 (molar ratio) at pH 5.0 (**A**) and pH 7.4 (**B**). The H7 tag showed no lipid-mixing activity at both pH values. The lipid-to-peptide molar ratio was 20:1, peptides were added at 50 seconds, and 1% (v/v) Triton X-100 was added at the end of the experiments to simulate 100% fusion. Buffers: 10 mM HEPES/MES, 150 mM NaCl, pH 5.0 or 7.4.

Table 3. Lipid-mixing assay results showing the fusogenic activity (%) of fusion peptides on SUVs with different membrane compositions. Experiments were primarily conducted at pH 5.0, except for PS-containing vesicles, which were also tested at pH 7.4. The lipid-to-peptide molar ratio was 20:1 (5 mol%). N/A values ("-") indicate conditions in which the peptide was not tested.

Membrane	pH	1FP1H7		2FP1H7		FP2H7		IFPH7		HIVFP	
		$\bar{x}$	$\Delta\bar{x}$	$\bar{x}$	σ	$\bar{x}$	$\Delta\bar{x}$	$\bar{x}$	$\Delta\bar{x}$	$\bar{x}$	$\Delta\bar{x}$
POPC/Chol 80/20	5.0	4.6	0.8	0.3	0.8	0.1	0.8	0.8	0.7	0.1	0.7
POPC/POPE/Chol 60/20/20	5.0	5.2	1.1	1.0	0.7	0.0	0.0	0.4	0.7	0.0	0.0
POPC/SM/Chol 60/20/20	5.0	2.2	0.3	0.9	0.4	0.0	0.3	1.0	0.3	-	-
POPC/DOTAP/Chol 60/20/20	5.0	4.1	0.4	1.4	0.4	0.0	0.0	5.6	0.5	-	-
POPC/POPG/Chol 60/20/20	5.0	55.4	0.7	35.9	2.9	87.4	1.8	6.9	0.5	46.8	1.0
POPC/POPS/Chol 60/20/20	5.0	44.9	1.5	22.7	1.4	58.4	0.1	7.2	0.6	31.6	0.8
POPC/POPS/Chol 60/20/20	7.4	87.8	1.8	21.1	2.0	50.6	3.9	55.7	1.6	42.0	0.3

As shown in **Fig. 6**, the H7-C tag alone exhibited no fusogenic activity at either pH 5.0 or pH 7.4, confirming that it does not interfere with the fusogenic activity of the peptides. The H7-C tag was used instead of the H7 tag due to the availability of the peptide in the laboratory. These results highlight the critical role of lipid composition and pH in modulating the fusogenic activity of SARS-CoV-2 fusion peptides, providing valuable insights into their potential mechanisms of action.

4.2.2. Negatively charged membranes promote changes on the secondary structure of SARS-CoV-2 fusion peptides

CD experiments were conducted to assess whether the secondary structure of fusion peptides is affected by membrane composition. For these assays, vesicles were prepared with a fixed composition of POPC (60 mol%) and cholesterol (20 mol%), while the remaining 20 mol% was varied among DOTAP, POPC, POPG, or POPS to assess the effect of different lipid environments. Additionally, micelles composed entirely of LPG (100%) were tested as an alternative and simpler membrane-mimetic system. Peptide concentrations were optimized to ensure reliable CD signal acquisition while avoiding photomultiplier voltage saturation (> 600 V). The concentrations used were 20 μM for 1FP1H7 and 2FP1H7, and 40 μM for FP2H7, IFPH7, and HIVFP. SUVs were tested at lipid-to-peptide molar ratios of 5:1 and 20:1, meaning that SUVs concentrations were 100 μM and 400 μM for 1FP1H7 and 2FP1H7, and 200 μM and 800 μM for FP2H7, IFPH7, and HIVFP. Vesicles concentrations higher than 1 mM can promote significant light scattering, leading to absorption flattening artifacts in the CD spectra[64]. The LPG micelles concentrations were set at 10 mM for 1FP1H7 and 2FP1H7, and 20 mM for FP2H7, IFPH7, and HIVFP.

CD measurements were primarily conducted at pH 5.0, as this condition is relevant to endosomal fusion pathway. However, to investigate potential physiologically relevant structural changes, experiments were also performed at pH 7.4, to mimic the plasma membrane entry pathway, with SUVs containing POPS. All experiments were carried out at 37 °C in the presence of 150 mM NaF, ensuring a stable ionic environment without strong absorbance interference in the CD spectra. To quantify structural changes, spectral deconvolution was carried out to determine the percentage of each secondary structure component (e.g., *α*-helix, *β*-sheet, random coil) for all peptides, both in solution and in the presence of membranes.

Representative CD spectra of fusion peptides in solution are illustrated in **Fig. 7**. Most peptides exhibited spectra with a prominent negative band around 200 nm, characteristic of disordered structures[65]. Notably, FP2H7 displayed two distinct negative bands at approximately 198 nm and 218 nm, suggesting a combination of disordered and ordered structural elements, potentially including β-strands. To illustrate the structural adaptations of fusion peptides in membrane environments, **Fig. 8** presents representative CD spectra of FP2H7 in the presence of each membrane composition studied. These spectra highlight significant structural only when FP2H7 interacts with negatively charged membranes under acidic conditions, revealing the importance of membrane charge in modulating peptide conformation. Additionally, distinct spectral patterns were observed for micelles and SUVs, indicating differential peptide-membrane interactions.

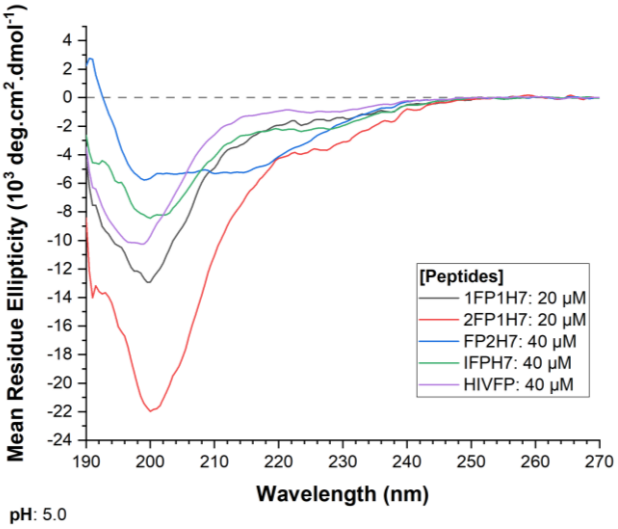

Fig. 7. CD spectra of all fusion peptides in solution at pH 5.0. Representative spectra of 1FP1H7, 2FP1H7, FP2H7, IFPH7, and HIVFP in 10 mM MES, 150 mM NaF, pH 5.0, at 37 °C. Concentration of peptides are indicated.

The CD spectra of all fusion peptides, organized by membrane composition, are provided in **Annexes 2 to 7**. To provide a comprehensive understanding of the effects of SUVs and micelles on the secondary structures of fusion peptides, the results are presented based on variations in the relative content of *α*-helices, *β*-strands (antiparallel and parallel), turns, and disordered or unstructured conformations. These structural components were quantified through spectral deconvolution, using data obtained at the highest membrane concentration tested for each condition (**Fig. 9**). All the deconvolution data is provided in **Annexes 8 and 9.**

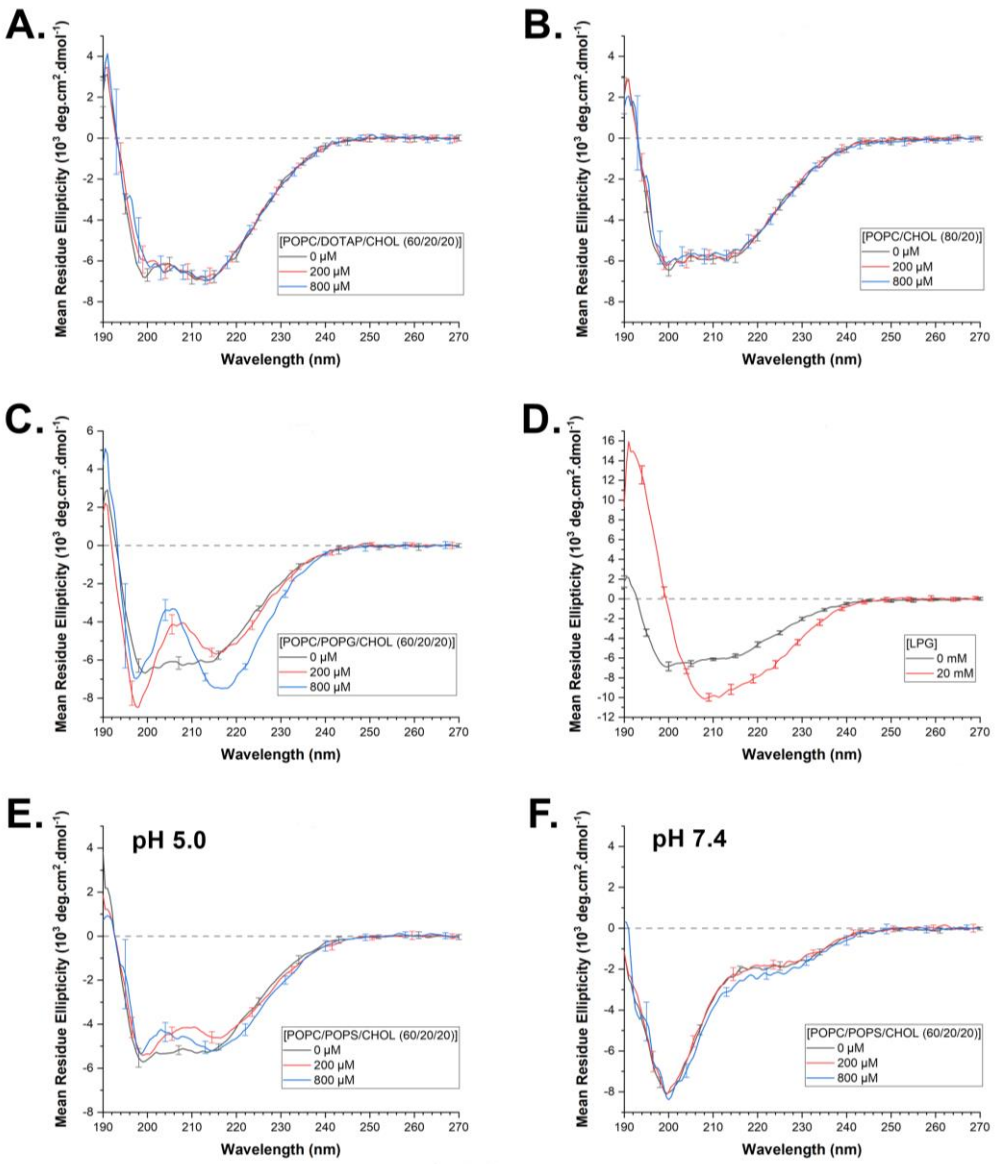

Fig. 8. Representative CD spectra of FP2H7 in the presence of membranes with different lipid compositions. FP2H7 (40 µM) was analyzed in solution and in the presence of SUVs at 200 µM and 800 µM, containing 20 mol% of DOTAP (**A**), POPC (**B**), POPG (**C**), and POPS (**E**) at pH 5.0. Additionally, POPS-containing SUVs were tested at the same concentrations at pH 7.4 (**F**). Micelles composed of LPG were also tested at a concentration of 20 mM at pH 5.0 (**D**). Spectra were recorded at 37 °C. The buffers used were 10 mM HEPES/MES, 150 mM NaF pH 5.0, and 10 mM Tris, 150 mM NaF, pH 7.4.

At pH 5.0, spectral deconvolution revealed an increase in α-helix content (%) of the fusion peptides in the presence of LPG micelles (**Fig. 9**), with IFPH7 exhibiting the most significant structural change, reaching 27.8% of the total (**Fig. 9.D**). In contrast, minimal changes in the overall secondary structure composition were observed in the presence of SUVs containing DOTAP or POPC, suggesting that neutral or positively charged membranes have little influence on peptide conformation.

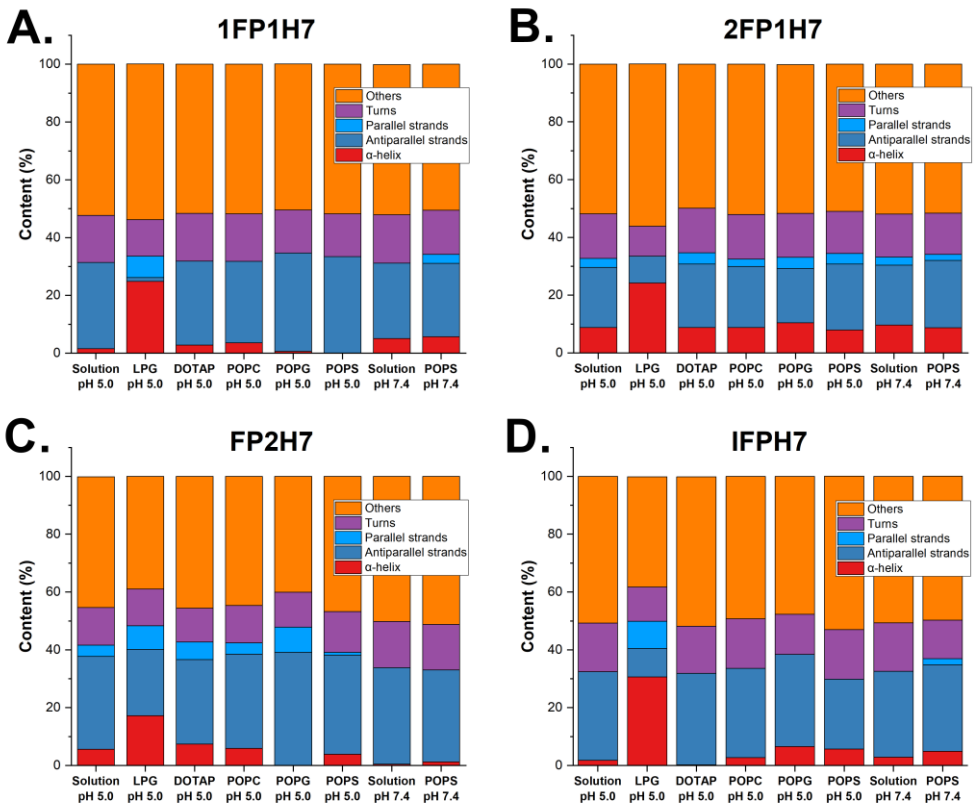

Fig. 9. Secondary structure content of fusion peptides in solution and in the presence model membranes at pH 5.0 and 7.4. Percentages of secondary structural elements for 1FP1H7 (**A**), 2FP1H7 (**B**), FP2H7 (**C**), and IFPH7 (**D**) in solution and in the presence of LPG micelles at pH 5.0, as well in the presence of POPC/Chol (60/20) SUVs containing 20 mol% of DOTAP, POPC, POPG, and POPS at pH 5.0, and POPS at pH 7.4. Spectral deconvolution was carried out with the samples exhibiting the highest lipid-to-peptide molar ratio (20:1).

On the other hand, SUVs enriched with negatively charged lipids, such as POPG and POPS, induced an increase in *β*-strand content across all fusion peptides. This effect was particularly evident in POPG-containing vesicles, where *β*-strand content increased by 4.6% for 1FP1H7 (**Fig. 9.A**) and 9.6% for FP2H7 (**Fig. 9.C**). Although this increase was not as pronounced as the α-helix enhancement observed with LPG micelles, it is likely to be more physiologically relevant, as membranes with anionic phospholipids better mimic biological environments compared to lysolipids. A similar *β*-strand enrichment (+7.9%) was observed for IFPH7 in SUVs containing POPS at pH 7.4 compared to pH 5.0 (**Fig. 9.D**). This result suggests a pH-dependent *β*-strand formation for IFPH7. Interestingly, 2FP1H7 (**Fig. 9.B**) maintained its secondary structure content across all SUVs, regardless of lipid composition, with the only structural alteration occurring in micelles, where α-helix content increased. Regardless of the membrane composition, all peptides retained a high proportion of

disordered conformations, which accounted for approximately half of the total secondary structure both in solution and in the presence of vesicles. Additionally, the percentage of turns remained relatively stable for all peptides under most conditions, with a notable decrease only in micelles, similar to the trend observed for disordered structures. Finally, the H7 tag remained primarily disordered both in solution and in the presence of membranes, as shown in **Annex 10**.

4.2.3. Membrane-ordering effect of fusion peptides is higher in negatively charged membranes

To evaluate the ability of peptides to alter membrane physical properties, specifically membrane packing and order, EPR assays were conducted. These experiments aimed to evaluate whether peptide-induced changes in lipid bilayer properties could facilitate membrane fusion. SUVs containing 20 mol% POPG or POPS were selected for analysis, as these lipid compositions exhibited the highest lipid-mixing activity and induced the most significant (and physiologically relevant) secondary structure changes in fusion peptides. Measurements were performed at pH 5.0 for both POPG- and POPS-containing vesicles and additionally at pH 7.4 for POPS-containing liposomes to investigate the influence of pH on the peptide-induced membranotropic effect. As a control group, SUVs containing 20 mol% POPE were tested at both pH 5.0 and 7.4, since peptides demonstrated minimal or no fusogenic activity in these membranes. To assess lipid rotational dynamics, EPR spectra were acquired using the nitroxide-labeled lipids 5-PCSL and DPPTC. 5-PCSL has a doxyl group positioned at C5 of the acyl chain (**Fig. 10.A**), allowing the evaluation of structural changes within the hydrophobic core of the bilayer around the C5 region. Meanwhile, DPPTC contains a TEMPO-choline headgroup (**Fig. 10.B**) and is sensitive to changes at the lipid/water interface, providing insights into alterations at the membrane surface[29,34].

To quantify membrane perturbation, the parameters $2A_{max}$, $2A_{min}$ and h_{+1}/h_0 were extracted from their respective EPR spectra. The outer ($2A_{max}$) and inner ($2A_{min}$) hyperfine splittings were obtained from the 5-PCSL spectra to calculate the effective order parameter (S_{zz})[58,66]. The h_{+1}/h_0 ratio was calculated from DPPTC spectra by dividing the amplitude of the low-field (h_{+1}) and central-field (h_0) spectral lines, offering an indicator of lipid rotational mobility[29]. Illustrative EPR spectra of 5-PCSL and DPPTC in POPC/POPS/Chol (60/20/20 molar ratio) SUVs, acquired in the absence and

presence of 1FP1H7 at pH 5.0, are provided in **Fig. 10.C and 10.D** to highlight the definition of these empirical parameters on the spectra**.** All EPR signals obtained and analyzed in this work are presented in **Annexes 11 to 19**. A higher h_{+1}/h_0 ratio and a lower $2A_{max}$ value (or lower S_{zz}) indicate increased spin-label mobility and a decrease in lipid chain order, suggesting membrane destabilization[67,68].

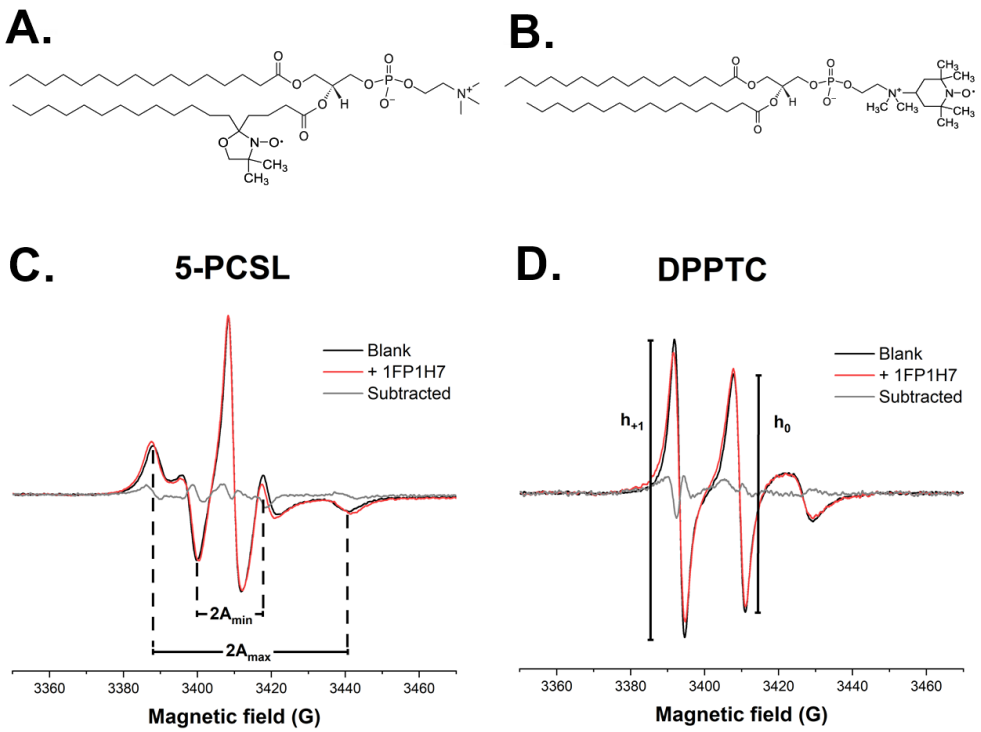

Fig. 10. **Illustrative EPR spectra for spin-labeled vesicles in the absence and presence of 1FP1H7.** Lipid structures of the spin labels 5-PCSL (**A**) and DPPTC (**B**). EPR spectra of 5-PCSL (**C**) and DPPTC (**D**) embedded in 5 mg/mL SUVs composed of POPC/POPS/Chol at a 60/20/20 molar ratio in the absence (black) and presence (red) of 1FP1H7. The figure highlights the definitions of $2A_{max}$ and $2A_{min}$ in the 5-PCSL spectra, and h_{+1} and h_0 in the DPPTC spectra. The residual (gray line), obtained by subtracting the peptide-containing spectrum from the vesicle-only one, is included to facilitate the identification of spectral changes. 1FP1H7 was added at a lipid-to-peptide ratio of 20:1. Buffer: 10 mM HEPES/MES, 150 mM NaCl, pH 5.0.

To provide a more quantitative and comprehensive assessment of how the fusion peptides influence spin probe mobility in phospholipid bilayers, the percentage change (%Δ) of the parameters S_{zz} and h_{+1}/h_0 ratio was calculated. A higher positive value of $\%\Delta S_{zz}$ indicates greater lipid ordering, suggesting increased membrane packing. Similarly, a more negative $\%\Delta h_{+1}/h_0$ reflects restricted probe mobility near the membrane surface, implying a more packed headgroup region. All EPR and calculated parameters are presented in **Annex 18**.

At the headgroup level, fusion peptides exhibited negative $\%\Delta h_{+1}/h_0$ values in negatively charged membranes containing POPS and POPG, indicating increased membrane packing at pH 5.0, as well as in POPS-containing vesicles at pH 7.4 (**Fig. 11.A**). In SUVs containing POPE, fusion peptides had little ordering effect at pH 5.0, but displayed the opposite behavior at pH 7.4, where they decreased headgroup ordering. Among the peptides, 1FP1H7 and IFPH7 induced the strongest ordering effects in POPS-containing membranes, with $\%\Delta h_{+1}/h_0$ values of -9.6% for 1FP1H7 at pH 7.4 and -6.8% for IFPH7 at pH 5.0. However, at pH 7.4, IFPH7's ordering effect in POPS vesicles was slightly reduced compared to pH 5.0, with its $\%\Delta h_{+1}/h_0$ value decreasing to -5.7%. In contrast, 2FP1H7 maintained an almost unchanged effect on headgroup ordering at pH 5.0 and 7.4 in POPS vesicles. FP2H7 showed the weakest ordering effect in negatively charged membranes, particularly in POPS-containing SUVs at pH 7.4, where its $\%\Delta h_{+1}/h_0$ value was only -1.7%. At pH 5.0, however, FP2H7 exhibited a stronger ordering effect, making it the most pH-dependent peptide. Due to the high membrane aggregation activity of 1FP1H7 and IFPH7 in POPG-containing membranes at pH 5.0, reliable EPR spectra could not be obtained for these conditions.

At the hydrophobic core level, the order parameters of the peptide-free membranes indicate that POPE SUVs are more ordered than those containing POPS and POPG, in that order. All membranes are also more packed (larger S_{zz} values) in neutral pH than under acidic conditions (**Annex 18**). This is likely due to the larger repulsive interaction between the more negatively charged lipids at neutral pH. Indeed, both POPG and POPS are more anionic than POPE (**Table 2**). Additionally, binding of protons (H_3O^+) to the membrane surface under more acidic conditions reduces the effective surface charge, increasing membrane packing.

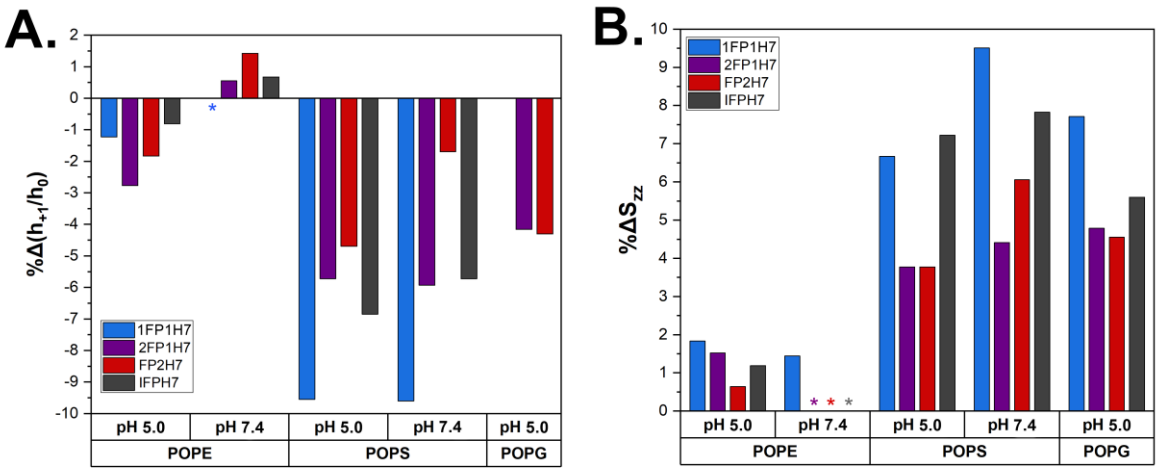

Fig. 11. Changes in the lipid ordering of negatively charged SUVs induced by fusion peptides at pH 5.0 and 7.4. The peptides-induced percentage change in h_{+1}/h_0 (**A**) and S_{zz} (**B**) for DPPTC and 5-PCSL, respectively, in POPC/POPE/Chol (POPE), POPC/POPS/Chol (POPS), and POPC/POPG/Chol (POPG) SUVs, at a 60/20/20 molar ratio and at the indicated pH values. An asterisk (*) indicates values that are too low to be represented at the scale of the graph. No $\%\Delta h_{+1}/h_0$ data were obtained for 1FP1H7 and IFPH7 in POPG membranes at pH 5.0.

Insertion fusion peptides increased lipid packing in all vesicles at both pH 5.0 and pH 7.4 (**Fig. 11.B**). The highest ordering effect of the FPs was observed in POPS-containing vesicles at pH 7.4, except for FP2H7, which displayed stronger ordering effect in POPG-containing membranes. Among the peptides, 1FP1H7 and IFPH7 induced the most pronounced ordering effects across all conditions, with their highest activity observed in POPS-containing membranes at pH 7.4, where $\%\Delta S_{zz}$ values reached 9.5% for 1FP1H7 and 7.8% for IFPH7. In POPS-containing vesicles at pH 5.0, IFPH7 induced a stronger packing effect than 1FP1H7, achieving a $\%\Delta S_{zz}$ value of 7.2%, while 1FP1H7 reached 6.7%. All peptides exhibited a moderate membrane-ordering effect in POPE vesicles at pH 5.0, whereas at pH 7.4, their effect was minimal, remaining close to zero. Taken together, these results suggest distinct interaction mechanisms and/or insertion depths of the fusion peptides in the different membranes.

4.3. Effect of cholesterol on fusion peptides properties

4.3.1. Fusion peptides exhibit cholesterol-dependent fusogenic activity

To evaluate whether the fusogenic activity of fusion peptides is influenced by cholesterol concentration in membranes, lipid-mixing assays were performed using SUVs with varying cholesterol content, ranging from 0% to 30%. For these experiments, vesicles containing 20 mol% POPG were selected, as our previous results demonstrated that fusion peptides exhibit higher activity in negatively charged membranes at pH 5.0. The following membrane compositions (in molar ratio) were tested: POPC/POPG (80/20), POPC/POPG/Chol (70/20/10), POPC/POPG/Chol (60/20/20), and POPC/POPG/Chol (50/20/30). In addition to the standard FPs (1FP1H7, 2FP1H7, FP2H7, and IFPH7), peptides containing CRAC (cholesterol recognition/interaction amino acid consensus) domains – namely crac1FP1H7 and crac2FP1H7 –were also tested to evaluate the specific role of cholesterol recognition in modulating fusogenic activity. All lipid mixing assays were conducted under acidic

conditions (pH 5.0), following the same protocols, parameters, and peptide and membrane concentrations previously described.

The results revealed that the fusogenic activity of the peptides was largely dependent on cholesterol concentration, though each peptide exhibited a distinct response to varying cholesterol levels (**Fig. 12**). 1FP1H7 displayed a linear increase in fusogenic activity with rising cholesterol content, ranging from 23.2% (0% cholesterol) to 68.5% (30% cholesterol), indicating a strong cholesterol-dependent effect. In contrast, FP2H7 maintained high activity (~87%) across cholesterol concentrations ranging from 0 to 20 mol%, but fusogenicity decreased to 72.4% at 30 mol% cholesterol, suggesting that excess cholesterol may inhibit its fusogenic potential. 2FP1H7 displayed a constant activity (36.1%) regardless of cholesterol concentration, indicating minimal sensitivity to cholesterol levels. IFPH7 consistently exhibited low fusogenic activity (~7.7%) under all tested conditions, suggesting that its membrane interaction is largely independent of cholesterol content under at pH 5.0.

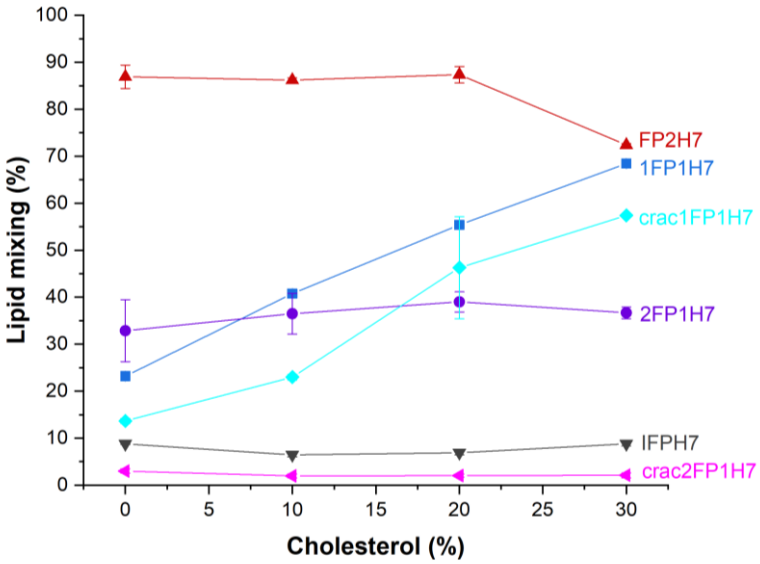

Fig. 12. **Lipid-mixing activity of fusion peptides in negatively charged vesicles with varying cholesterol content at pH 5.0**. The fusogenic activity of peptides 1FP1H7, 2FP1H7, FP2H7, IFPH7, and the CRAC-containing ones crac1FP1H7 and crac2FP1H7 was evaluated at 37 °C by increasing the cholesterol concentration in anionic vesicles from 0 to 30 mol%. SUVs with the following compositions (in molar ratio) were tested: POPC/POPG (80/20), POPC/POPG/Chol (70/20/10), POPC/POPG/Chol (60/20/20), and POPC/POPG/Chol (50/20/30). The total peptide and membrane concentrations were, respectively, 3.75 μM and 75 μM. Buffer: 10 mM HEPES/MES, 150 mM NaCl, pH5.0. Error bars represent standard error of the mean calculated from three independent replicates for each condition.

The inclusion of CRAC domains further highlighted the putative role of cholesterol recognition in modulating fusogenicity. crac1FP1H7 followed a trend similar to 1FP1H7, increasing linearly its activity alongside cholesterol content but reaching lower fusogenicity values (13.7% to 57.4%) compared to its non-CRAC counterpart. The addition of the CRAC domain reduced the peptide activity by approximately 10%. This result suggests that while the CRAC domain might putatively enhance cholesterol recognition, it may also impose structural constraints that reduce overall fusogenic efficiency. On the other hand, crac2FP1H7 maintained a consistently low and unresponsive activity (~2%) across all cholesterol concentrations, indicating that the CRAC domain not only did not enhance its interaction with cholesterol-rich membranes but also abrogates the peptide activity. These findings underscore the complex interplay between cholesterol concentration and peptide primary structure in modulating membrane fusion efficiency, with implications for understanding how viral fusion peptides exploit membrane composition to facilitate host cell entry.

4.3.2. Membrane-ordering effect of fusion peptides increases with higher cholesterol content in negatively charged membranes

To investigate how cholesterol concentration influences the membrane-ordering effects of fusion peptides, EPR assays were performed using POPG-containing vesicles, following the same lipid compositions applied in the previous lipid-mixing assays, with cholesterol concentrations varying from 0% to 30%. The membranes were labeled with 5-PCSL and DPPTC, allowing for the analysis of membrane dynamics both at the lipid-water interface and within the hydrophobic core. Key parameters, including $2A_{max}$ and h_{+1}/h_0, were extracted from the spectra (and S_{zz} was calculated from $2A_{max}$), and their percentage variations ($\%\Delta S_{zz}$ and $\%\Delta h_{+1}/h_0$) were calculated to quantify changes in lipid ordering. All EPR spectra are provided in **Annexes 15 to 18**, while detailed data for all calculated parameters are presented in **Annex 20**.

At the lipid-water interface, the fusion peptides generally increased lipid ordering, with the effect intensifying as cholesterol content increased (**Fig. 13**). This trend was consistent across all peptides, though the extent of the effect varied. 1FP1H7 exhibited the strongest ordering effect among all peptides, with a $\%\Delta h_{+1}/h_0$ value of -11.6% at 30 mol% cholesterol. IFPH7 followed closely, inducing a -9.3% change under the same conditions. In contrast, FP2H7 showed a slight disordering effect at 0 mol% cholesterol, with a $\%\Delta h_{+1}/h_0$ value of 0.1%, indicating minimal impact on headgroup

packing in the absence of cholesterol. Despite this, FP2H7's ordering effect increased progressively with higher cholesterol concentrations. 2FP1H7 displayed low to moderate ordering effects but followed the same overall trend as 1FP1H7 and IFPH7 of increased headgroup packing with rising cholesterol content.

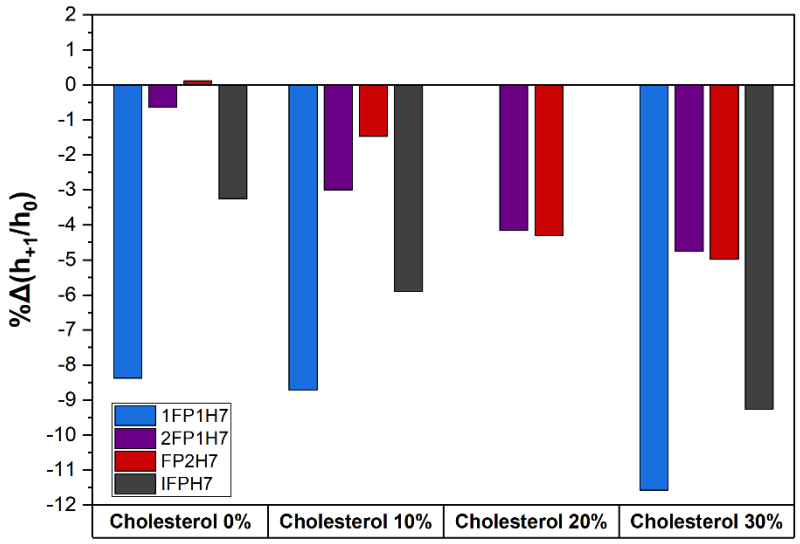

Fig. 13. Percentage change of the $\Delta h_{+1}/h_0$ parameter of DPPTC in POPG-containing vesicles with varying cholesterol content at pH 5.0. SUVs containing 20 mol% POPG with cholesterol concentrations ranging from 0 to 30 mol% were analyzed in the absence and presence of fusion peptides, and $\%\Delta h_{+1}/h_0$ was determined to quantify the impact of peptides on lipid packing at the headgroup level. The labeled SUVs were prepared at a concentration of 5 mg/mL, with peptides added at a lipid-to-peptide ratio of 20:1. Buffer: 10 mM HEPES/MES, 150 mM NaCl, pH 5.0. No data was obtained for 1FP1H7 and IFPH7 in membranes containing 20 mol% cholesterol.

In the hydrophobic core of the membranes, fusion peptides increased membrane packing and lipid ordering, but their behavior did not follow a clear pattern with increasing cholesterol content. Peptides exhibited an initial increase in membrane packing, as indicated by higher S_{zz} values, when cholesterol rose from 0 mol% to 10 mol%, but their ordering activity either slightly decreased or stabilized in membranes with 20 mol% and 30 mol% cholesterol (**Fig. 14**). The highest degree of lipid ordering was observed at 10 mol% cholesterol, where 1FP1H7 again induced the most substantial effect, with a $\%\Delta S_{zz}$= 9.6%. The other peptides exhibited similar levels of membrane packing under these conditions, with $\%\Delta S_{zz}$ values ranging from 4.6% to 6.4%.

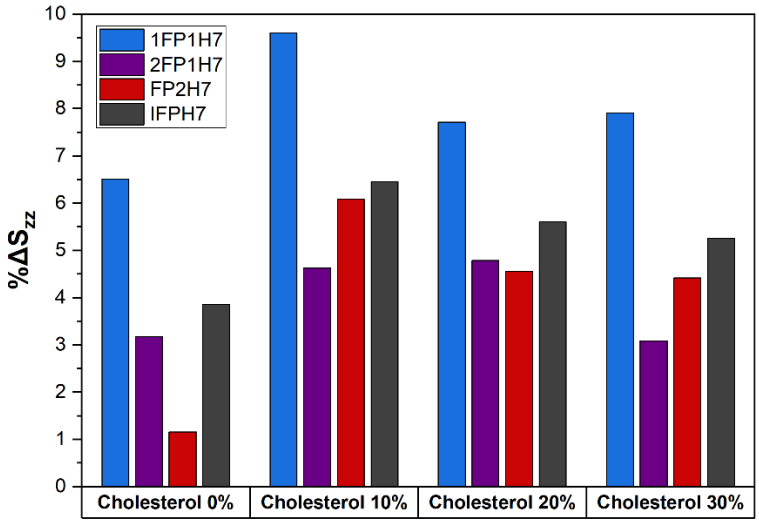

Fig 14. Percentage change of ΔS_{zz} of 5-PCSL in POPG-containing vesicles with varying cholesterol content at pH 5.0. SUVs containing 20 mol% POPG with cholesterol concentrations ranging from 0 to 30 mol% were analyzed in the absence and presence of fusion peptides, and $\%\Delta 2A_{max}$ was determined to quantify the impact of peptides on lipid packing at the hydrophobic core level. The labeled SUVs were prepared at a concentration of 5 mg/mL, with peptides added at a lipid-to-peptide ratio of 20:1. Buffer: 10 mM HEPES/MES, 150 mM NaCl, pH 5.0.

In summary, the data clearly demonstrate that cholesterol plays a pivotal role in modulating the membrane-ordering effects of fusion peptides, particularly at the lipid-water interface, where higher cholesterol concentrations consistently enhanced headgroup packing. Although the peptides generally increased lipid ordering within the hydrophobic core, their activity peaked at 10 mol% cholesterol, with additional cholesterol leading to either stabilization or a slight reduction in ordering effects. Importantly, cholesterol enrichment alone significantly increased the baseline membrane packing, with S_{zz} values rising from 0.565 at 0 mol% cholesterol to 0.667 at 30 mol% cholesterol (**Annex 20**). This intrinsic increase in membrane order is likely to impact the interaction dynamics of fusion peptides, as more ordered membranes can restrict peptide insertion, alter membrane curvature, and potentially modulate the fusion process. The observation that fusion peptides exhibit varying sensitivities to cholesterol-induced membrane ordering underscores the complexity of peptide-membrane interactions and highlights the critical role of membrane composition in regulating fusion efficiency.

4.4. Calcium effect on fusion peptides-membranes interactions

4.4.1. Fusogenic activity of fusion peptides is decreased by calcium interactions

To assess the impact of calcium ions on the fusogenic activity of fusion peptides, lipid-mixing assays were performed using negatively charged vesicles. These membranes were selected due to the high fusogenic activity exhibited by the peptides in such environments and the potential for electrostatic interactions between the negatively charged lipid headgroups and the divalent Ca^{2+} cations. The fusion peptides 1FP1H7, 2FP1H7, IFPH7, and HIVFP were tested using SUVs with the following compositions: POPC/POPG/Chol (60/20/20) at pH 5.0, POPC/POPS/Chol (60/20/20) at pH 5.0, and POPC/POPS/Chol (60/20/20) at pH 7.4. The membranes were incubated with 2 mM $CaCl_2$ prior to the experiments, to allow calcium binding to the membrane surface. All assays were conducted following the same protocols, parameters, and peptide and membrane concentrations previously described.

Our results showed that calcium consistently decreased the lipid mixing activity of the fusion peptides across all tested conditions (**Table 4**). To quantify the extent of this inhibition, the percentage of inhibition was calculated as follows:

$$Inhibition\ (\%) = 100\% - \frac{Activity\ with\ calcium * 100\%}{Activity\ without\ calcium}$$

Table 4. Lipid mixing activity of fusion peptides on negatively charged vesicles in the absence and presence of calcium. Lipid-mixing experiments were conducted using SUVs composed of POPC/POPG/Chol and POPC/POPS/Chol at pH 5.0, and POPC/POPS/Chol at pH 7.4 in the absence and presence of 2 mM $CaCl_2$.

Peptide	Calcium	pH 5.0				pH 7.4	
		POPC/POPG/CHOL 60/20/20		POPC/POPS/CHOL 60/20/20		POPC/POPS/CHOL 60/20/20	
		$\bar{x}$	$\Delta\bar{x}$	$\bar{x}$	$\Delta\bar{x}$	$\bar{x}$	$\Delta\bar{x}$
1FP1H7	Without Ca	55.4	0.7	44.9	1.5	87.8	1.8
	With Ca	50.7	2.2	21.3	0.6	62.9	5.1
2FP1H7	Without Ca	39.0	2.1	22.7	1.4	21.1	2.0
	With Ca	30.3	2.3	20.0	0.7	16.4	2.8
FP2H7	Without Ca	87.4	1.8	58.4	0.1	50.6	3.9
	With Ca	72.7	3.5	52.6	0.1	22.0	1.5
IFPH7	Without Ca	6.9	0.5	7.2	0.6	55.7	1.6
	With Ca	6.9	0.5	7.1	0.2	25.3	1.9
HIVFP	Without Ca	46.8	1.0	31.6	0.8	42.0	0.3
	With Ca	33.0	0.8	16.0	0.7	31.7	0.5

The results revealed that the degree of calcium-mediated inhibition varied depending on both membrane composition and the specific fusion peptide tested (**Fig. 15**). In general, POPG-containing membranes at pH 5.0 exhibited the lowest inhibition, while POPS-containing vesicles at pH 7.4 showed the highest inhibition. This suggests that membrane composition and pH-dependent electrostatic properties significantly modulate the effect of calcium on peptide-membrane interactions. Among the peptides, 1FP1H7 was least affected by Ca^{2+} in POPG-containing vesicles at pH 5.0, with only 8.5% inhibition. However, in POPS membranes at pH 5.0, the inhibition increased significantly to 52.6%, highlighting the sensitivity of this peptide to the specific membrane environment. 2FP1H7 displayed moderate inhibition (~22%) in both POPG at pH 5.0 and POPS at pH 7.4, with lower inhibition in POPS at pH 5.0 (11.8%), suggesting a relatively stable interaction across varying conditions. FP2H7 and IFPH7 were strongly inhibited by calcium only in POPS-containing vesicles at pH 7.4, reaching 56.6% and 54.6%, respectively. This indicates a pronounced sensitivity of these peptides to both membrane composition and pH in the presence of calcium. HIVFP, used as a comparative control, was also highly affected, with 49.5% inhibition in POPS at pH 5.0, suggesting that calcium can broadly interfere with fusogenic peptides, regardless of their origin.

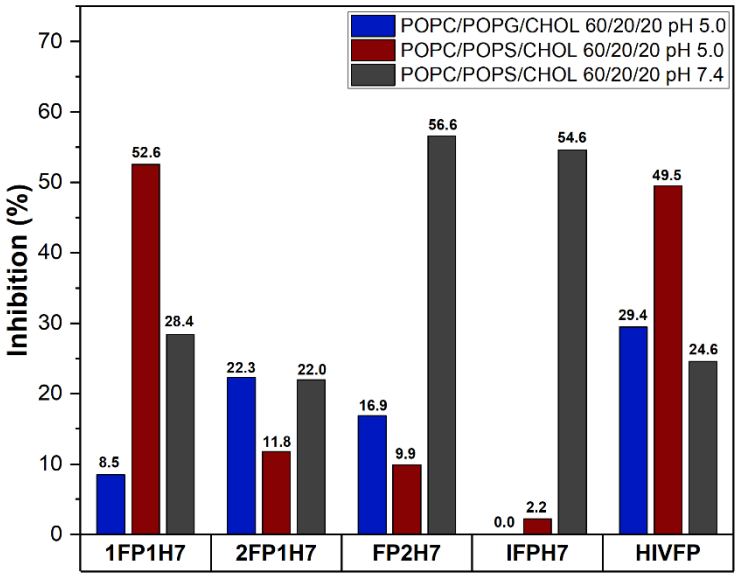

Fig. 15. Inhibition of FPs fusogenic activity by calcium in negatively charged membranes. Percentage of inhibition of fusogenic activity of 1FP1H7, 2FP1H7, FP2H7, IFPH7, and HIVFP caused by 2 mM calcium in SUVs composed of POPC/POPG/Chol and POPC/POPS/Chol at pH 5.0, and POPC/POPS/Chol (60/20/20) at pH 7.4.

Interestingly, IFPH7 was least affected by calcium in POPG- and POPS-containing vesicles at pH 5.0, while its impact on FP2H7 under the same membranes was low to moderate (**Table 4** and **Fig. 15**). Overall, the strongest calcium-mediated inhibitory effect on fusogenic activity were observed in POPS-containing vesicles both at pH 7.4, where FP2H7 and IFPH7 were the most affected peptides, and at pH 5.0, where 1FP1H7 was the most affected coronavirus FP.

4.4.2. Membrane ordering of vesicles is moderately affected by calcium

To investigate the influence of calcium on the membrane-ordering effect of fusion peptides, EPR assays were performed using spin-labeled SUVs with the same lipid composition described in Section 4.2.3. Vesicles were incubated both with and without 2 mM $CaCl_2$, and the percentage variations of the EPR parameters ($\%\Delta S_{zz}$ and $\%\Delta h_{+1}/h_0$) were calculated to quantify changes in membrane packing and ordering. The complete dataset, including all calculated parameters, is provided in **Annex 21.**

At the lipid-water interface, with a few exceptions, calcium mainly increased the $\%\Delta h_{+1}/h_0$ negative value in anionic membranes, indicating higher calcium-induced lipid headgroup ordering both in the presence and absence of fusion peptides (**Fig. 16**). This effect was most pronounced in POPS vesicles at pH 7.4, where 1FP1H7 and FP2H7 induced changes of about -3.0%, suggesting tighter headgroup packing. Conversely, 2FP1H7 showed the opposite trend, with a positive $\%\Delta h_{+1}/h_0$ value (+1.5%), indicating increased headgroup dynamics at the interface under the same conditions. At pH 5.0, calcium enhanced lipid packing in peptide-free POPS-containing vesicles, though it had minimal impact in the presence of most fusion peptides. An exception was FP2H7, which showed a slight decrease in headgroup ordering. In POPG vesicles at pH 5.0, calcium increased the $\%\Delta h_{+1}/h_0$ values uniformly in both the absence and presence of 2FP1H7 and FP2H7, indicating enhanced packing. In contrast, in POPE-containing vesicles, the overall calcium effect was negligible, except for 1FP1H7 at pH 7.4, which caused a moderate increase in headgroup packing. This suggests that calcium's ability to influence lipid ordering at the interface is highly dependent on both membrane composition and peptide identity.

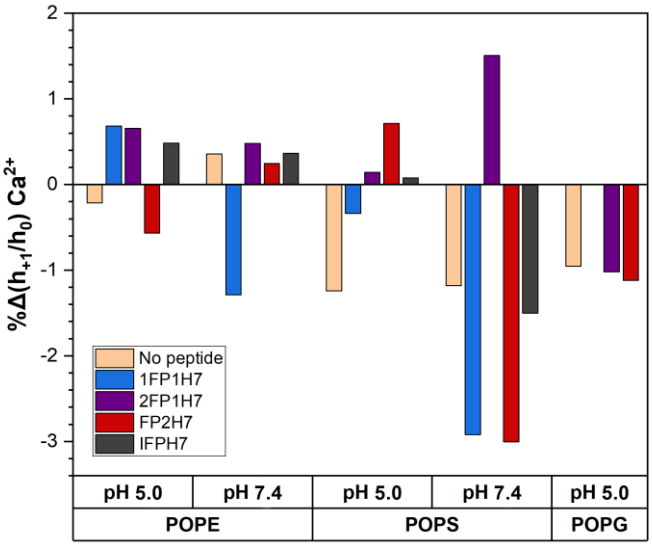

Fig. 16. Calcium changes of the peptide-induced ordering effect of DPPTC (%$\Delta h_{+1}/h_0$) in negatively charged vesicles. The percentage of variation of the $\Delta h_{+1}/h_0$ parameter of DPPTC embedded in SUVs containing 20 mol% of POPE, POPG, or POPS vesicles was calculated in the presence and absence of calcium at pH 5.0 and pH 7.4. SUVs concentration was 5 mg/mL, peptides were added at a lipid-to-peptide ratio of 20:1, and $CaCl_2$ concentration was 2 mM. Buffer: 10 mM HEPES/MES, 150 mM NaCl, pH 5.0. No $\%\Delta h_{+1}/h_0$ data were obtained for 1FP1H7 and IFPH7 in POPG membranes at pH 5.0.

At the hydrophobic core, the effect of calcium also varied with membrane composition, pH, and the specific fusion peptide tested (**Fig. 17**). Calcium generally increased lipid packing across most vesicles, except for POPE SUVs at pH 5.0, where a decrease in $\%\Delta S_{zz}$ observed for 1FP1H7, 2FP1H7, and the empty vesicles indicated increased membrane fluidity. Similarly, in peptide-free POPS-containing vesicles at pH 5.0, binding of calcium slightly reduced membrane ordering, although the changes were less pronounced than in POPE vesicles. At pH 5.0, calcium promoted lipid packing in POPG vesicles, with IFPH7 showing the highest increase in $\%\Delta S_{zz}$ (+3.406%), whereas 1FP1H7 exhibited the opposite effect, decreasing membrane ordering. In vesicles with POPS at pH 5.0, calcium had little to no influence, with FP2H7 experiencing the most notable, yet minor, increase in lipid packing (0.7%), suggesting peptide-specific interactions with the calcium-altered membrane. At pH 7.4, calcium increased membrane ordering in POPS-containing vesicles with and without 2FP1H7. POPE vesicles displayed an overall increase in $\%\Delta S_{zz}$ in all cases, except for 1FP1H7, which reduced membrane ordering.

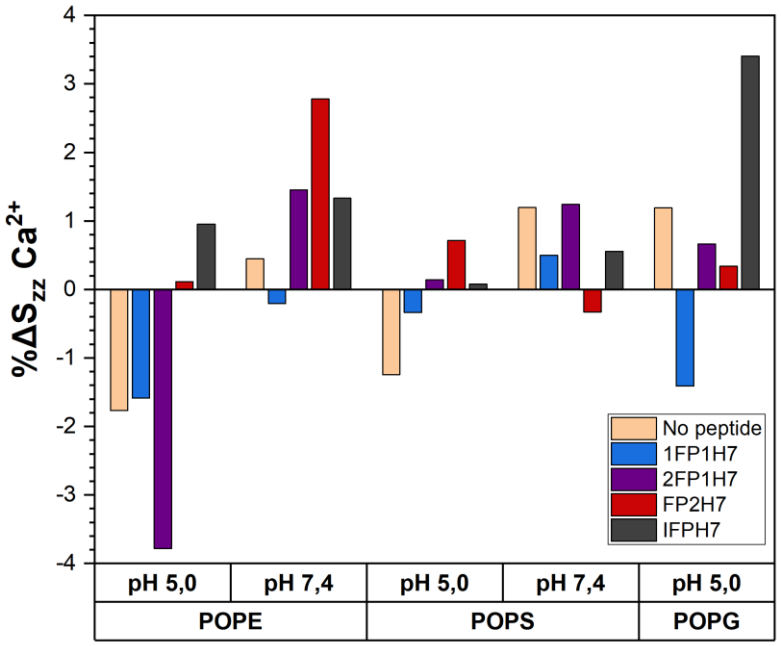

Fig. 17. Calcium changes the peptide-induced ordering effect of 5-PCSL (%ΔS_{zz}) in negatively charged vesicles. The percentage of the order parameter S_{zz} of 5-PCSL embedded in SUVs containing 20 mol% of POPE, POPG, or POPS was calculated in the presence and absence of calcium at pH 5.0 and pH 7.4. SUVs concentration was 5 mg/mL, peptides were added at a lipid-to-peptide ratio of 20:1, and $CaCl_2$ concentration was 2 mM. Buffer: 10 mM HEPES/MES, 150 mM NaCl, pH 5.0.

4.4.3. Calcium causes subtle changes in the secondary structure of fusion peptides in the presence of membranes

CD experiments were conducted to evaluate the effect of calcium ions (Ca^{2+}) on the secondary structure of fusion peptides, both in solution and in the presence of negatively charged vesicles. The fusion peptides analyzed included 1FP1H7, 2FP1H7, FP2H7, and IFPH7, selected based on their previously observed high fusogenic activity in anionic membrane environments. The tested SUVs included: POPC/POPG/Chol (60/20/20) at pH 5.0, POPC/POPS/Chol (60/20/20) at pH 5.0 and 7.4, and LPG micelles at pH 5.0. A final calcium concentration of 2 mM was used at the highest vesicle concentration tested. All CD experiments followed the previously established protocols, using consistent peptide and vesicle concentrations under identical conditions for direct comparison.

CD spectra of each peptide, both in solution and in the presence of membranes, with and without calcium, are provided in **Annexes 4 to 7**. The deconvolution data for these spectra, detailing the percentage content of different secondary structures (*α*-

helix, *β*-strand, turn, and disordered structures), is available in **Annex 8**. To enable a more quantitative analysis of the impact of calcium on peptide secondary structure, the difference in the percentage of each secondary structure was calculated by comparing their content with and without calcium (**Table 5**). For simplicity, POPC/POPG/Chol is referred to as POPG vesicles, and POPC/POPS/Chol is described as POPS vesicles.

Table 5. Changes in secondary structures of the fusion peptides by calcium in solution and in the presence of negatively charged membranes. The difference of each type of secondary structure between the calcium-rich and calcium-free samples is shown here. Spectral deconvolution was carried out using BeStSel.

Peptide	Membrane	pH	Secondary structure (%)					
			α-helix	Strand		Total Strands	Turn	Others
				Antiparallel	Parallel			
1FP1H7	Solution	5.0	0.1	0.5	0.0	0.5	0.7	-1.3
	LPG	5.0	-3.1	9.9	-1.1	8.8	0.3	-6.1
	POPG	5.0	-0.1	-1.1	0.0	-1.1	-0.6	1.8
	POPS	5.0	2.3	-4.3	1.5	-2.8	-0.4	0.9
	Solution	7.4	1.0	0.7	0.0	0.7	-0.7	-0.8
	POPS	7.4	-0.8	2.7	-2.5	0.2	-0.7	1.3
2FP1H7	Solution	5.0	0.2	-0.5	-0.5	-1.0	-0.2	1.0
	LPG	5.0	1.6	-0.9	0.0	-0.9	0.7	-1.6
	POPG	5.0	-1.4	2.9	0.9	3.8	-0.6	-1.7
	POPS	5.0	1.0	-0.9	-1.2	-2.1	0.4	0.7
	Solution	7.4	-0.1	1.9	-0.5	1.4	-0.8	-0.5
	POPS	7.4	-0.2	0.4	-0.4	0.0	-0.2	0.4
FP2H7	Solution	5.0	-1.8	0.3	-0.4	-0.1	0.1	1.9
	LPG	5.0	-1.6	1.3	0.4	1.7	-1.2	1.1
	POPG	5.0	0.0	0.2	-1.2	-1.0	0.0	1.0
	POPS	5.0	-1.1	1.7	0.5	2.2	-1.2	0.1
	Solution	7.4	0.0	-0.3	0.0	-0.3	0.4	-0.2
	POPS	7.4	0.4	-0.7	0.0	-0.7	0.5	-0.3
lFPH7	Solution	5.0	-0.8	0.5	0.0	0.5	-0.2	0.5
	LPG	5.0	1.6	-1.0	0.1	-0.9	-0.4	-0.3
	POPG	5.0	-2.5	0.0	0.0	0.0	0.7	1.7
	POPS	5.0	-0.7	5.1	0.0	5.1	-0.9	-3.6
	Solution	7.4	2.7	-2.5	0.0	-2.5	0.2	-0.4
	POPS	7.4	1.2	-1.9	-0.9	-2.8	1.8	-0.3

The effect of calcium on the secondary structure of fusion peptides was found to be minimal across most conditions, with membrane composition and pH having little influence on the degree of structural change. In solution, calcium caused no significant structural changes at either pH 5.0 or pH 7.4. The minor differences in *α*-helices and

β-strands observed for 2FP1H7 and IFPH7 at pH 7.4 (**Table 5**) are likely artifacts from spectral deconvolution, as the CD spectra of the peptides under these conditions are highly similar within the experimental uncertainties **(Annexes 4 to 7)**.

Among the tested model membranes, the most pronounced structural changes were observed in LPG micelles, particularly for 1FP1H7. In this environment, calcium induced a significant increase in *β*-strands (+8.8%), with a marked enhancement of antiparallel *β*-strands (+9.9%), while simultaneously reducing the proportion of disordered structures. This suggests that 1FP1H7 is particularly sensitive to the membrane-mimetic properties of LPG micelles, adopting more ordered *β*-structures upon calcium binding. In contrast, calcium had a minimal impact on the secondary structure of the other peptides, both in LPG micelles and in lipid vesicles, with only slight adjustments in structural elements that fall within experimental variability. Indeed, the CD spectra shows only minor to no alterations upon calcium addition (**Annexes 4 to 7**), supporting the conclusion that calcium does not significantly influence peptide secondary structure in these environments.

In summary, the secondary structure of the peptides was mostly affected by calcium only in the presence of LPG micelles, while in the presence of lipid vesicles, the structural profiles of all peptides remained largely unaltered. This finding suggests that the inhibitory effect of calcium on fusogenic activity – as previously observed in lipid-mixing assays – is not directly linked to significant structural rearrangements of the fusion peptides. Instead, the reduction in fusogenicity is likely driven by calcium's impact on membrane properties, such as surface charge neutralization, increased membrane rigidity, and altered lipid packing. The ability of calcium to inhibit fusion without inducing major conformational changes in the peptides highlights its role as a modulator of membrane dynamics rather than a direct effector of peptide structure.

4.4.4. Calcium affects zeta potential values of negatively charged membranes

To evaluate the impact of calcium on the surface charge of negatively charged vesicles, zeta potential measurements were performed using SUVs composed of POPC/POPG/Chol and POPC/POPS/Chol (both at 60/20/20 molar%). The membranes were prepared at a final concentration of 50 µM tested at pH 5.0. Vesicles were incubated with increasing concentrations of $CaCl_2$ (0 µM, 50 µM, 100 µM, 250 µM, 500 µM, 750 µM, 1 mM, 1.5 mM, and 2 mM) prior to the zeta potential

measurement. Due to equipment limitations, NaCl was excluded from these assays to avoid interference with conductivity.

The results showed a logarithmic increase in positive charge – and consequently, a reduction in negative ζ-potential values – upon calcium addition in both POPG- and POPS-containing vesicles (**Fig. 18**). In the absence of calcium, SUVs with POPG were initially more negatively charged than ones with POPS, with ζ-potential values of -25.2 mV and -18.2 mV, respectively. This difference aligns with the intrinsic charge properties of the phospholipid headgroups, as POPG carries a stronger net negative charge compared to POPS under acidic conditions.

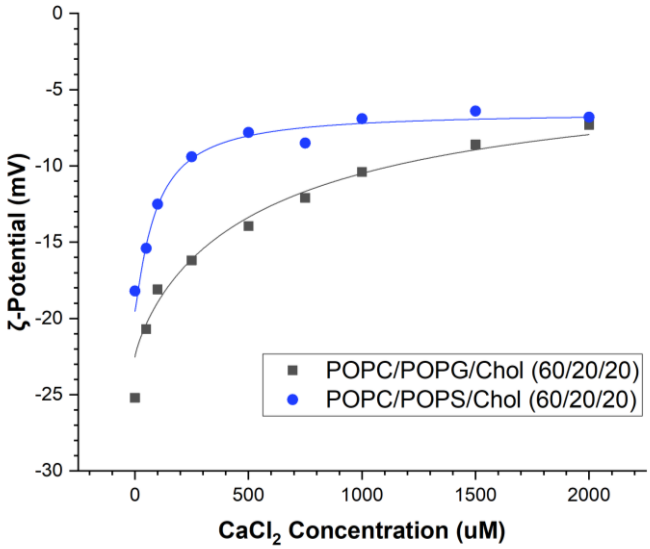

Fig. 18. Effect of calcium on ζ-potential values of negatively charged membranes. SUVs of POPC/POPG/Chol and POPC/POPS/Chol (both at 60/20/20 molar%) at a concentration of 50 μM and pH 5.0 were incubated with increasing $CaCl_2$ concentration). Buffer: 10 mM HEPES/MES, pH 5.0. Fitting curves were generated using the Hill equation.

As calcium concentration increased, both membranes experienced a progressive reduction in ζ-potential, and consequently, in surface charge (**Fig. 18**). However, the rate and extent of charge neutralization differed between the two membrane compositions. Vesicles with POPS began stabilizing their charge at relatively low calcium concentrations (500 μM $CaCl_2$), suggesting a rapid binding of calcium to the membrane surface. In contrast, POPG vesicles displayed a gradual and continuous reduction in negative charge across the entire calcium titration range, without reaching full stabilization even at the highest tested concentration (2 mM $CaCl_2$). At 2 mM $CaCl_2$, both vesicle types eventually converged to similar ζ-potential

values of -6.8 mV (POPS) and -7.3 mV (POPG). The faster charge neutralization and saturation observed in POPS vesicles compared to the slower, gradual charge reduction in POPG vesicles, suggests that calcium has a higher affinity for POPS membranes. This is likely due to the unique chemical structure of PS headgroups, which can form more stable coordination complexes with divalent cations like Ca^{2+} through their carboxyl and phosphate groups.

5. DISCUSSION

The fusion of host and viral membranes is essential for the infectivity of enveloped viruses. This process is orchestrated by several key factors, among which fusion peptides play a crucial role. These peptides are responsible for binding target membranes, modifying their physical properties, and ultimately facilitating membrane fusion. In SARS-CoV and SARS-CoV-2, these fusion peptides are located within the N-terminal region of the S2 subunit of the Spike glycoprotein, a region that undergoes conformational changes upon activation to mediate membrane merging. In this study, we analyzed the fusogenic activity, secondary structure, and membrane-ordering effects of the synthetic fusion peptides 1FP1H7, 2FP1H7, FP2H7, and IFPH7 under varying experimental conditions, including differences in lipid composition, cholesterol content in artificial membrane models, and the presence of calcium ions. Our findings confirmed that the fusion peptides are indeed capable of inducing membrane fusion, as evidenced by their lipid-mixing activity, while also increasing membrane ordering and undergoing minor but context-dependent structural changes.

Membrane model characterization: Charge and size as determinants of peptide-membrane interactions

A critical first step in this study was the characterization of the SUVs used in this study, focusing on their surface charge and size to provide, as these parameters are essential for understanding their interactions with fusion peptides.

ζ-potential measurements at pH 5.0 revealed differences in surface charge among the vesicles, primarily driven by the headgroup composition of the lipids. Vesicles containing POPE, SM, or pure POPC were slightly negatively charged, while those containing DOTAP were positively charged. In contrast, SUVs with POPS or POPG were more negatively charged due to their anionic nature. Although POPE- and

POPC-containing vesicles are expected to be zwitterionic, studies indicate that cholesterol reduces the surface charge of POPC-based phospholipid membranes[69], while phosphatidylethanolamine enhances the slight negative charge of the phosphate group in POPC, contributing to their overall charge profile[70,71]. Conversely, SUVs containing DOTAP displayed a strong positive charge, as expected from the presence of a cationic ammonium group (NH_4^+), which remains positively charged regardless of pH changes[72,73]. Vesicles with POPS and POPG were negatively charged, consistent with their chemical structures. The carboxylate ($-COO^-$) and phosphate ($-PO_4^-$) groups in the headgroups of phosphatidylserine and phosphatidylglycerol contribute to their strong negative zeta potential under the same conditions[74,75]. Notably, the initial ζ-potential of POPG vesicles (-25.2 mV) was more negative than that of POPS vesicles (-18.2 mV), a difference that aligns with previous reports indicating that, under acidic conditions, POPG retains its negative charge more effectively than POPS, where the protonation of the carboxylate group of PS can reduce surface charge[74].

Size measurements of SUVs showed interesting results under varying ionic conditions. In the absence of NaCl, vesicles exhibited larger sizes, particularly those composed solely of phospholipids and cholesterol. The addition of NaCl led to a significant reduction in vesicle size for most lipid compositions. This effect can be explained by two well-established mechanisms: 1) the addition of Na^+ ions screens the electrostatic interactions between headgroups, reducing repulsion between the negatively charged groups, leading to tighter lipid packing and a decrease in vesicle size. This ion-mediated neutralization also alter the intrinsic curvature of the bilayer favoring more compact vesicle formation.[76] 2) The salt concentration gradient across the membrane generates an osmotic force, leading to the efflux of water molecules from the vesicle interior, thus contributing to the observed size reduction[77].The increase of size in DOTAP vesicles in the presence of NaCl was an exception to this trend but is in concordance with previous studies[78].

Fusogenic and membranotropic activities, but not the structure, of fusion peptides are influenced by lipid composition

The first major finding of this study highlights the crucial role of membrane lipid composition in influencing the activity and structure of SARS-CoV and SARS-CoV-2 fusion peptides. These peptides exhibited high fusogenic activity and significant membrane-ordering effect in negatively charged membranes, with only minor structural

modifications. In contrast, their activity was minimal or nonexistent in zwitterionic or cationic membranes, underscoring a clear preference for anionic environments that likely facilitate membrane destabilization and fusion.

All fusion peptides analyzed in this study contained a C-terminal H7 tag (GGGKKKK) used to enhance peptide solubility, which may have contributed to their electrostatic affinity for negatively charged membranes. Importantly, this tag did not interfere with fusogenic activity, as confirmed by the lack of lipid-mixing activity of H7-C tag (GCGKKK), which shares an almost identical amino acid composition (**Fig. 6A and B**). This observation aligns with previous studies that employed this H7-C tag, in studies of SARS-CoV[26,34], SARS-CoV-2[29,36], and other viral fusion peptides[79–81], all of which reported no effect on FP function. Our CD measurements also revealed that the secondary structure of the H7 tag is predominantly disordered conformations both in solution and in the presence of membranes (**Annex 10**). This flexibility likely minimizes its influence on the structural and functional dynamics of the fusion peptides, validating its use as a solubilizing tool in peptide studies.

1FP1 is one of the earliest putative fusion peptides identified in SARS-CoV[26], with a relatively conserved sequence across betacoronaviruses, including SARS-CoV-2 2FP1(**Table 1**). This study demonstrated that 1FP1H7 exhibits high fusogenic activity in negatively charged membranes, and a strong ability to induce membrane ordering at both the headgroup and hydrophobic core of anionic lipid bilayers. These findings corroborate previous work highlighting the critical role of anionic lipids in facilitating the membrane fusion process Sainz *et al*.[27] reported significant lipid mixing activity in large unilamellar vesicles (LUVs) containing the anionic phosphatidylinositol (PI), while Basso and colleagues[29] observed the same level of activity in POPC/POPG (3:2) membranes at pH 5.0, which further increased at pH 7.4, the same tendency observed in this study.

CD spectra of 1FP1H7 revealed a high content of disordered conformations (52.0%), with 26.1% *β*-sheet content at pH 7.4, which slightly increased to 28.5% upon interaction with negatively charged POPC/POPS/Chol SUVs. Sainz *et al*.[27] reported a *β*-sheet conformation of the H7-free 1FP1 peptide in solution at pH 7.0, which persisted in the presence of 1 mM LUVs composed of POPC/PI (9:1). Guillen *et al*. also reported an increase in extended *β*-strand conformation of the H7-free 1FP1 from 31% in solution to ~35–36% in phospholipid membranes[62]. Basso *et al*.[29] also observed a predominantly disordered structure at both pH 5.0 and 7.4, with a transition to an α-

helix conformation in LPG and lysophosphocholine (LPC) micelles. A nuclear magnetic resonance (NMR) study by Mahajan and Bhattacharjya[82] further confirmed the peptide's ability to adopt different structures depending on the environment. In dodecylphosphocholine (DPC) micelles, 1FP1 was shown to adopt an α-helical conformation with a notable distortion at the central glycine residues, emphasizing the peptide's structural plasticity in membrane-mimetic systems.

The membrane ordering effect and interaction of 1FP1H7 have been previously investigated using various techniques, all of which align with our findings. Lai *et al*.[34] referred to the 1FP1 peptide as an alternative fusion peptide (AltFP-A) and demonstrated an increase in the ordering of both DPPTC and 5-PCSL in POPC/POPS/Chol (60/20/20 mol%) using EPR. However, the effect was less pronounced than that of FP2 (referred to as FP1 in their study). Similarly, Basso *et al*.[29,35] used EPR to confirm the membrane ordering effect of both 1FP1 and 1FP1H7, showing an increased order parameter of DPPTC and 5-PCSL, with a more substantial effect on negatively charged membranes. Indeed, the 2021 study of Basso[29] showed that 1FP1H7 (referred to as FP1H7) was identified as the second most effective peptide in inducing membrane ordering, surpassed only by cIFPH7 (an extended version of IFPH7). This study identified 1FP1H7 as the peptide with the highest membrane-packing ability among the tested SARS-CoV and SARS-CoV-2 fusion peptides, in agreement with the previous EPR studies[29,35]. Additional evidence of peptide's penetration into membranes comes from studies showing that the tryptophan residue in 1FP1 is less exposed to the aqueous environment when bound to negatively charged membranes, indicating deeper membrane insertion[83]. Such insertion likely facilitates membrane destabilization, an essential step in the fusion process[82].

Fusion peptide 2FP1H7, a close homolog of 1FP1H7, differs by only five amino acid residues but exhibits distinct functional properties. Molecular dynamics (MD) simulations have shown that 2FP1 (without the H7 tag) has a higher affinity for negatively charged membranes (e.g., POPG) compared to zwitterionic ones[84]. This preference was attributed to the peptide’s positive charge at both pH 7.0 and pH 5.0, primarily driven by a lysine (K) residue[84] that mediates electrostatic interactions with anionic headgroups[85].

In the current study, 2FP1H7 displayed a similar membrane-binding preference, with higher fusogenic activity in negatively charged environments. Its secondary structure remained predominantly disordered, even upon membrane binding,

consistent with MD simulations data suggesting that structural flexibility is preserved during membrane interaction[84]. This flexibility may allow 2FP1H7 to adapt to different membrane curvatures and compositions, a property that could be functionally significant during membrane fusion.

Regarding its secondary structure, it was reported that 2FP1 was predominantly disordered in solution, with a notable presence of *β*-sheets at pH 7, and this unstructured conformation was largely retained upon POPG membrane binding, similar to the results in present work.[84] This highlight a structural preference for anionic environments while maintaining flexibility, which may be relevant for its role in membrane fusion.

The FP2 fusion peptide – commonly referred to as “FP1” in the SARS-CoV-2 literature[34,36] – has been the subject of considerable debate regarding its sequence boundaries and functional properties. While 1FP1 was the first FP sequence identified in SARS-CoV, many studies on SARS-CoV-2 have focused on the FP2 region (residues 834 to 855 in SARS-CoV-2 or 816 to 837 in SARS-CoV), often overlooking 1FP1. Furthermore, there remains no consensus on the optimal sequence length for FP2, with both short and extended fragments being employed in the literature, leading to variations in reported structural and functional characteristics.

A hallmark of the FP2H7 peptide is its pH-depended fusogenic activity, particularly in negatively charged membranes. Our results confirm this behavior, with FP2H7 showing higher lipid-mixing activity at pH 5.0 compared to pH 7.4, in alignment with previous findings, regardless of sequence length.[26,8629] This pH sensitivity is crucial for understanding FP2’s role during viral entry, as the endosomal environment, where viral fusion often occurs, is acidic, favoring FP2 activation.

Contrary to the observed preference of FP2 for negatively charged membranes, Santamaria *et al*.[44] calculated the binding affinity of this peptide (referred to as FP1 in their study) to a PS-containing plasma membrane-like monolayer using a Langmuir trough, and reported a negative cooperative binding. This behavior was attributed to FP2’s overall negative charge at physiological pH, which impairs its interaction with the negatively charged phosphatidylserine (PS) lipids in the membrane’s outer leaflet. Adding further complexity, a study of Shekunov *et al*.[87] demonstrated that FP2’s fusogenic potential is highly influenced by membrane composition. Their leakage assays showed that FP2’s fusogenicity was enhanced by the presence of phosphatidylethanolamine (PE) but inhibited by PS. However, characterizing its

fusogenic activity based solely on content leakage experiments does not provide definitive evidence of membrane fusion, and further analyses are required[50].

A consistent theme in FP2 research is its conformational adaptability**.** Regardless the extension of the FP2 sequence length or the pH, previous studies have shown that FP2 in solution changed from a disordered structure to a helical or helical-like conformation in negatively charged membranes[26,29,34,88–90]. However, our findings differ from this pattern in two key aspects. First, in solution at pH 5.0, FP2H7 exhibited partial structural organization, with CD spectra showing two negative peaks (~200 nm and ~216 nm) attributed to a coexistence of *β*-strands conformations and disordered structures, a feature that has been underreported in previous studies. Only in the presence of LPG micelles did the peptide shift to a fully α-helical conformation. Second, in our study, FP2H7 showed a tendency to increase β-strand content while slightly reducing or maintaining its α-helix levels. Basso and colleagues[29], using the same FP2H7 sequence, reported a transition from an unstructured conformation in solution to an α-helix in the presence of LPC and LPG micelles, aligning with our observations. However, a recent study by Sumarokova *et al.*[91], utilizing the same spectral deconvolution tool (BeStSel), observed that the FP2 helical content increased from 8% in solution (which the peptide is primarily unstructured) to 55% in the presence of methanol and to 27% in DOPS LUVs at pH 7.0. In contrast, our experiments showed only a minimal increase of the helices in POPS membranes at pH 7.4 (from 0.4% to 1.2%), which is within the experimental error.

In terms of membrane ordering effects, our study found that FP2H7 exhibited the lowest lipid packing ability among the fusion peptides tested, affecting both the headgroup and hydrophobic core regions at pH 5.0 and pH 7.4. These results align with findings from Basso *et al*.[29], who also reported that FP2H7 had the weakest membrane ordering effect, showing only moderate ordering both in the hydrophobic and in the headgroup levels. In contrast, Lai *et al*.[34] demonstrated that FP2 (referred to as FP1 in their study) exhibited the strongest membrane ordering effect among tested fusion peptides, surpassing both 1FP1 and IFP. This discrepancy may stem from differences in experimental conditions or peptide constructs, particularly regarding sequence length and the presence of the H7 tag in our study. Despite its weak overall ordering effect compared to the other peptides, FP2H7 appears to have a distinct membrane penetration profile. Neutron reflectometry[44] studies and MD simulations[87] have shown that FP2 interacts with both lipid headgroups and aliphatic tails of anionic

membranes, primarily due to its LLF motif, a well-known membrane anchoring sequence in viral fusion peptides.

The interactions between FP2 and membranes are heavily influenced by specific amino acid residues that dictate its depth of insertion and fusogenic potential. It has been shown that the aspartic acid at position 830 (Asp830) plays a crucial role in regulating the depth of peptide insertion. Neutralization of its charge significantly reduces the insertion of FP2 into DMPC bicelles, highlighting its role in peptide-membrane electrostatic interactions [92]. While hydrophobic residues primarily facilitate membrane interactions, lysine residues are key in binding to the headgroups of negatively charged lipids[93]. Specifically, the lysine at position 825 (Lys825), highly conserved across Betacoronaviruses, anchors the peptide to membrane surfaces. Interestingly, the K825A mutation has been shown to enhance fusogenic activity and increase *α*-helix conformation, suggesting that Lys825's presence stabilizes membrane binding but may restrict conformational flexibility[94]. Hydrophobic residues are equally critical.[95,96] Phenylalanine (Phe), isoleucine (Ile), and leucine (Leu) stabilize the FP2 α-helical conformation, facilitating deeper membrane insertion and promoting fusion.[95] The LLF motif further enhances this membrane-penetrating capacity.

The IFPH7 fusion peptide stands out among the SARS-CoV and SARS-CoV-2 fusion peptides due to its distinct pH-dependent fusogenic activity and its strong membrane-ordering effects. Unlike other fusion peptides that show high activity at acidic pH, IFPH7 demonstrates minimal fusogenic activity on negatively charged membranes at pH 5.0 (~7.0%) but exhibits a substantial increase in activity at pH 7.4 (55.7%). The observed increase in fusogenic activity at neutral pH is consistent with previous studies. Santamaria *et al*. reported that IFP exhibits positively cooperative binding to anionic membranes, facilitated by its positive charge at both acidic and physiological pH. This charge profile enhances its interaction with negatively charged lipids, such as phosphatidylserine, commonly found in the inner leaflet of the plasma membrane and endosomal compartments[44]. The higher fusogenicity at pH 7.4 observed in this study aligns with Basso *et al*.,[29] who demonstrated that an extended version of IFPH7, known as cIFPH7, displayed high lipid mixing activity – surpassing both 1FP1H7 and FP2H7 – with activity reaching 100% at pH 7.4. These findings highlight the pH sensitivity of IFPH7 and its potential role in facilitating fusion events outside the endosomal environment.

The secondary structure of IFPH7 characterized in this study revealed an unstructured conformation in solution, which transitions into a more α-helix conformation upon interaction with the negatively charged LPG micelles (from 2.8% to 30.6%). This finding is consistent with the work of Basso *et al*.,[29] who observed a similar transition for IFPH7 in the presence of LPC and LPG micelles at both pH 5.0 and 7.4. Additionally, an NMR study confirmed that IFP adopts a relatively straight α-helical structure in DPC micelles, stabilized by packing interactions among the side chains of aromatic and aliphatic residues[82]. In the presence of lipid vesicles, though, the IFPH7 conformation remained mainly unstructured, with a slight increase in *β*-strands in POPS triggered by neutral pH. This result is consistent with the work by Guillén *et al*., who demonstrated that the H7-free IFP undergoes a conformational change from a predominantly unstructured conformation in solution to *β*-sheet aggregates in the presence of anionic membranes comprised of PG or phosphatidic acid (PA) lipids[97].

A key finding of this study is the strong membrane-ordering effect of IFPH7, making it the second most potent membrane packer after 1FP1H7. IFPH7 significantly increased lipid packing at both the headgroup and the hydrophobic core regions of negatively charged membranes across both pH 5.0 and pH 7.4. Basso *et al*.[35] demonstrated that IFP increased the order parameter in DPPG and DPPS membranes using EPR spectroscopy, with effects similar to those observed in this study. Also, in a most recent work,[29] the same authors showed that the extended version of IFPH7 (cIFPH7) displayed even stronger membrane-ordering effects, emerging as the most potent inducer among the fusion peptides tested. In contrast, Lai *et al*.,[34] who referred to IFP as AltFP-B, reported a moderate increase in membrane ordering, smaller than that of FP2 (referred to as FP1 in their work) and 1FP1 (referred to as AltFP-A), possibly due to differences in experimental conditions or peptide constructs.

The extent of IFPH7's membrane insertion has been explored using various experimental techniques. Mahajan and Bhattacharjya[82] showed, through paramagnetic spin-labeled NMR, that IFP inserts into the hydrophobic core of DPC micelles, stabilizing its α-helical conformation. Similarly, Santamaría *et al*.[44] demonstrated that IFP interacts strongly within the lipid headgroup region of membranes. However, the depth of insertion appears to be highly lipid composition-dependent. One work found that the presence of POPG diminished the IFP's ability to

penetrate the membranes, while the addition of cholesterol completely abolished its insertion[83].

Fusion peptides exhibit a strong preference for and are more active in negatively charged membranes, properties driven by electrostatic interactions between positively charged peptide residues and anionic lipid headgroups. In this study, we highlighted the interaction of SARS-CoV and SARS-CoV-2 fusion peptides primarily with anionic lipids, such as phosphatidylserine (PS) and phosphatidylglycerol (PG), consistent with their known roles in facilitating membrane fusion.

PS is typically located in the inner leaflet of the plasma membrane and in endosomal membranes[98], playing a critical role in synaptic fusion events[99] and acting as a key lipid in viral entry through membrane fusion[100–102]. PG, while less abundant in mammalian membranes, is commonly used in membrane fusion studies due to its strong anionic character. It is predominantly found in bacteria, archaea and pulmonary surfactants[103,104]. Another common anionic lipid in eukaryotic membranes is phosphatidylinositol, which is primarily involved in cellular signaling, and PI derivatives, known as phosphoinositides, also participate in membrane fusion events.[105] Despite the above, PS, PG, and PI are not the only negatively charged lipids implicated in membrane fusion. A study demonstrated that an extended version of the SARS-CoV-2 FP2 peptide (residues 816 to 855) preferentially initiates fusion in membranes resembling the late endosomal compartment due to the presence of bis(monoacylglycero)phosphate (BMP).[106] LUVs containing BMP exhibited significantly higher FP2-mediated fusion compared to those containing POPS or POPG. An intriguing observation from that study was the inverse correlation between lipid packing and fusion efficiency, as POPS membranes were slightly more tightly packed than BMP-containing membranes. This contrasts with the findings in our study for 1FPH7 and crac1FP1H7, as their fusion activities increase with cholesterol content, which makes the bilayers more ordered (higher S_{zz} values).

The role of cholesterol in modulating peptide's fusogenic and membrane ordering activities

The second main section of the results delves into the influence of cholesterol concentration on the fusogenic activity, secondary structure, and membrane ordering properties of the fusion peptides. Cholesterol is a key component of eukaryotic membranes, known to regulate membrane fluidity, curvature, and domain formation.

Its involvement in viral entry has been widely documented, particularly in enveloped viruses that rely on membrane fusion for infection. The spike proteins of both SARS-CoV and SARS-CoV-2 contain cholesterol-recognition motifs (CRAC and CARC), which facilitate specific interactions with cholesterol-rich membrane domains. Notably, Baier and Barrantes identified a residual CARC motif within the N-terminal region of FP2, supporting the idea that cholesterol can modulate its activity[107]. In this study, we identified a CARC domain in extended versions of FP1 from both SARS-CoV and SARS-CoV-2.

Our results revealed a peptide-specific response to increasing cholesterol concentrations. We observed a strong cholesterol-dependent increase in the fusogenic activity of 1FP1H7 and its CRAC-contained variant (crac1FP1H7), although at slightly reduced levels. 2FP1H7 and IFPH7 maintained consistent fusogenic activity levels regardless of cholesterol concentration, indicating a lesser dependence on membrane cholesterol for fusion promotion. FP2H7, in contrast, exhibited decreased fusogenic activity in negatively charged membranes at pH 5.0 only when 30 mol% cholesterol was present. This reduced activity of FP2H7 at high cholesterol content contrasts with findings by Niort *et al*.[39], who reported enhanced lipid mixing activity of FP2 in POPC-based SUVs at pH 7.5 upon the addition of DOPE and cholesterol, with further increases when ceramides were included. This discrepancy likely arises from differences in pH and membrane composition and charge (as the inclusion of PE and cholesterol make the membrane slightly more anionic), underscoring the context-dependent nature of fusion peptide behavior. Moreover, Santamaria *et al*.[44] reported an increase in the secondary structure content of extended FP2 and IFP in the presence of cholesterol-rich liposomes, suggesting that cholesterol can stabilize fusion peptide conformations. Another study confirmed that an extended FP2 variant binds cholesterol-containing vesicles fivefold faster than cholesterol-free ones, and cholesterol depletion was shown to reduce viral infectivity[108].

For 1FP1 and IFP, a study by Pattnaik[38] demonstrated that both peptides (referred to as IFP1 and FP in that study) exhibited increased fusogenic activity with higher cholesterol content in SUVs containing PG, indicating cholesterol-dependent lipid mixing activity. However, despite this increase, 1FP1 was not highly efficient in inducing lipid mixing. Furthermore, both peptides failed to promote substantial content mixing between membranes, suggesting that while they could induce hemifusion, they were unable to facilitate complete pore formation between merging membranes.

Interestingly, our findings contrast with these observations. We demonstrated that 1FP1H7 exhibited strong cholesterol-dependent fusogenic activity under acidic conditions, with a significant increase in lipid mixing in the presence of cholesterol, establishing it as a potent fusion inducer. In contrast, IFPH7 displayed minimal fusogenic activity under all tested conditions. These discrepancies likely stem from differences in experimental setups. While Pattnaik's study varied cholesterol content in DOPC/DOPE/DOPG/Chol SUVs at pH 7.4 and used H7 tag-free peptides, our experiments were conducted at pH 5.0 using POPC/POPG/Chol. Notably, our data also showed that IFPH7 exhibited significantly enhanced lipid mixing activity at pH 7.4, highlighting the pH-dependence of these peptides' fusogenic activity.

The role of calcium ions in modulating SARS-CoV and SARS-CoV-2 fusion peptide structure and activity

Calcium ions (Ca^{2+}) play a pivotal role in a wide range of biological processes, including cell signaling, membrane fusion, and viral entry. In the context of viral infections, several viruses exploit host cell calcium homeostasis to facilitate key stages of their life cycle, such as attachment, membrane fusion, and genome delivery.[109,110] Enveloped viruses, including coronaviruses, often rely on calcium-dependent mechanisms to fine-tune their fusion processes, making calcium a critical factor in understanding viral infectivity and identifying potential therapeutic targets.[111,112]

In this study, we explored the effects of calcium on the fusogenic activity, secondary structure, and membrane-ordering properties of SARS-CoV and SARS-CoV-2 fusion peptides. Our results reveal that calcium consistently reduces the lipid mixing activity of these peptides, acting as an inhibitor of membrane fusion. Additionally, calcium moderately impacts membrane ordering but induces minimal changes in peptide secondary structure. These findings align with and expand upon previous literature, offering insights into the complex role of calcium in coronavirus membrane fusion.

One of the key findings of this study is that calcium consistently decreases the fusogenic activity of the SARS-CoV and SARS-CoV-2 fusion peptides. This inhibition was particularly evident in POPS-containing membranes, where calcium induced a significant reduction in lipid mixing, while the effect was less pronounced in POPG-containing vesicles. This trend correlates with zeta potential measurements, which demonstrated that calcium increased the positive surface charge of the POPS vesicles

more efficiently than to POPG ones by binding to negatively charged lipid headgroups, thus reducing electrostatic attraction between the fusion peptides and the membrane.

Our findings align with those of Basso *et al*.[29], who also observed a reduction in FP2H7's lipid mixing activity in the presence of calcium using POPC/POPS/Chol (60/20/20) LUVs at pH 5.0. However, this inhibitory effect contrasts with studies suggesting that calcium can enhance viral infectivity. For example, Lai *et al*. observed that the depletion of extracellular calcium significantly reduced the infectivity of SARS-CoV pseudotyped particles.[34] This apparent contradiction can be reconciled by considering the multifaceted role of calcium in viral entry and infection. While calcium binding to membrane lipids can reduce the fusogenic activity of fusion peptides by screening negative charges and altering membrane properties, calcium simultaneously acts as a critical cellular signaling molecule that viruses can exploit. During viral infection, calcium can trigger clathrin-mediated endocytosis, facilitating viral internalization; it can regulate endosomal acidification and trafficking, essential steps for viral uncoating and replication; and it can bind to both host and viral proteins, including calcium-dependent enzymes, ion channels, and viroporins, etc., thereby modulating membrane dynamics and intracellular signaling. These complex cellular responses extend beyond the scope of our biophysical assays, which focus on direct peptide-membrane interactions. Therefore, the reduction in fusogenic activity observed in our study is not directly comparable to the broader cellular effects inferred by Lai *et al*. in their work.[34]

Our CD analyses revealed that calcium had a minimal impact on the secondary structure of the fusion peptides under the conditions tested. This result suggests that the observed reduction in fusogenic activity is primarily driven by electrostatic effects rather than calcium-induced conformational changes. In contrast, some studies reported more pronounced structural changes upon calcium binding. For instance, Lai *et al*. demonstrated that calcium promotes an increase in the α-helical content in extended FP2, particularly in cholesterol-rich membranes, suggesting that calcium can influence the peptide's conformation in specific environments.[36,113] The lack of significant structural changes in our experiments could be attributed to differences in membrane composition, peptide sequence length, or specific different experimental conditions (type of buffers, pH values, presence of NaCl, etc.).

EPR analyses provided further insights into the membrane-ordering effects of calcium. Our findings showed that calcium moderately enhances the ordering of lipid

headgroups in negatively charged membranes, while exerting minimal influence on the packing of the hydrophobic core. Our findings align with the results of Lai *et al.*,[34] who found that Ca^{2+} ions increased membrane ordering at the headgroup level in POPC/POPS/Chol MLVs (60/20/20) but had no noticeable effect on the acyl chains. This localized ordering effect could restrict peptide access to the membrane surface, contributing to the observed reduction in fusogenic activity.

In a related study, Lai *et al.*[36] demonstrated that an extended version of the SARS-CoV-2 FP2 induced greater membrane ordering than its SARS-CoV counterpart, with both peptides showing a calcium-dependent membrane ordering effect. EPR studies confirmed that calcium increases headgroup ordering in negatively charged membranes (POPC/POPG/Chol), and the presence of calcium also amplified membrane ordering induced by the extended FP2 peptide. Furthermore, isothermal titration calorimetry (ITC) revealed that the SARS-CoV-2 FP2 binds two calcium ions, while the sequence corresponding to our FP2 binds one.

Interestingly, Santamaria and colleagues[44] reported that calcium promotes deeper insertion of FP2 (referred to as FP1 in their study) into lipid bilayers. In the presence of 2 mM calcium, FP2 penetrated from the outer leaflet to fully traverse the membrane, with most of the peptide residing in the hydrophobic tail region rather than near the headgroups. This deeper insertion could explain the reduced fusogenic activity observed in our study, as the peptide would be less available to interact with outer headgroups to mediate membrane fusion.

The interaction between calcium ions and fusion peptides is highly dependent on specific amino acid residues that coordinate calcium binding. NMR studies on extended FP2 (42 residues, spanning 816–857) suggested that the peptide can coordinate divalent calcium ions alongside lipid phosphoryl groups to promote membrane fusion[88]. Asp843 and Asp839 were identified as key residues likely participating in Ca^{2+} binding, whereas Asp830 appears uninvolved in calcium coordination due to its critical role in membrane insertion. Another study highlighted the contribution of six negatively charged residues in the extended FP2 to its membrane-ordering effect, driven by their calcium-binding capacity[113]. Among these, Asp812 in SARS-CoV FP2 (corresponding to Asp830 in SARS-CoV-2) was identified as particularly crucial. Mutating this residue resulted in a significant reduction in FP2's ability to enhance membrane ordering, further underscoring the importance of specific residues in calcium-mediated fusion dynamics.

Our findings indicate that calcium primarily affects the electrostatic interactions between the anionic membranes and fusion peptides rather than inducing significant changes in the peptides' secondary structure or their membrane ordering effects. This electrostatic modulation appears to play a key role in the observed inhibition of peptide-mediated fusion.

6. CONCLUSIONS

This study systematically investigated how membrane lipid composition, cholesterol content, and calcium ions influence the structure, fusogenic activity, and membrane-ordering effects of SARS-CoV and SARS-CoV-2 fusion peptides –1FP1H7, 2FP1H7, FP2H7, and IFPH7 – using a combination of biophysical techniques such as fluorescence spectroscopy, circular dichroism, and electron paramagnetic resonance. The findings provided valuable insights into the biophysical mechanisms underlying viral membrane fusion and identify key factors that modulate interactions between fusion peptides and host membranes.

First, we demonstrated that the fusogenic activity, secondary structure, and membrane-ordering effects of fusion peptides are strongly dependent on lipid composition and pH. The FP's fusogenic activity was significantly enhanced in negatively charged membranes containing POPS and POPG, while zwitterionic and cationic membranes exhibited minimal or no fusion activity. The pH-dependence of fusogenic activity was particularly notable. Most peptides showed increased lipid mixing activity in POPG membranes under acidic pH conditions. However, IFPH7 displayed an opposite trend, with a marked increase in fusogenicity at pH 7.4, suggesting a pH-induced conformational shift that enhances membrane fusion under physiological conditions. This pH-sensitivity reflects the environmental cues that coronaviruses may exploit during cell entry.

Circular dichroism analyses revealed that the secondary structures of the fusion peptides were sensitive to membrane composition. Negatively charged membranes promoted the formation of *β*-strands for some peptides, while micelles induced a shift toward α-helical conformations. These membrane-induced structural changes – especially within vesicles – likely facilitate membrane fusion by enabling deeper peptide insertion into the bilayer or enhancing membrane-peptide interactions. Interestingly, the degree of conformational change varied among peptides. While 1FP1H7 and IFPH7 exhibited marked structural rearrangements upon membrane

binding and pH, respectively, FP2H7 maintained a relatively stable structure but displayed subtle *β*-strand enhancements in negatively charged vesicles. These differences highlight the sequence-specific adaptability of each fusion peptide, reflecting their distinct roles during the membrane fusion process.

EPR studies demonstrated that the fusion peptides increased lipid ordering and membrane packing, particularly in negatively charged vesicles. The most pronounced ordering effects were observed for 1FP1H7 and IFPH7, which significantly enhanced packing at both the headgroup and the hydrophobic core regions of the bilayer. The peptides not only changed membrane curvature but also stabilized the bilayer, potentially facilitating hemifusion and pore formation.

We also explored the complex role of cholesterol in modulating peptide-membrane interactions. Cholesterol influenced fusogenic activity and membrane ordering in a peptide-specific manner. For example, 1FP1H7 displayed a linear increase in fusogenic activity with higher cholesterol concentrations, aligning with the known role of cholesterol in promoting lipid raft formation and creating favorable microenvironments for viral fusion. Conversely, FP2H7 displayed reduced activity at elevated cholesterol levels, suggesting that excessive membrane rigidity can inhibit its fusogenic potential. The presence of cholesterol recognition/interaction amino acid consensus (CRAC) motifs further modulated peptide function, enhancing membrane association but occasionally imposing structural constraints that limited fusogenicity.

Calcium ions exhibited a notable inhibitory effect on the fusogenic activity of the peptides, though this inhibition was pH-dependent and varied with membrane composition. However, calcium had minimal impact on the peptides' secondary structures, suggesting that its effects are primarily mediated through alterations in membrane properties rather than direct peptide conformational changes. EPR analyses indicated that calcium slightly enhanced membrane packing at the headgroup level and subtly altered the dynamics of the hydrophobic core. Additionally, zeta potential measurements confirmed that calcium binding to negatively charged membranes reduced the overall negative surface charge, further limiting peptide-membrane interactions.

These findings highlight the dual role of calcium in viral infections. While it can stabilize membranes and reduce fusogenic activity in simplified biophysical systems, calcium can also trigger host cell signaling pathways that viruses exploit for entry and

replication. This complexity underscores the importance of contextualizing *in vitro* findings within the broader cellular environment.

This study highlights the multifaceted nature of peptide-membrane interactions and underscores the importance of membrane composition, pH, cholesterol, and calcium ions in modulating the fusogenic activity of SARS-CoV and SARS-CoV-2 fusion peptides. The findings provide a detailed biophysical framework for understanding how these peptides interact with host membranes and how environmental conditions can enhance or inhibit membrane fusion. These insights have potential therapeutic implications. Targeting membrane properties (e.g., cholesterol content or membrane charge) or modulating calcium signaling could offer novel strategies to disrupt viral entry and limit infection.

7. REFERENCES

1. Wu, F. *et al.* A new coronavirus associated with human respiratory disease in China. *Nature 2020 579:7798* **579**, 265–269 (2020).
2. Barrantes, F. J. The Contribution of Biophysics and Structural Biology to Current Advances in COVID-19. *https://doi.org/10.1146/annurev-biophys-102620-080956* **50**, 493–523 (2021).
3. COVID-19 epidemiological update – 17 January 2025. https://www.who.int/publications/m/item/covid-19-epidemiological-update-edition-175.
4. COVID-19 cases | WHO COVID-19 dashboard. https://data.who.int/dashboards/covid19/cases.
5. Coronavírus Brasil. https://covid.saude.gov.br/.
6. Covid-19 Casos e Óbitos. https://infoms.saude.gov.br/extensions/covid-19_html/covid-19_html.html.
7. Schmidt, N. *et al.* The SARS-CoV-2 RNA–protein interactome in infected human cells. *Nature Microbiology 2020 6:3* **6**, 339–353 (2020).
8. Rahmandoust, M. & Ranaei-Siadat, S. O. COVID-19: Science to Social Impact. *COVID-19: Science to Social Impact* 1–263 (2021) doi:10.1007/978-981-16-3108-5/COVER.
9. Gorbalenya, A. E. *et al.* The species Severe acute respiratory syndrome-related coronavirus: classifying 2019-nCoV and naming it SARS-CoV-2. *Nature Microbiology 2020 5:4* **5**, 536–544 (2020).
10. Fang, R. *et al.* SARS-CoV-2 infection in animals: Patterns, transmission routes, and drivers. *Eco-Environment & Health* **3**, 45–54 (2024).

11. Chan, J. F. W. *et al.* Genomic characterization of the 2019 novel human-pathogenic coronavirus isolated from a patient with atypical pneumonia after visiting Wuhan. *Emerg Microbes Infect* **9**, 221–236 (2020).

12. Lu, R. *et al.* Genomic characterisation and epidemiology of 2019 novel coronavirus: implications for virus origins and receptor binding. *The Lancet* **395**, 565–574 (2020).

13. Zhou, P. *et al.* A pneumonia outbreak associated with a new coronavirus of probable bat origin. *Nature 2020 579:7798* **579**, 270–273 (2020).

14. Wrapp, D. *et al*. Cryo-EM structure of the 2019-nCoV spike in the prefusion conformation. *Science*. https://www.science.org/doi/10.1126/science.abb2507.

15. Lippi, G., Sanchis-Gomar, F., Mattiuzzi, C. & Henry, B. M. SARS-CoV-2: An Update on the Biological Interplay with the Human Host. *COVID 2023, Vol. 3, Pages 1586-1600* **3**, 1586–1600 (2023).

16. Jackson, C. B., Farzan, M., Chen, B. & Choe, H. Mechanisms of SARS-CoV-2 entry into cells. *Nature Reviews Molecular Cell Biology 2021 23:1* **23**, 3–20 (2021).

17. Negi, G., Sharma, A., Dey, M., Dhanawat, G. & Parveen, N. Membrane attachment and fusion of HIV-1, influenza A, and SARS-CoV-2: resolving the mechanisms with biophysical methods. *Biophysical Reviews 2022 14:5* **14**, 1109–1140 (2022).

18. Sternberg, A. & Naujokat, C. Structural features of coronavirus SARS-CoV-2 spike protein: Targets for vaccination. *Life Sci* **257**, 118056 (2020).

19. Arya, R. *et al.* Structural insights into SARS-CoV-2 proteins. *J Mol Biol* **433**, 166725 (2021).

20. Zhang, J., Xiao, T., Cai, Y. & Chen, B. Structure of SARS-CoV-2 spike protein. *Curr Opin Virol* **50**, 173–182 (2021).

21. Andersen, K. G., Rambaut, A., Lipkin, W. I., Holmes, E. C. & Garry, R. F. The proximal origin of SARS-CoV-2. *Nature Medicine 2020 26:4* **26**, 450–452 (2020).

22. Epand, R. M. Fusion peptides and the mechanism of viral fusion. *Biochimica et Biophysica Acta (BBA) - Biomembranes* **1614**, 116–121 (2003).

23. Apellániz, B., Huarte, N., Largo, E. & Nieva, J. L. The three lives of viral fusion peptides. *Chem Phys Lipids* **181**, 40–55 (2014).

24. Millet, J. K. & Whittaker, G. R. Physiological and molecular triggers for SARS-CoV membrane fusion and entry into host cells. *Virology* **517**, 3–8 (2018).

25. Shi, W. *et al.* Cryo-EM structure of SARS-CoV-2 postfusion spike in membrane. *Nature 2023 619:7969* **619**, 403–409 (2023).

26. Madu, I. G., Roth, S. L., Belouzard, S. & Whittaker, G. R. Characterization of a Highly Conserved Domain within the Severe Acute Respiratory Syndrome Coronavirus Spike Protein S2 Domain with Characteristics of a Viral Fusion Peptide. *J Virol* **83**, 7411–7421 (2009).

27. Sainz, B., Rausch, J. M., Gallaher, W. R., Garry, R. F. & Wimley, W. C. Identification and Characterization of the Putative Fusion Peptide of the Severe

Acute Respiratory Syndrome-Associated Coronavirus Spike Protein. *J Virol* **79**, 7195–7206 (2005).

28. Guillén, J., Pérez-Berná, A. J., Moreno, M. R. & Villalaín, J. Identification of the Membrane-Active Regions of the Severe Acute Respiratory Syndrome Coronavirus Spike Membrane Glycoprotein Using a 16/18-Mer Peptide Scan: Implications for the Viral Fusion Mechanism. *J Virol* **79**, 1743–1752 (2005).

29. Basso, L. G. M., Zeraik, A. E., Felizatti, A. P. & Costa-Filho, A. J. Membranotropic and biological activities of the membrane fusion peptides from SARS-CoV spike glycoprotein: The importance of the complete internal fusion peptide domain. *Biochimica et Biophysica Acta (BBA) - Biomembranes* **1863**, 183697 (2021).

30. Harrison, S. C. Viral membrane fusion. *Virology* **479–480**, 498–507 (2015).

31. White, J. M. & Whittaker, G. R. Fusion of Enveloped Viruses in Endosomes. *Traffic* **17**, 593–614 (2016).

32. Koch, J. *et al.* TMPRSS2 expression dictates the entry route used by SARS-CoV-2 to infect host cells. *EMBO J* **40**, 107821 (2021).

33. Meher, G. & Chakraborty, H. Membrane Composition Modulates Fusion by Altering Membrane Properties and Fusion Peptide Structure. *Journal of Membrane Biology* **252**, 261–272 (2019).

34. Lai, A. L., Millet, J. K., Daniel, S., Freed, J. H. & Whittaker, G. R. The SARS-CoV Fusion Peptide Forms an Extended Bipartite Fusion Platform that Perturbs Membrane Order in a Calcium-Dependent Manner. *J Mol Biol* **429**, 3875–3892 (2017).

35. Basso, L. G. M., Vicente, E. F., Crusca, E., Cilli, E. M. & Costa-Filho, A. J. SARS-CoV fusion peptides induce membrane surface ordering and curvature. *Scientific Reports 2016 6:1* **6**, 1–19 (2016).

36. Lai, A. L. & Freed, J. H. SARS-CoV-2 Fusion Peptide has a Greater Membrane Perturbating Effect than SARS-CoV with Highly Specific Dependence on Ca2+. *J Mol Biol* **433**, 166946 (2021).

37. Ge, M. & Freed, J. H. Fusion peptide from influenza hemagglutinin increases membrane surface order: An electron-spin resonance study. *Biophys J* **96**, 4925–4934 (2009).

38. Pattnaik, G. P., Bhattacharjya, S. & Chakraborty, H. Enhanced Cholesterol-Dependent Hemifusion by Internal Fusion Peptide 1 of SARS Coronavirus-2 Compared to Its N-Terminal Counterpart. *Biochemistry* **60**, 559–562 (2021).

39. Niort, K. *et al.* Cholesterol and Ceramide Facilitate Membrane Fusion Mediated by the Fusion Peptide of the SARS-CoV-2 Spike Protein. *ACS Omega* **8**, 32729–32739 (2023).

40. Barrantes, F. J. The constellation of cholesterol-dependent processes associated with SARS-CoV-2 infection. *Prog Lipid Res* **87**, 101166 (2022).

41. Lloyd-Evans, E. & Platt, F. M. Lysosomal Ca2+ homeostasis: Role in pathogenesis of lysosomal storage diseases. *Cell Calcium* **50**, 200–205 (2011).

42. Singh, P., Mukherji, S., Basak, S., Hoffmann, M. & Das, D. K. Dynamic Ca2+ sensitivity stimulates the evolved SARS-CoV-2 spike strain-mediated membrane fusion for enhanced entry. *Cell Rep* **39**, 110694 (2022).

43. Bronner, F. Extracellular and Intracellular Regulation of Calcium Homeostasis. *The Scientific World Journal* **1**, 919–925 (2001).

44. Santamaria, A. *et al.* Strikingly Different Roles of SARS-CoV-2 Fusion Peptides Uncovered by Neutron Scattering. *J Am Chem Soc* **144**, 2968–2979 (2022).

45. Carten, J. D. *et al.* A Mechanistic Understanding of the Modes of Ca2+ Ion Binding to the SARS-CoV-1 Fusion Peptide and Their Role in the Dynamics of Host Membrane Penetration. *ACS Infect Dis* **10**, 398–411 (2024).

46. Palacios-Rápalo, S. N. *et al.* Cholesterol-Rich Lipid Rafts as Platforms for SARS-CoV-2 Entry. *Front Immunol* **12**, 796855 (2021).

47. Han, X. & Tamm, L. K. A host-guest system to study structure-function relationships of membrane fusion peptides. *Proc Natl Acad Sci U S A* **97**, 13097–13102 (2000).

48. Swinehart, D. F. The Beer-Lambert Law. *J Chem Educ* **39**, 333–335 (1962).

49. Miles, A. J. & Wallace, B. A. Circular dichroism spectroscopy of membrane proteins. *Chem Soc Rev* **45**, 4859–4872 (2016).

50. Joardar, A., Pattnaik, G. P. & Chakraborty, H. Mechanism of Membrane Fusion: Interplay of Lipid and Peptide. *Journal of Membrane Biology* **255**, 211–224 (2022).

51. Clegg, R. M. Fluorescence resonance energy transfer. *Curr Opin Biotechnol* **6**, 103–110 (1995).

52. Hoekstra, D. & Düzgüneş, N. [2] Lipid mixing assays to determine fusion in liposome systems. *Methods Enzymol* **220**, 15–32 (1993).

53. Struck, D. K., Hoekstra, D. & Pagano, R. E. Use of Resonance Energy Transfer To Monitor Membrane Fusion. *Biochemistry* **20**, 4093–4099 (1981).

54. Bürck, J., Wadhwani, P., Fanghänel, S. & Ulrich, A. S. Oriented Circular Dichroism: A Method to Characterize Membrane-Active Peptides in Oriented Lipid Bilayers. *Acc Chem Res* **49**, 184–192 (2016).

55. Kelly, S. M., Jess, T. J. & Price, N. C. How to study proteins by circular dichroism. *Biochimica et Biophysica Acta (BBA) - Proteins and Proteomics* **1751**, 119–139 (2005).

56. Miles, A. J. & Wallace, B. A. CDtoolX, a downloadable software package for processing and analyses of circular dichroism spectroscopic data. *Protein Science* **27**, 1717–1722 (2018).

57. Micsonai, A. *et al.* Accurate secondary structure prediction and fold recognition for circular dichroism spectroscopy. *Proc Natl Acad Sci U S A* **112**, E3095–E3103 (2015).

58. Schorn, K. & Marsh, D. Extracting order parameters from powder EPR lineshapes for spin-labelled lipids in membranes. *Spectrochim Acta A Mol Biomol Spectrosc* **53**, 2235–2240 (1997).

59. Philip L. Yeagle. *The Structure of Biological Membranes*. (CRC Press, 2005).

60. Zimmerberg, J. & Chernomordik, L. V. Membrane fusion. *Adv Drug Deliv Rev* **38**, 197–205 (1999).

61. Nieva, J. L. & Agirre, A. Are fusion peptides a good model to study viral cell fusion? *Biochimica et Biophysica Acta (BBA) - Biomembranes* **1614**, 104–115 (2003).

62. Guillén, J., De Almeida, R. F. M., Prieto, M. & Villalaín, J. Structural and Dynamic Characterization of the Interaction of the Putative Fusion Peptide of the S2 SARS-CoV Virus Protein with Lipid Membranes. *Journal of Physical Chemistry B* **112**, 6997–7007 (2008).

63. Kay, J. G. & Fairn, G. D. Distribution, dynamics and functional roles of phosphatidylserine within the cell. *Cell Communication and Signaling* **17**, 1–8 (2019).

64. Miles, A. J. & Wallace, B. A. Circular dichroism spectroscopy of membrane proteins. *Chem Soc Rev* **45**, 4859–4872 (2016).

65. Greenfield, N. J. Using circular dichroism spectra to estimate protein secondary structure. *Nature Protocols 2007 1:6* **1**, 2876–2890 (2007).

66. Anso, I. *et al.* Molecular ruler mechanism and interfacial catalysis of the integral membrane acyltransferase PatA. *Sci Adv* **7**, (2021).

67. Basso, L. G. M., Mendes, L. F. S. & Costa-Filho, A. J. The two sides of a lipid-protein story. *Biophys Rev* **8**, 179–191 (2016).

68. Rozenfeld, J. H. K., Duarte, E. L., Oliveira, T. R. & Lamy, M. T. Structural insights on biologically relevant cationic membranes by ESR spectroscopy. *Biophys Rev* **9**, 633–647 (2017).

69. Magarkar, A. *et al.* Cholesterol level affects surface charge of lipid membranes in saline solution. *Scientific Reports 2014 4:1* **4**, 1–5 (2014).

70. Roy, M. T., Gallardo, M. & Estelrich, J. Influence of Size on Electrokinetic Behavior of Phosphatidylserine and Phosphatidylethanolamine Lipid Vesicles. *J Colloid Interface Sci* **206**, 512–517 (1998).

71. Her, C. *et al.* The Charge Properties of Phospholipid Nanodiscs. *Biophys J* **111**, 989–998 (2016).

72. Miatmoko, A., Asmoro, F. H., Azhari, A. A., Rosita, N. & Huang, C. S. The effect of 1,2-dioleoyl-3-trimethylammonium propane (DOTAP) Addition on the physical characteristics of β-ionone liposomes. *Scientific Reports 2023 13:1* **13**, 1–13 (2023).

73. Smith, M. C., Crist, R. M., Clogston, J. D. & McNeil, S. E. Zeta potential: a case study of cationic, anionic, and neutral liposomes. *Anal Bioanal Chem* **409**, 5779–5787 (2017).

74. Abhinav, Jurkiewicz, P., Hof, M., Allolio, C. & Sýkora, J. Modulation of Anionic Lipid Bilayers by Specific Interplay of Protons and Calcium Ions. *Biomolecules* **12**, 1894 (2022).

75. Klein, M. E. *et al.* Phosphatidylserine (PS) and phosphatidylglycerol (PG) nanodispersions as potential anti-inflammatory therapeutics: Comparison of in vitro activity and impact of pegylation. *Nanomedicine* **23**, 102096 (2020).

76. Zidovska, A. *et al.* The effect of salt and pH on block liposomes studied by cryogenic transmission electron microscopy. *Biochimica et Biophysica Acta (BBA) - Biomembranes* **1788**, 1869–1876 (2009).

77. Sabín, J., Prieto, G., Ruso, J. M., Hidalgo-Álvarez, R. & Sarmiento, F. Size and stability of liposomes: A possible role of hydration and osmotic forces. *The European Physical Journal E 2006 20:4* **20**, 401–408 (2006).

78. Yan, W. & Huang, L. The effects of salt on the physicochemical properties and immunogenicity of protein based vaccine formulated in cationic liposome. *Int J Pharm* **368**, 56–62 (2009).

79. Lai, A. L. & Freed, J. H. HIV gp41 Fusion Peptide Increases Membrane Ordering in a Cholesterol-Dependent Fashion. *Biophys J* **106**, 172–181 (2014).

80. Lai, A. L., Park, H., White, J. M. & Tamm, L. K. Fusion Peptide of Influenza Hemagglutinin Requires a Fixed Angle Boomerang Structure for Activity. *Journal of Biological Chemistry* **281**, 5760–5770 (2006).

81. Han, X., Steinhauer, D. A., Wharton, S. A. & Tamm, L. K. Interaction of mutant influenza virus hemagglutinin fusion peptides with lipid bilayers: Probing the role of hydrophobic residue size in the central region of the fusion peptide. *Biochemistry* **38**, 15052–15059 (1999).

82. Mahajan, M. & Bhattacharjya, S. NMR structures and localization of the potential fusion peptides and the pre-transmembrane region of SARS-CoV: Implications in membrane fusion. *Biochimica et Biophysica Acta (BBA) - Biomembranes* **1848**, 721–730 (2015).

83. Guillén, J., Kinnunen, P. K. J. & Villalaín, J. Membrane insertion of the three main membranotropic sequences from SARS-CoV S2 glycoprotein. *Biochimica et Biophysica Acta (BBA) - Biomembranes* **1778**, 2765–2774 (2008).

84. Hao, Y. *et al.* Functional Peptides from SARS-CoV-2 Binding with Cell Membrane: From Molecular Dynamics Simulations to Cell Demonstration. *Cells* **11**, 1738 (2022).

85. Henao, M. C. *et al.* Translocating Peptides of Biomedical Interest Obtained from the Spike (S) Glycoprotein of the SARS-CoV-2. *Membranes 2022, Vol. 12, Page 600* **12**, 600 (2022).

86. Birtles, D., Oh, A. E. & Lee, J. Exploring the pH dependence of the SARS-CoV-2 complete fusion domain and the role of its unique structural features. *Protein Science* **31**, e4390 (2022).

87. Shekunov, E. V. *et al.* Lipid specificity of action of SARS-CoV-2 fusion peptide fragments on model membranes. *bioRxiv* 2024.12.11.627892 (2024) doi:10.1101/2024.12.11.627892.

88. Koppisetti, R. K., Fulcher, Y. G. & Van Doren, S. R. Fusion Peptide of SARS-CoV-2 Spike Rearranges into a Wedge Inserted in Bilayered Micelles. *J Am Chem Soc* **143**, 13205–13211 (2021).

89. Qiu, C., Whittaker, G. R., Gellman, S. H., Daniel, S. & Abbott, N. L. Interactions of SARS-CoV-2 and MERS-CoV fusion peptides measured using single-molecule force methods. *Biophys J* **122**, 646–660 (2023).

90. Birtles, D. & Lee, J. Identifying Distinct Structural Features of the SARS-CoV-2 Spike Protein Fusion Domain Essential for Membrane Interaction. *Biochemistry* **60**, 2978–2986 (2021).

91. Sumarokova, M. *et al.* SARS-CoV-2 FP1 Destabilizes Lipid Membranes and Facilitates Pore Formation. *International Journal of Molecular Sciences 2025, Vol. 26, Page 686* **26**, 686 (2025).

92. Van Doren, S. R., Scott, B. S. & Koppisetti, R. K. SARS-CoV-2 fusion peptide sculpting of a membrane with insertion of charged and polar groups. *Structure* **31**, 1184-1199.e3 (2023).

93. Villalaín, J. SARS-CoV-2 Protein S Fusion Peptide Is Capable of Wrapping Negatively-Charged Phospholipids. *Membranes (Basel)* **13**, 344 (2023).

94. Birtles, D., Guiyab, L., Abbas, W. & Lee, J. Positive residues of the SARS-CoV-2 fusion domain are key contributors to the initiation of membrane fusion. *Journal of Biological Chemistry* **300**, 107564 (2024).

95. Schaefer, S. L., Jung, H. & Hummer, G. Binding of SARS-CoV-2 Fusion Peptide to Host Endosome and Plasma Membrane. *Journal of Physical Chemistry B* **125**, 7732–7741 (2021).

96. Shen, H., Wu, Z. & Chen, L. Different Binding Modes of SARS-CoV-1 and SARS-CoV-2 Fusion Peptides to Cell Membranes: The Influence of Peptide Helix Length. *Journal of Physical Chemistry B* (2022) doi:10.1021/ACS.JPCB.2C01295/SUPPL_FILE/JP2C01295_SI_001.PDF.

97. Guillén, J., Pérez-Berná, A. J., Moreno, M. R. & Villalaín, J. A second SARS-CoV S2 glycoprotein internal membrane-active peptide. Biophysical characterization and membrane interaction. *Biochemistry* **47**, 8214–8224 (2008).

98. Van Meer, G., Voelker, D. R. & Feigenson, G. W. Membrane lipids: where they are and how they behave. *Nature Reviews Molecular Cell Biology 2008 9:2* **9**, 112–124 (2008).

99. Lai, A. L., Tamm, L. K., Ellena, J. F. & Cafiso, D. S. Synaptotagmin 1 modulates lipid acyl chain order in lipid bilayers by demixing phosphatidylserine. *Journal of Biological Chemistry* **286**, 25291–25300 (2011).

100. Patel, A., Mohl, B. P. & Roy, P. Entry of bluetongue virus capsid requires the late endosome-specific lipid lysobisphosphatidic acid. *Journal of Biological Chemistry* **291**, 12408–12419 (2016).

101. Matos, P. M. *et al.* Anionic lipids are required for vesicular stomatitis virus G protein-mediated single particle fusion with supported lipid bilayers. *Journal of Biological Chemistry* **288**, 12416–12425 (2013).

102. Zaitseva, E. *et al.* Fusion Stage of HIV-1 Entry Depends on Virus-Induced Cell Surface Exposure of Phosphatidylserine. *Cell Host Microbe* **22**, 99-110.e7 (2017).

103. Luévano-Martínez, L. A. & Kowaltowski, A. J. Phosphatidylglycerol-derived phospholipids have a universal, domain-crossing role in stress responses. *Arch Biochem Biophys* **585**, 90–97 (2015).

104. Veldhuizen, R., Nag, K., Orgeig, S. & Possmayer, F. The role of lipids in pulmonary surfactant. *Biochimica et Biophysica Acta (BBA) - Molecular Basis of Disease* **1408**, 90–108 (1998).

105. Poccia, D. & Larijani, B. Phosphatidylinositol metabolism and membrane fusion. *Biochemical Journal* **418**, 233–246 (2009).

106. Birtles, D., Abbas, W. & Lee, J. Bis(Monoacylglycero)Phosphate Promotes Membrane Fusion Facilitated by the SARS-CoV-2 Fusion Domain. *Journal of Physical Chemistry B* **128**, 2675–2683 (2024).

107. Baier, C. J. & Barrantes, F. J. Role of cholesterol-recognition motifs in the infectivity of SARS-CoV-2 variants. *Colloids Surf B Biointerfaces* **222**, 113090 (2023).

108. Zhang, Q. *et al.* Probing SARS-CoV-2 membrane binding peptide via single-molecule AFM-based force spectroscopy. *Nature Communications 2024 16:1* **16**, 1–14 (2025).

109. Zhou, Y., Frey, T. K. & Yang, J. J. Viral calciomics: Interplays between Ca2+ and virus. *Cell Calcium* **46**, 1–17 (2009).

110. Qu, Y., Sun, Y., Yang, Z. & Ding, C. Calcium Ions Signaling: Targets for Attack and Utilization by Viruses. *Front Microbiol* **13**, 889374 (2022).

111. Berlansky, S. *et al.* Calcium Signals during SARS-CoV-2 Infection: Assessing the Potential of Emerging Therapies. *Cells 2022, Vol. 11, Page 253* **11**, 253 (2022).

112. Tang, T., Bidon, M., Jaimes, J. A., Whittaker, G. R. & Daniel, S. Coronavirus membrane fusion mechanism offers a potential target for antiviral development. *Antiviral Res* **178**, 104792 (2020).

113. Lai, A. L. & Freed, J. H. Negatively charged residues in the membrane ordering activity of SARS-CoV-1 and -2 fusion peptides. *Biophys J* **121**, 207–227 (2022).

8. ANNEXES

ANNEX 1

Fusion peptides characteristics (extended). The name, position within the Spike protein, sequence, length, organism, theorical isoelectric point, charge at pH 5.0 and 7.4, molecular weight, extinction coefficient at 280 nm, grand average of hydropathicity (GRAVY), instability index, ΔG of insertion from water to POPC interface, ΔG of insertion from water to octanol are specified. Positively charged amino acid residues are colored in red, negatively charged ones in blue, aromatic residues in green, and the lysine tag in purple. In addition to SARS-CoV and SARS-CoV-2 fusion peptides, the characteristics of the HIV fusion peptide (HIVFP) and the H7 tag are also shown. Most of the parameters were calculated using Expasy Protparam tool (available at https://web.expasy.org/protparam/) and Prot pi Protein tool (available at https://www.protpi.ch/Calculator/ProteinTool). ΔG of insertion were determined according to previous studies[1]. CRAC domain residues are highlighted in yellow. aa: amino acid residue; Ac-: acetylated; -Am: amidated; N/A: not applicable.

Peptide	Position (N° aa.)	Sequence	Length (aa.)	Origin	Theorical pI	Charge (pH 5,0)	Charge (pH 7,4)	Molecular Weight (g/mol)	Ext. Coefficient (280 nm)	GRAVY	Instability index	Aliphatic index	ΔG from water to POPC interface (kcal/mol)	ΔG from water to Octanol (kcal/mol)
1FP1	770-788	Ac-MWKTPTLKYFGGFNFSQIL-Am	19	SARS-CoV	9.70	+2.04	+1.26	2278.70	6990	0.042	23.86	61.58	-3.98	-1.60
1FP1H7	770-788	Ac-MWKTPTLKYFGGFNFSQILGGGKKKK-Am	26	SARS-CoV	10.40	+6.01	+5.25	2962.55	6990	-0.615	26.36	45.00	0.01	13.05
crac1FP1H7	767-788	Ac-VKQMWKTPTLKYFGGFNFSQILGGGKKKK-Am	29	SARS-CoV	10.48	+7.02	+6.50	3317.99	6990	-0.662	31.84	50.34	1.65	16.16
2FP1H7	788-806	Ac-IYKTPPIKDFGGFNFSQILGGGKKKK-Am	26	SARS-CoV-2	10.13	+5.13	+4.52	2869.40	1490	-0.623	30.87	60.00	3.57	18.35
crac2FP1H7	785-806	Ac-VKQIYKTPPIKDFGGFNFSQILGGGKKKK-Am	29	SARS-CoV-2	10.22	+6.12	+5.50	3224.84	1490	-0.669	35.88	63.79	5.21	21.46
FP2H7	798-815 / 816-833	Ac-SFIEDLLFNKVTLADAGFGGGKKKK-Am	25	SARS-CoV / SARS-CoV-2	9.40	+2.44	+1.21	2684.13	N/A	-0.180	40.64	82.00	5.19	21.61
IFPH7	873-888 / 891-906	Ac-GAALQIPFAMQMAYRFGGGKKKK-Am	23	SARS-CoV / SARS-CoV-2	10.58	+5.02	+4.54	2499.03	1490	-0.291	28.94	51.30	2.57	13.45
HIVFPH7	512-534	Ac-AVGIGALFLGFLGAAGSTMGAASGGGKKKKK-Am	31	HIV	10.60	+5.02	+4.59	2851.40	N/A	0.419	1.21	79.03	2.05	19.10
H7-C	N/A	Ac-GCGKKKK-Am	7	synthetic	10.04	+4.02	+3.43	747.95	N/A	-1,986	-3.56	0.00	3.74	13.48
H7	N/A	Ac-GGGKKKK-Am	7	synthetic	10.48	+4.20	+3.54	701.87	N/A	-2.400	31.70	0.00	3.99	14.65

[1]Wimley, W.C. and White, S.H. (1996). Experimentally determined hydrophobicity scale for proteins at membrane interfaces. *Nature Structural & Molecular Biology*, 3(10), pp.842–848. doi: https://doi.org/10.1038/nsb1096-842.

ANNEX 2

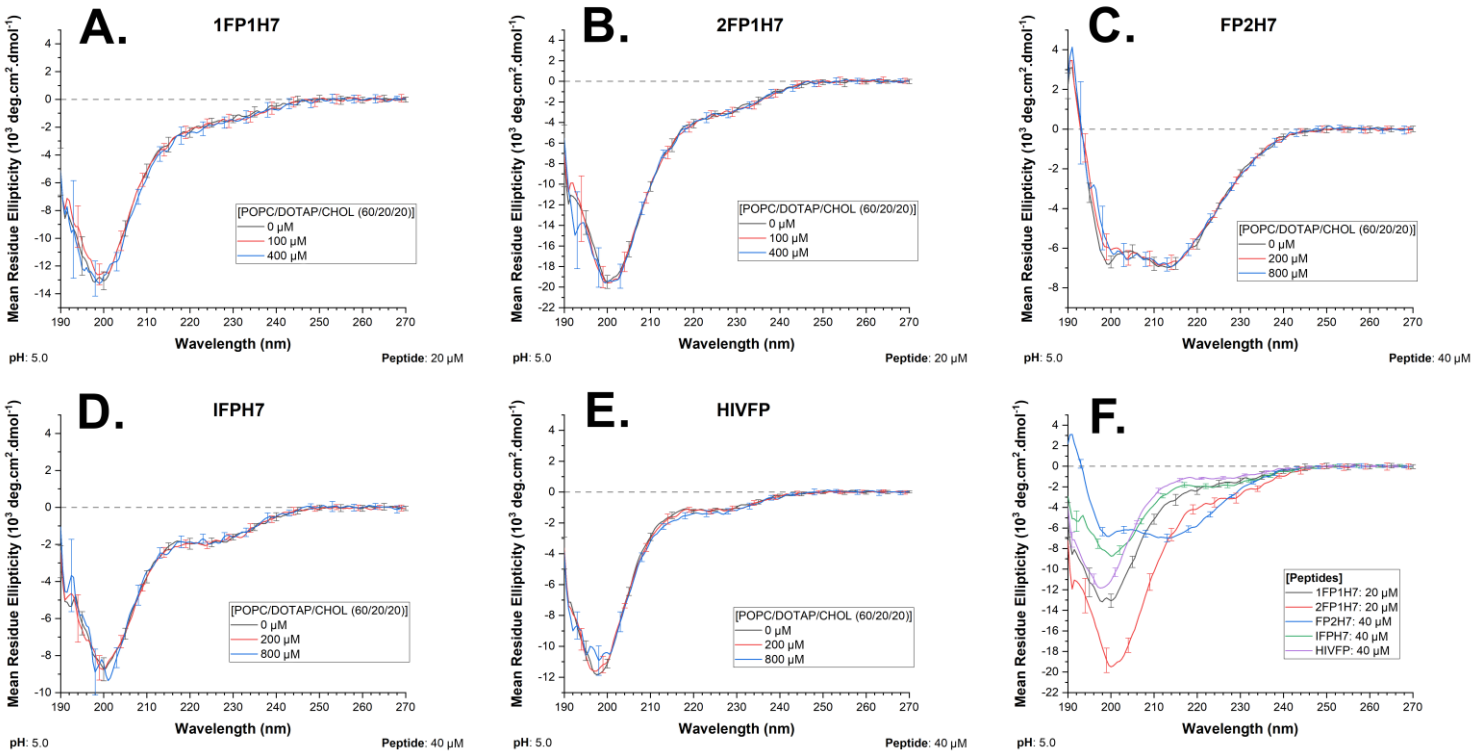

CD spectra of fusion peptides in solution and in the presence of SUVs containing DOTAP at pH 5.0. Spectra of peptides 1FP1H7 (**A**), 2FP1H7 (**B**), FP2H7 (**C**), IFPH7 (**D**), and HIVFP (**E**) in POPC/DOTAP/Chol (60/20/20 mol%) SUVs.at concentrations of 100 µM and 400 µM, for 1FP1H7 and 2F1H7, and 200 µM and 800 µM, for FP2H7, IFPH7, and HIVFP. Spectra of peptides in solution without SUVs (**F**) are shown for comparison. Spectra were recorded at 37 °C. Buffer: 10 mM MES 150 mM NaF, pH 5.0.

ANNEX 3

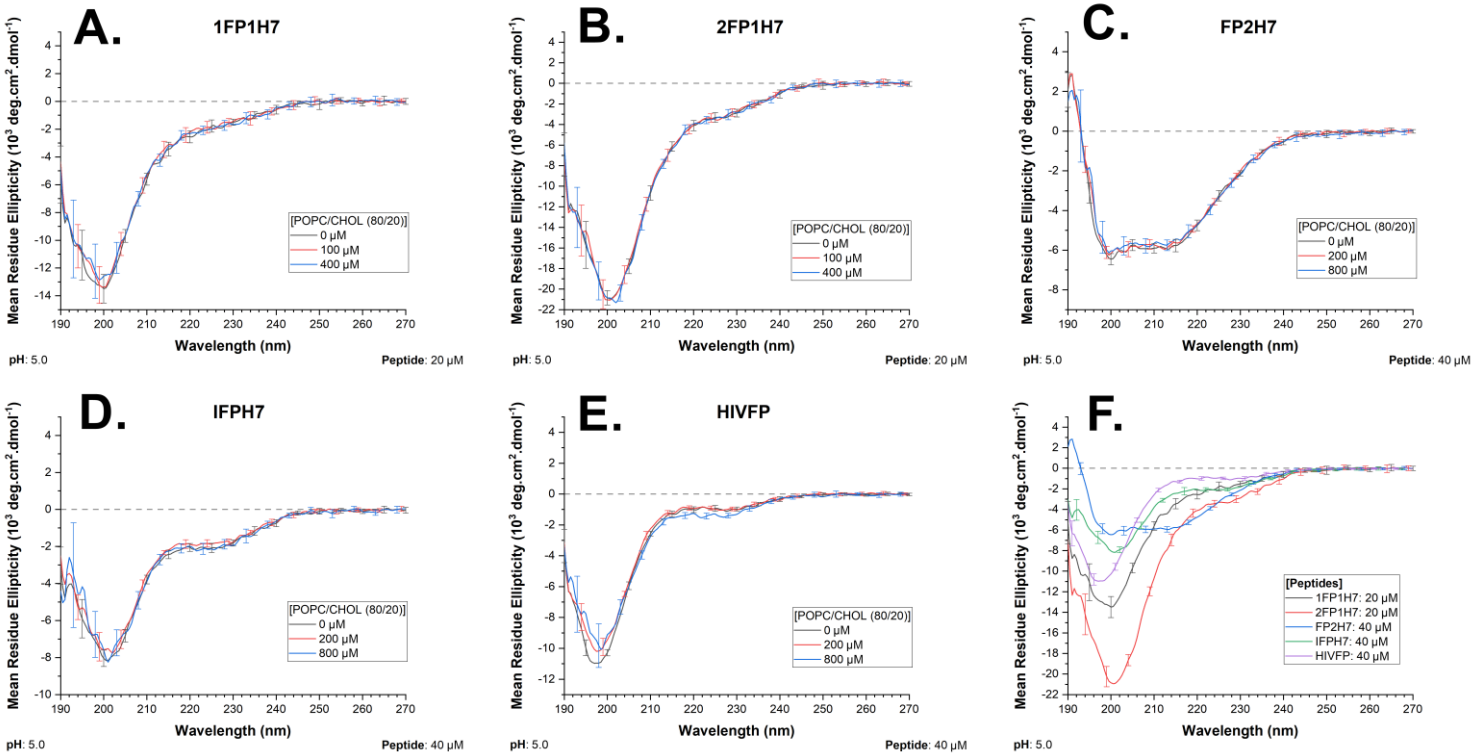

CD spectra of fusion peptides in solution and in the presence of SUVs containing POPC at pH 5.0. Spectra of peptides 1FP1H7 (**A**), 2FP1H7 (**B**), FP2H7 (**C**), IFPH7 (**D**), and HIVFP (**E**) in POPC /Chol (80/20 mol%) SUVs.at concentrations of 100 µM and 400 µM, for 1FP1H7 and 2F1H7, and 200 µM and 800 µM, for FP2H7, IFPH7, and HIVFP. Spectra of peptides in solution without SUVs (**F**) are shown for comparison. Spectra were recorded at 37 °C. Buffer: 10 mM MES 150 mM NaF, pH 5.0.

ANNEX 4

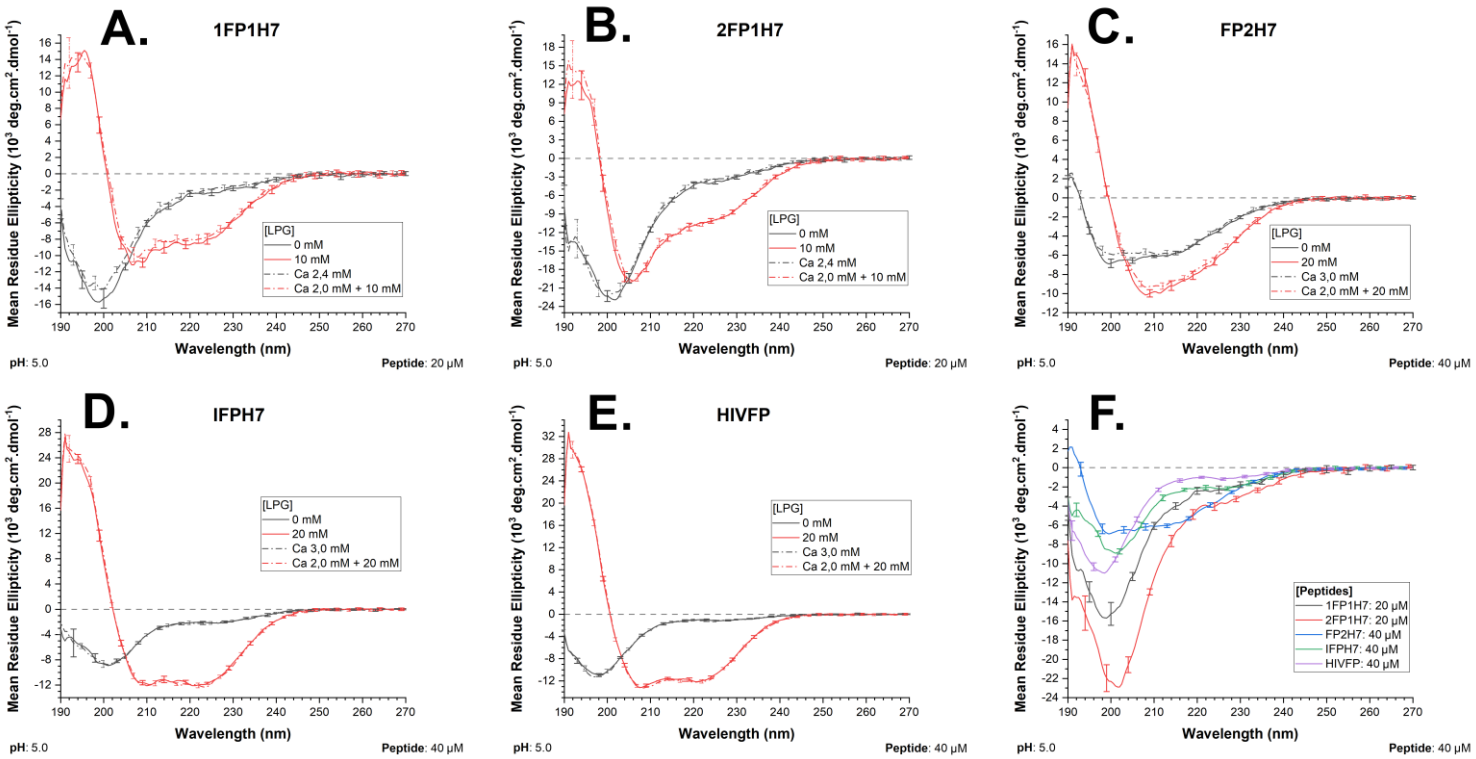

CD spectra of fusion peptides in solution and in the presence of LPG micelles at pH 5.0. Spectra of peptides 1FP1H7 (**A**), 2FP1H7 (**B**), FP2H7 (**C**), IFPH7 (**D**) and HIVFP (**E**) in LPG micelles at concentrations of 10 mM for 1FP1H7 and 2F1H7, and 20 mM for FP2H7, IFPH7, and HIVFP. Additionally, measurements were performed with the addition of $CaCl_2$ to evaluate the effect of calcium in each case. Spectra of peptides in solution without micelles (**F**) are shown for comparison. Spectra were recorded at 37 °C. Buffer: 10 mM MES 150 mM NaF, pH 5.0.

ANNEX 5

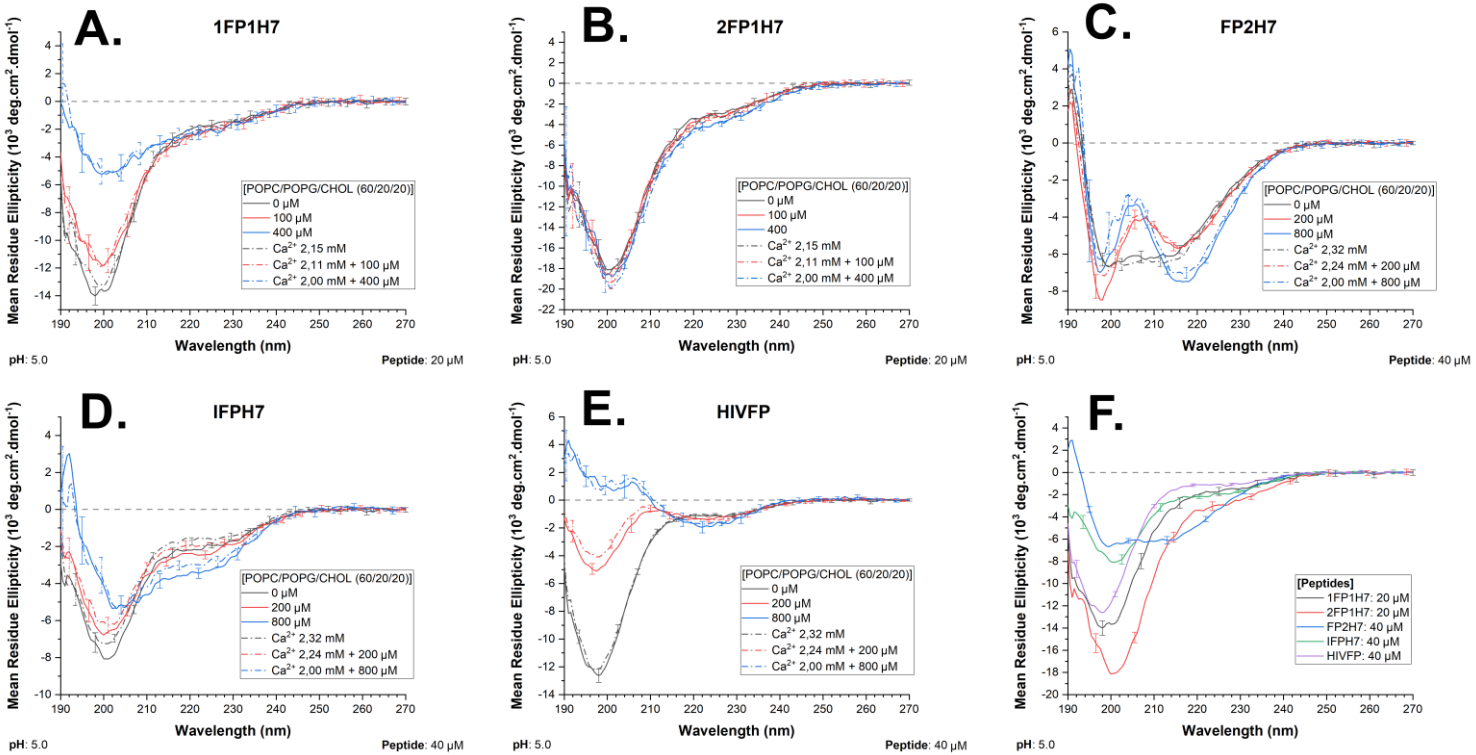

CD spectra of fusion peptides in solution and in the presence of SUVs containing POPG at pH 5.0. Spectra of peptides 1FP1H7 (**A**), 2FP1H7 (**B**), FP2H7 (**C**), IFPH7 (**D**) and HIVFP (**E**) in POPC/POPG/Chol (60/20/20 mol%) SUVs.at concentrations of 100 µM and 400 µM, for 1FP1H7 and 2F1H7, and 200 µM and 800 µM, for FP2H7, IFPH7, and HIVFP. Additionally, measurements were performed with the addition of $CaCl_2$ to evaluate the effect of calcium in each case. Spectra of peptides in solution without SUVs (**F**) are shown for comparison. Spectra were recorded at 37 °C. Buffer: 10 mM MES 150 mM NaF, pH 5.0.

ANNEX 6

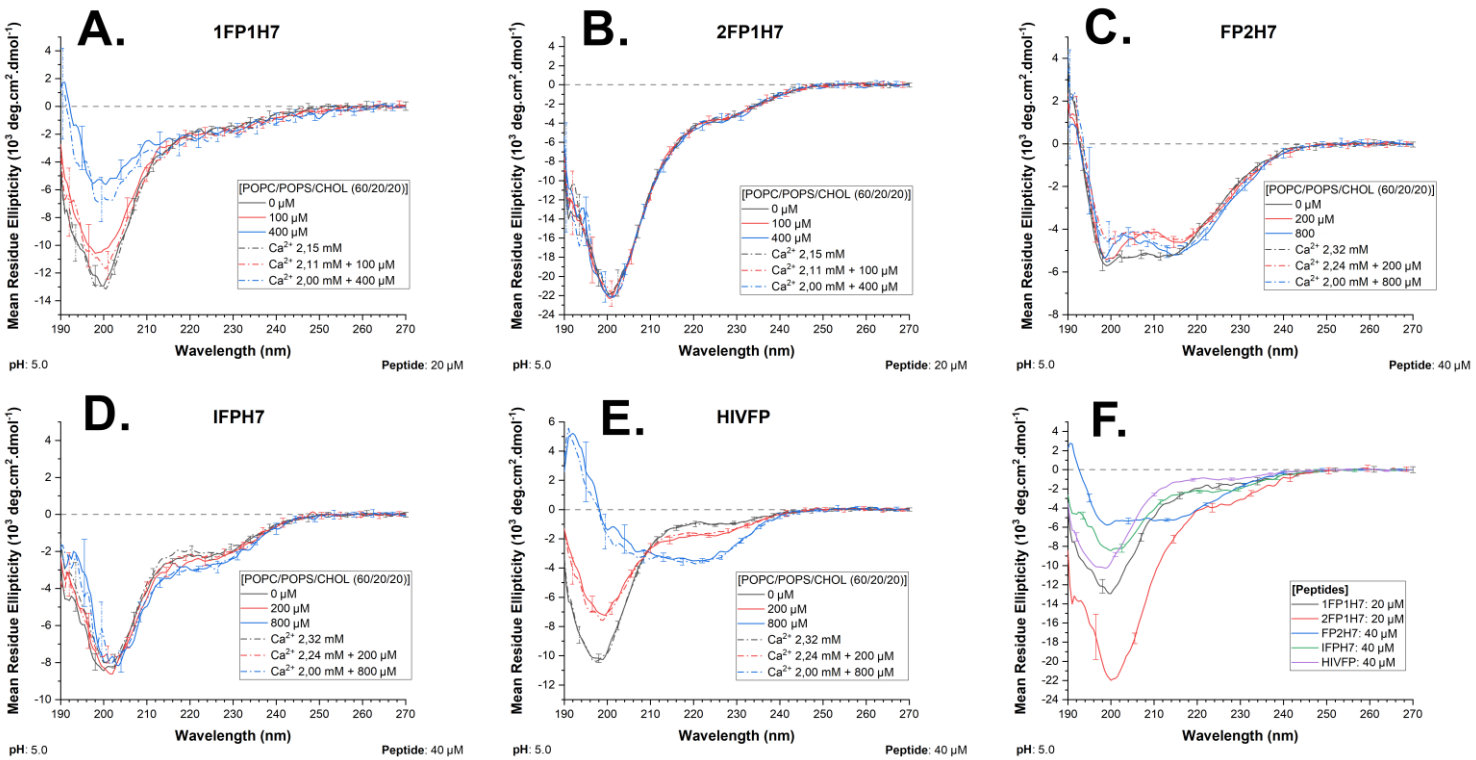

CD spectra of fusion peptides in solution and in the presence of SUVs containing POPS at pH 5.0. Spectra of peptides 1FP1H7 (**A**), 2FP1H7 (**B**), FP2H7 (**C**), IFPH7 (**D**) and HIVFP (**E**) in POPC/POPS/Chol (60/20/20 mol%) SUVs.at concentrations of 100 µM and 400 µM, for 1FP1H7 and 2F1H7, and 200 µM and 800 µM, for FP2H7, IFPH7, and HIVFP. Additionally, measurements were performed with the addition of $CaCl_2$ to evaluate the effect of calcium in each case. Spectra of peptides in solution without SUVs (**F**) are shown for comparison. Spectra were recorded at 37 °C. Buffer: 10 mM MES, 150 mM NaF, pH 5.0.

ANNEX 7

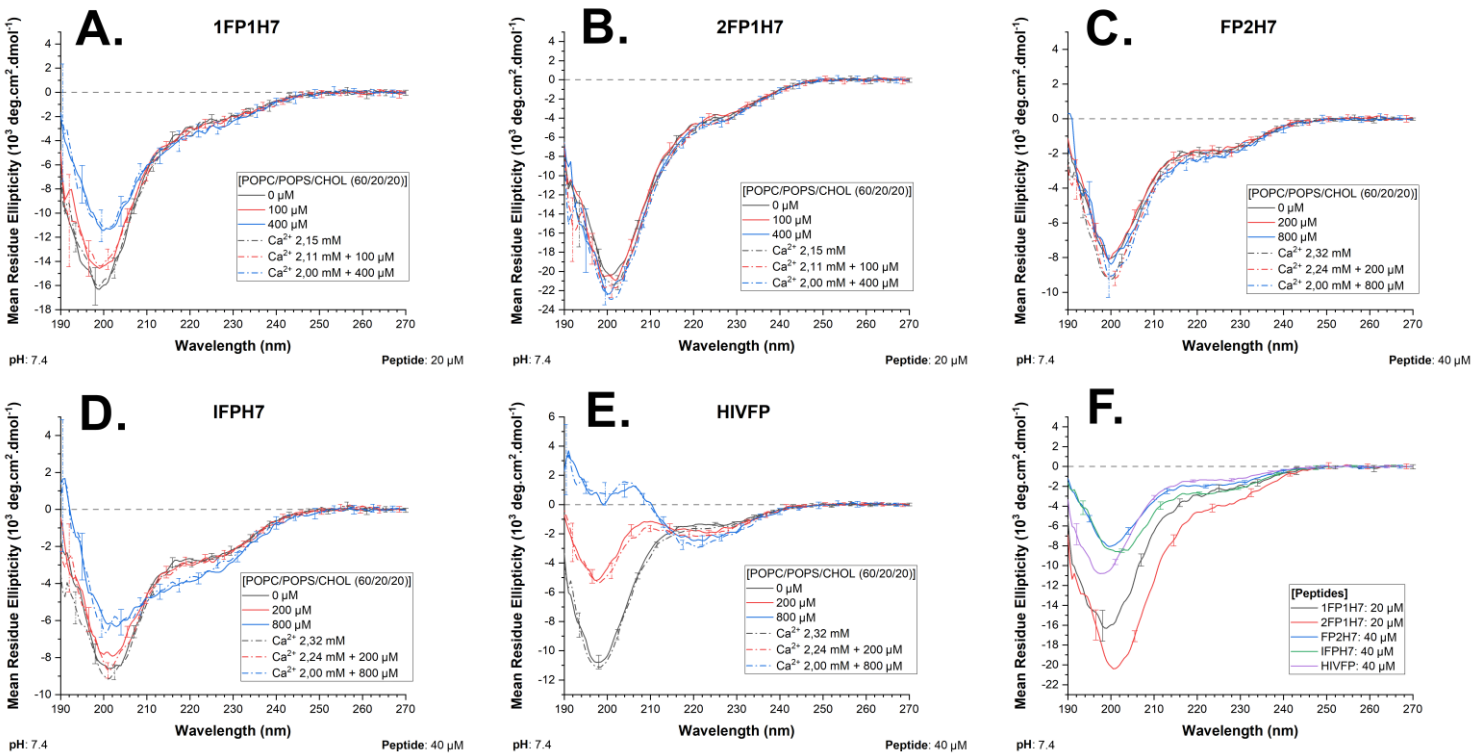

CD spectra of fusion peptides in solution and in the presence of SUVs containing POPS at pH 7.4. Spectra of peptides 1FP1H7 (**A**), 2FP1H7 (**B**), FP2H7 (**C**), IFPH7 (**D**) and HIVFP (**E**) in POPC/POPS/Chol (60/20/20 mol%) SUVs.at concentrations of 100 µM and 400 µM, for 1FP1H7 and 2F1H7, and 200 µM and 800 µM, for FP2H7, IFPH7, and HIVFP. Additionally, measurements were performed with the addition of $CaCl_2$ to evaluate the effect of calcium in each case. Spectra of peptides in solution without SUVs (**F**) are shown for comparison. Spectra were recorded at 37 °C. Buffer: 10 mM Tris 150 mM NaF, pH 7.4.

ANNEX 8

Deconvolution of CD spectra for fusion peptides in SUVs of varying phospholipid compositions. The table includes information on the peptides, presence or absence of calcium, membrane composition and concentration, pH, percentage of secondary structures, and associated errors (Root mean square deviation or RMSD, and Normalized root mean square deviation or NRMSD).

Peptide	Calcium	Membrane	Mol%	Membrane concentration (μM)	pH	α-Helix (%)	β-Strand (%)		Turn (%)	Others (%)	All Strands (%)	All (%)	RMSD	NRMSD
							Antiparallel	Parallel						
1FP1H7	No	POPC/DOTAP/CHOL	60/20/20	0	5.0	1.6	31.1	0.0	17.0	50.3	31.1	100	0.0778	0.01522
1FP1H7	No	POPC/DOTAP/CHOL	60/20/20	100	5.0	1.9	29.9	0.0	16.7	51.5	29.9	100	0.0758	0.01814
1FP1H7	No	POPC/DOTAP/CHOL	60/20/20	400	5	2.8	29.1	0.0	16.5	51.6	29.1	100	0.0825	0.014
2FP1H7	No	POPC/DOTAP/CHOL	60/20/20	0	5.0	9.9	19.4	3.7	15.6	51.4	23.1	100	0.2033	0.03707
2FP1H7	No	POPC/DOTAP/CHOL	60/20/20	100	5.0	8.8	20.7	4.5	15.4	50.5	25.2	99.9	0.1685	0.03252
2FP1H7	No	POPC/DOTAP/CHOL	60/20/20	400	5.0	8.8	22.0	3.9	15.4	49.9	25.9	100	0.21	0.032
FP2H7	No	POPC/DOTAP/CHOL	60/20/20	0	5.0	5.8	31.7	7.7	12.1	42.8	39.4	100.1	0.0779	0.01833
FP2H7	No	POPC/DOTAP/CHOL	60/20/20	200	5.0	5.5	32.2	5.7	12.3	44.3	37.9	100	0.0621	0.01124
FP2H7	No	POPC/DOTAP/CHOL	60/20/20	800	5.0	7.4	29.2	6.1	11.7	45.6	35.3	100	0.0929	0.01767
IFPH7	No	POPC/DOTAP/CHOL	60/20/20	0	5.0	1.1	31.6	0.0	16.9	50.4	31.6	100	0.0706	0.02056
IFPH7	No	POPC/DOTAP/CHOL	60/20/20	200	5.0	1.2	31.2	0.0	16.8	50.8	31.2	100	0.0734	0.01815
IFPH7	No	POPC/DOTAP/CHOL	60/20/20	800	5.0	0.2	31.7	0.0	16.3	51.7	31.7	99.9	0.1136	0.0239
HIVFP	No	POPC/DOTAP/CHOL	60/20/20	0	5.0	0.0	34.6	0.0	17.1	48.2	34.6	99.9	0.0821	0.01843
HIVFP	No	POPC/DOTAP/CHOL	60/20/20	200	5.0	0.0	34.4	0.0	17.0	48.6	34.4	100	0.0873	0.01622
HIVFP	No	POPC/DOTAP/CHOL	60/20/20	800	5.0	0.0	33.6	0.0	16.5	50.0	33.6	100.1	0.1185	0.02131
1FP1H7	No	POPC/CHOL	80/20	0	5.0	3.6	29.3	0.0	16.6	50.5	29.3	100	0.089	0.02685
1FP1H7	No	POPC/CHOL	80/20	100	5.0	3.0	28.0	0.0	16.7	52.3	28.0	100	0.1031	0.01748
1FP1H7	No	POPC/CHOL	80/20	400	5.0	3.6	28.2	0.0	16.4	51.8	28.2	100	0.1061	0.01821
2FP1H7	No	POPC/CHOL	80/20	0	5.0	8.8	20.8	3.1	15.5	51.8	23.9	100	0.207	0.03457
2FP1H7	No	POPC/CHOL	80/20	100	5.0	8.7	20.3	3.4	15.6	52.0	23.7	100	0.226	0.03645
2FP1H7	No	POPC/CHOL	80/20	400	5.0	8.8	21.1	2.6	15.4	52.1	23.7	100	0.2188	0.03324

FP2H7	No	POPC/CHOL	80/20	0	5.0	3.7	35.2	3.6	12.5	45.0	38.8	100	0.0731	0.01962
FP2H7	No	POPC/CHOL	80/20	200	5.0	5.3	33.8	3.7	12.5	44.7	37.5	100	0.059	0.01519
FP2H7	No	POPC/CHOL	80/20	800	5.0	5.9	32.6	3.9	12.9	44.7	36.5	100	0.082	0.02322
IFPH7	No	POPC/CHOL	80/20	0	5.0	1.7	30.6	0.0	16.6	51.2	30.6	100.1	0.0605	0.02164
IFPH7	No	POPC/CHOL	80/20	200	5.0	1.4	31.2	0.0	16.3	51.2	31.2	100.1	0.0561	0.01946
IFPH7	No	POPC/CHOL	80/20	800	5.0	2.7	30.9	0.0	17.1	49.3	30.9	100	0.0879	0.03034
HIVFP	No	POPC/CHOL	80/20	0	5.0	0.0	34.5	0.0	16.9	48.5	34.5	99.9	0.0763	0.01848
HIVFP	No	POPC/CHOL	80/20	200	5.0	0.0	34.5	0.0	16.8	48.7	34.5	100	0.0845	0.01972
HIVFP	No	POPC/CHOL	80/20	800	5.0	0.0	34.1	0.0	16.8	49.2	34.1	100.1	0.0732	0.01999
1FP1H7	No	POPC/POPG/CHOL	60/20/20	0	5.0	1.6	29.5	0.0	17.0	51.9	29.5	100	0.1026	0.01627
1FP1H7	No	POPC/POPG/CHOL	60/20/20	100	5.0	2.6	29.4	0.0	16.2	51.8	29.4	100	0.0685	0.0125
1FP1H7	No	POPC/POPG/CHOL	60/20/20	400	5.0	0.6	34.1	0.0	14.9	50.5	34.1	100.1	0.0557	0.02869
1FP1H7	Yes	POPC/POPG/CHOL	60/20/20	0	5.0	2.0	29.2	0.0	16.6	52.2	29.2	100	0.1065	0.01844
1FP1H7	Yes	POPC/POPG/CHOL	60/20/20	100	5.0	5.8	27.9	0.0	16.2	50.1	27.9	100	0.1087	0.01972
1FP1H7	Yes	POPC/POPG/CHOL	60/20/20	400	5.0	0.5	33.0	0.0	14.3	52.3	33.0	100.1	0.0752	0.03123
2FP1H7	No	POPC/POPG/CHOL	60/20/20	0	5.0	9.7	20.9	2.7	15.4	51.2	23.6	99.9	0.1675	0.3285
2FP1H7	No	POPC/POPG/CHOL	60/20/20	100	5.0	10.1	20.2	2.1	15.5	52.1	22.3	100	0.1723	0.03203
2FP1H7	No	POPC/POPG/CHOL	60/20/20	400	5.0	10.4	18.8	3.9	15.2	51.6	22.7	99.9	0.1842	0.03103
2FP1H7	Yes	POPC/POPG/CHOL	60/20/20	0	5.0	10.3	20.2	2.4	15.4	51.7	22.6	100	0.2	0.03519
2FP1H7	Yes	POPC/POPG/CHOL	60/20/20	100	5.0	9.7	19.9	4.3	15.5	50.7	24.2	100.1	0.1801	0.0333
2FP1H7	Yes	POPC/POPG/CHOL	60/20/20	400	5.0	9.0	21.7	4.8	14.6	49.9	26.5	100	0.1581	0.02809
FP2H7	No	POPC/POPG/CHOL	60/20/20	0	5.0	5.6	34.0	4.2	12.6	43.5	38.2	99.9	0.0716	0.01799
FP2H7	No	POPC/POPG/CHOL	60/20/20	200	5.0	0.0	40.2	2.3	14.2	43.3	42.5	100	0.105	0.02855
FP2H7	No	POPC/POPG/CHOL	60/20/20	800	5.0	0.0	39.1	8.7	12.1	40.1	47.8	100	0.1655	0.03935
FP2H7	Yes	POPC/POPG/CHOL	60/20/20	0	5.0	3.8	34.3	3.8	12.7	45.4	38.1	100	0.083	0.01895
FP2H7	Yes	POPC/POPG/CHOL	60/20/20	200	5.0	0.3	40.7	1.2	13.9	43.9	41.9	100	0.1043	0.03021
FP2H7	Yes	POPC/POPG/CHOL	60/20/20	800	5.0	0.0	39.3	7.5	12.1	41.1	46.8	100	0.192	0.04934
IFPH7	No	POPC/POPG/CHOL	60/20/20	0	5.0	0.9	31.9	0.0	16.4	50.7	31.9	99.9	0.0489	0.02064
IFPH7	No	POPC/POPG/CHOL	60/20/20	200	5.0	0.0	32.5	0.0	15.7	51.8	32.5	100	0.05	0.02367

IFPH7	No	POPC/POPG/CHOL	60/20/20	800	5.0	6.5	31.9	0.0	13.9	47.7	31.9	100	0.1153	0.03273
IFPH7	Yes	POPC/POPG/CHOL	60/20/20	0	5.0	0.2	33.2	0.0	16.2	50.4	33.2	100	0.0615	0.0187
IFPH7	Yes	POPC/POPG/CHOL	60/20/20	200	5.0	0.0	32.6	0.0	15.4	52.0	32.6	100	0.0526	0.02301
IFPH7	Yes	POPC/POPG/CHOL	60/20/20	800	5.0	4.0	31.9	0.0	14.6	49.4	31.9	99.9	0.0717	0.03113
HIVFPH7	No	POPC/POPG/CHOL	60/20/20	0	5.0	0.0	34.0	0.0	17.2	48.8	34.0	100	0.0876	0.01701
HIVFPH7	No	POPC/POPG/CHOL	60/20/20	200	5.0	0.0	37.2	0.0	15.4	47.4	37.2	100	0.0798	0.05001
HIVFPH7	No	POPC/POPG/CHOL	60/20/20	800	5.0	0.0	41.1	0.0	13.7	45.2	41.1	100	0.1061	0.0542
HIVFPH7	Yes	POPC/POPG/CHOL	60/20/20	0	5.0	0.0	33.8	0.0	17.2	49.0	33.8	100	0.0739	0.01582
HIVFPH7	Yes	POPC/POPG/CHOL	60/20/20	200	5.0	0.0	38.1	0.0	15.1	46.8	38.1	100	0.0776	0.06062
HIVFPH7	Yes	POPC/POPG/CHOL	60/20/20	800	5.0	0.0	41.2	0.0	13.7	45.1	41.2	100	0.1009	0.06278
1FP1H7	No	POPC/POPS/CHOL	60/20/20	0	5.0	1.6	29.8	0.0	16.3	52.3	29.8	100	0.0898	0.01745
1FP1H7	No	POPC/POPS/CHOL	60/20/20	100	5.0	1.0	29.9	0.0	15.8	53.3	29.9	100	0.0687	0.01759
1FP1H7	No	POPC/POPS/CHOL	60/20/20	400	5.0	0.0	33.4	0.0	14.8	51.8	33.4	100	0.1015	0.04062
1FP1H7	Yes	POPC/POPS/CHOL	60/20/20	0	5.0	1.7	30.3	0.0	17.0	51.0	30.3	100	0.0842	0.01609
1FP1H7	Yes	POPC/POPS/CHOL	60/20/20	100	5.0	2.0	28.7	0.0	16.4	52.9	28.7	100	0.1027	0.02198
1FP1H7	Yes	POPC/POPS/CHOL	60/20/20	400	5.0	2.3	29.1	1.5	14.4	52.7	30.6	100	0.1271	0.04579
2FP1H7	No	POPC/POPS/CHOL	60/20/20	0	5.0	8.4	21.8	3.3	15.2	51.3	25.1	100	0.2579	0.04144
2FP1H7	No	POPC/POPS/CHOL	60/20/20	100	5.0	8.4	22.2	1.6	15.4	52.3	23.8	99.9	0.2339	0.0377
2FP1H7	No	POPC/POPS/CHOL	60/20/20	400	5.0	7.9	22.9	3.6	14.6	51.0	26.5	100	0.214	0.03234
2FP1H7	Yes	POPC/POPS/CHOL	60/20/20	0	5.0	8.6	21.3	2.8	15.0	52.3	24.1	100	0.225	0.03731
2FP1H7	Yes	POPC/POPS/CHOL	60/20/20	100	5.0	8.4	21.9	2.7	15.0	52.0	24.6	100	0.2163	0.03454
2FP1H7	Yes	POPC/POPS/CHOL	60/20/20	400	5.0	8.9	22.0	2.4	15.0	51.7	24.4	100	0.3256	0.04182
FP2H7	No	POPC/POPS/CHOL	60/20/20	0	5.0	4.4	35.5	1.5	13.0	45.6	37.0	100	0.0568	0.01623
FP2H7	No	POPC/POPS/CHOL	60/20/20	200	5.0	1.1	36.2	0.0	13.7	49.0	36.2	100	0.0487	0.02429
FP2H7	No	POPC/POPS/CHOL	60/20/20	800	5.0	3.9	34.3	0.9	14.1	46.8	35.2	100	0.0635	0.02819
FP2H7	Yes	POPC/POPS/CHOL	60/20/20	0	5.0	4.9	35.3	1.5	12.9	45.4	36.8	100	0.0691	0.01548
FP2H7	Yes	POPC/POPS/CHOL	60/20/20	200	5.0	1.6	36.8	0.0	13.4	48.2	36.8	100	0.0401	0.02281
FP2H7	Yes	POPC/POPS/CHOL	60/20/20	800	5.0	2.8	36.0	1.4	12.9	46.9	37.4	100	0.0739	0.0253
IFPH7	No	POPC/POPS/CHOL	60/20/20	0	5.0	1.8	30.6	0.0	16.8	50.8	30.6	100	0.0607	0.01866

IFPH7	No	POPC/POPS/CHOL	60/20/20	200	5.0	3.3	30.1	0.0	16.5	50.1	30.1	100	0.0558	0.01882
IFPH7	No	POPC/POPS/CHOL	60/20/20	800	5.0	5.7	24.1	0.0	17.2	53.1	24.1	100.1	0.0778	0.02695
IFPH7	Yes	POPC/POPS/CHOL	60/20/20	0	5.0	1.0	31.1	0.0	16.6	51.3	31.1	100	0.0541	0.01768
IFPH7	Yes	POPC/POPS/CHOL	60/20/20	200	5.0	1.7	30.6	0.0	16.8	50.8	30.6	99.9	0.0475	0.01982
IFPH7	Yes	POPC/POPS/CHOL	60/20/20	800	5.0	5.0	29.2	0.0	16.3	49.5	29.2	100	0.0694	0.01948
HIVFPH7	No	POPC/POPS/CHOL	60/20/20	0	5.0	0.0	34.7	0.0	16.7	48.6	34.7	100	0.0754	0.01789
HIVFPH7	No	POPC/POPS/CHOL	60/20/20	200	5.0	0.0	35.3	0.0	15.8	48.9	35.3	100	0.0502	0.02203
HIVFPH7	No	POPC/POPS/CHOL	60/20/20	800	5.0	2.4	36.2	0.0	14.2	47.2	36.2	100	0.1031	0.02371
HIVFPH7	Yes	POPC/POPS/CHOL	60/20/20	0	5.0	0.0	34.6	0.0	16.8	48.7	34.6	100.1	0.076	0.01831
HIVFPH7	Yes	POPC/POPS/CHOL	60/20/20	200	5.0	0.0	34.8	0.0	15.9	49.3	34.8	100	0.0596	0.02129
HIVFPH7	Yes	POPC/POPS/CHOL	60/20/20	800	5.0	2.5	36.9	0.0	13.1	47.6	36.9	100.1	0.0951	0.02158
H7-C	No	POPC/POPS/CHOL	60/20/20	0	5.0	0.0	37.7	0.0	21.4	40.9	37.7	100	0.2201	0.02495
H7-C	No	POPC/POPS/CHOL	60/20/20	800	5.0	0.0	39.3	0.0	21.2	39.5	39.3	100	0.3149	0.03048
1FP1H7	No	POPC/POPS/CHOL	60/20/20	0	7.4	5.1	26.1	0.0	16.7	52.0	26.1	99.9	0.105	0.0131
1FP1H7	No	POPC/POPS/CHOL	60/20/20	100	7.4	3.7	27.7	0.0	16.9	51.7	27.7	100	0.0987	0.0189
1FP1H7	No	POPC/POPS/CHOL	60/20/20	400	7.4	5.7	25.4	3.1	15.3	50.5	28.5	100	0.0655	0.01548
1FP1H7	Yes	POPC/POPS/CHOL	60/20/20	0	7.4	6.1	26.8	0.0	16.0	51.2	26.8	100.1	0.0903	0.01904
1FP1H7	Yes	POPC/POPS/CHOL	60/20/20	100	7.4	6.2	26.5	0.5	15.9	50.9	27.0	100	0.1233	0.01826
1FP1H7	Yes	POPC/POPS/CHOL	60/20/20	400	7.4	4.9	28.1	0.6	14.6	51.8	28.7	100	0.0739	0.01812
2FP1H7	No	POPC/POPS/CHOL	60/20/20	0	7.4	9.6	20.8	2.8	14.9	51.9	23.6	100	0.2179	0.03727
2FP1H7	No	POPC/POPS/CHOL	60/20/20	100	7.4	8.7	21.5	3.2	14.8	51.9	24.7	100.1	0.1887	0.03279
2FP1H7	No	POPC/POPS/CHOL	60/20/20	400	7.4	8.7	23.3	2.1	14.3	51.6	25.4	100	0.1912	0.02899
2FP1H7	Yes	POPC/POPS/CHOL	60/20/20	0	7.4	9.5	22.7	2.3	14.1	51.4	25.0	100	0.218	0.03567
2FP1H7	Yes	POPC/POPS/CHOL	60/20/20	100	7.4	8.6	23.5	2.5	14.3	51.1	26.0	100	0.3223	0.04489
2FP1H7	Yes	POPC/POPS/CHOL	60/20/20	400	7.4	8.5	23.7	1.7	14.1	52.0	25.4	100	0.3229	0.04641
FP2H7	No	POPC/POPS/CHOL	60/20/20	0	7.4	0.4	33.4	0.0	16.0	50.2	33.4	100	0.0458	0.1855
FP2H7	No	POPC/POPS/CHOL	60/20/20	200	7.4	0.4	33.9	0.0	15.9	49.8	33.9	100	0.049	0.02049
FP2H7	No	POPC/POPS/CHOL	60/20/20	800	7.4	1.2	31.8	0.0	15.8	51.2	31.8	100	0.0742	0.02048
FP2H7	Yes	POPC/POPS/CHOL	60/20/20	0	7.4	0.4	33.1	0.0	16.4	50.0	33.1	99.9	0.0539	0.02062

FP2H7	Yes	POPC/POPS/CHOL	60/20/20	200	7.4	0.4	31.9	0.0	16.8	50.9	31.9	100	0.0633	0.0221
FP2H7	Yes	POPC/POPS/CHOL	60/20/20	800	7.4	1.6	31.1	0.0	16.3	50.9	31.1	99.9	0.0563	0.01728
IFPH7	No	POPC/POPS/CHOL	60/20/20	0	7.4	2.9	29.7	0.0	16.7	50.7	29.7	100	0.0386	0.01391
IFPH7	No	POPC/POPS/CHOL	60/20/20	200	7.4	4.4	29.7	0.0	15.7	50.2	29.7	100	0.0623	0.01898
IFPH7	No	POPC/POPS/CHOL	60/20/20	800	7.4	4.9	29.9	2.1	13.4	49.8	32.0	100.1	0.0538	0.01822
IFPH7	Yes	POPC/POPS/CHOL	60/20/20	0	7.4	5.6	27.2	0.0	16.9	50.3	27.2	100	0.0495	0.01758
IFPH7	Yes	POPC/POPS/CHOL	60/20/20	200	7.4	4.3	30.0	0.0	16.4	49.3	30.0	100	0.0515	0.01818
IFPH7	Yes	POPC/POPS/CHOL	60/20/20	800	7.4	6.1	28.0	1.2	15.2	49.5	29.2	100	0.0665	0.01883
HIVFPH7	No	POPC/POPS/CHOL	60/20/20	0	7.4	0.0	34.0	0.0	16.8	49.2	34.0	100	0.0634	0.01509
HIVFPH7	No	POPC/POPS/CHOL	60/20/20	200	7.4	0.0	38.2	0.0	15.1	46.7	38.2	100	0.0735	0.0462
HIVFPH7	No	POPC/POPS/CHOL	60/20/20	800	7.4	0.0	41.2	0.0	13.4	45.4	41.2	100	0.1118	0.05868
HIVFPH7	Yes	POPC/POPS/CHOL	60/20/20	0	7.4	0.0	33.8	0.0	16.7	49.5	33.8	100	0.0588	0.01895
HIVFPH7	Yes	POPC/POPS/CHOL	60/20/20	200	7.4	0.0	37.7	0.0	14.9	47.4	37.7	100	0.0711	0.04071
HIVFPH7	Yes	POPC/POPS/CHOL	60/20/20	800	7.4	0.0	42.2	0.0	12.9	44.9	42.2	100	0.0985	0.05085
H7-C	No	POPC/POPS/CHOL	60/20/20	0	7.4	0.0	34.9	0.0	20.4	44.7	34.9	100	0.1849	0.02025
H7-C	No	POPC/POPS/CHOL	60/20/20	800	7.4	0.0	34.2	0.0	19.8	46.0	34.2	100	0.2069	0.02255

ANNEX 9

Deconvolution of CD spectra for fusion peptides in LPG micelles. The table includes information on the peptides, presence or absence of calcium, membrane composition and concentration, pH, percentage of secondary structures, and associated errors (RMSD and NRMSD).

Peptide	Calcium	Membrane	Mol%	Membrane concentration (mM)	pH	α-Helix (%)	B-Strand (%)		Turn (%)	Others (%)	All Strands (%)	All (%)	RMSD	NRMSD
							Antiparallel	Parallel						
1FP1H7	No	LPG	100	0	5.0	3.5	27.7	0.0	16.9	51.9	27.7	100.0	0.1226	0.01515
1FP1H7	No	LPG	100	10	5.0	24.9	1.3	7.4	12.6	53.9	8.7	100.1	0.1817	0.01507
1FP1H7	Yes	LPG	100	0	5.0	3.0	29.6	0.0	16.4	51.1	29.6	100.1	0.0918	0.01138
1FP1H7	Yes	LPG	100	10	5.0	21.8	11.2	6.3	12.9	47.8	17.5	100.0	0.1528	0.00908
2FP1H7	No	LPG	100	0	5.0	8.3	22.8	2.1	14.9	51.9	24.9	100.0	0.2738	0.04202
2FP1H7	No	LPG	100	10	5.0	24.2	9.3	0.0	10.4	56.2	9.3	100.1	0.3686	0.03122
2FP1H7	Yes	LPG	100	0	5.0	8.1	22.5	1.7	15.5	52.2	24.2	100.0	0.2782	0.04471
2FP1H7	Yes	LPG	100	10	5.0	25.8	8.4	0.0	11.1	54.6	8.4	99.9	0.3471	0.02449
FP2H7	No	LPG	100	0	5.0	5.6	32.1	3.9	13.0	45.3	36.0	99.9	0.0621	0.01791
FP2H7	No	LPG	100	20	5.0	17.2	22.9	8.2	12.7	39.0	31.1	100.0	0.1937	0.00804
FP2H7	Yes	LPG	100	0	5.0	3.9	34.6	3.5	12.4	45.5	38.1	99.9	0.0617	0.01803
FP2H7	Yes	LPG	100	20	5.0	15.6	24.2	8.6	11.5	40.1	32.8	100.0	0.1806	0.00714
IFPH7	No	LPG	100	0	5.0	2.8	28.8	0.0	17.1	51.4	28.8	100.1	0.067	0.02018
IFPH7	No	LPG	100	20	5.0	30.6	9.8	9.5	11.8	38.2	19.3	99.9	0.2992	0.00553
IFPH7	Yes	LPG	100	0	5.0	2.0	30.1	0.0	15.7	52.1	30.1	99.9	0.0501	0.01559
IFPH7	Yes	LPG	100	20	5.0	32.2	8.8	9.6	11.4	37.9	18.4	99.9	0.2865	0.00582
HIVFPH7	No	LPG	100	0	5.0	0.0	34.1	0.0	16.8	49.1	34.1	100.0	0.0799	0.01694
HIVFPH7	No	LPG	100	20	5.0	27.2	15.6	3.0	13.3	40.9	18.6	100.0	0.3537	0.00626
HIVFPH7	Yes	LPG	100	0	5.0	0.0	34.4	0.0	16.9	48.6	34.4	99.9	0.078	0.0168
HIVFPH7	Yes	LPG	100	20	5.0	28.3	15.0	4.2	12.0	40.5	19.2	100.0	0.3523	0.00598
H7-C	No	LPG	100	0	5.0	0.0	33.5	0.0	21.0	45.6	33.5	100.1	0.2173	0.0226
H7-C	No	LPG	100	20	5.0	0.0	32.0	0.0	19.9	48.1	32.0	100.0	0.207	0.02192

ANNEX 10

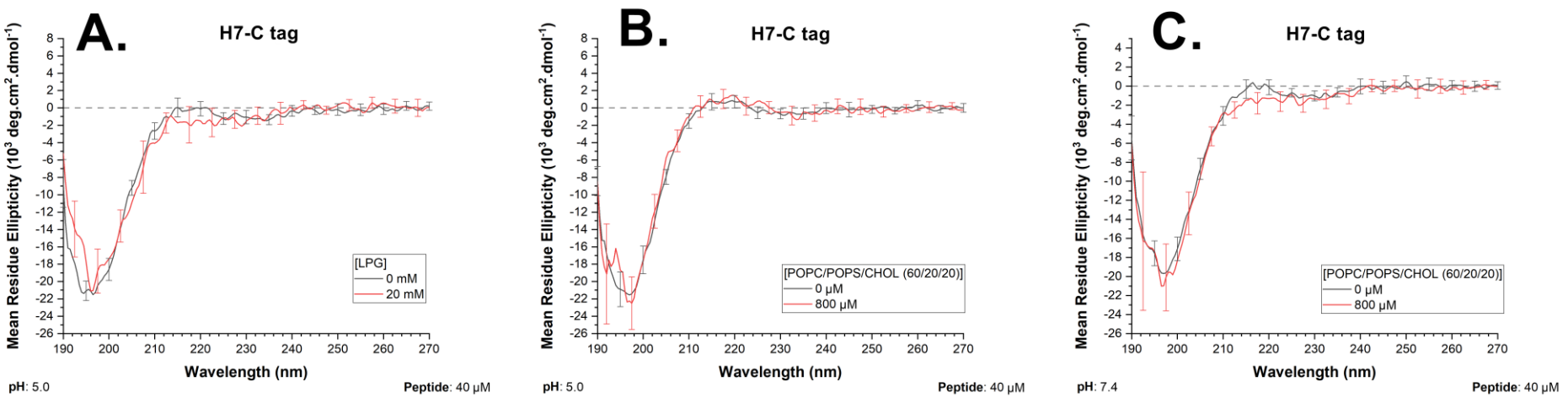

CD spectra of H7-C tag in solution and in the presence of LPG micelles and SUVs containing POPS. The spectra were recorded at 37 °C in solution and in the presence of **(A)** LPG micelles (20 mM) at pH 5.0 and POPC/POPS/Chol (60/20/20) SUVs (800 µM) at **(B)** pH.5.0 and **(C)** pH 7.4. Buffers: 10 mM MES 150 mM NaF, pH 5.0; and 10 mM Tris 150 mM NaF, pH 7.4.

ANNEX 11

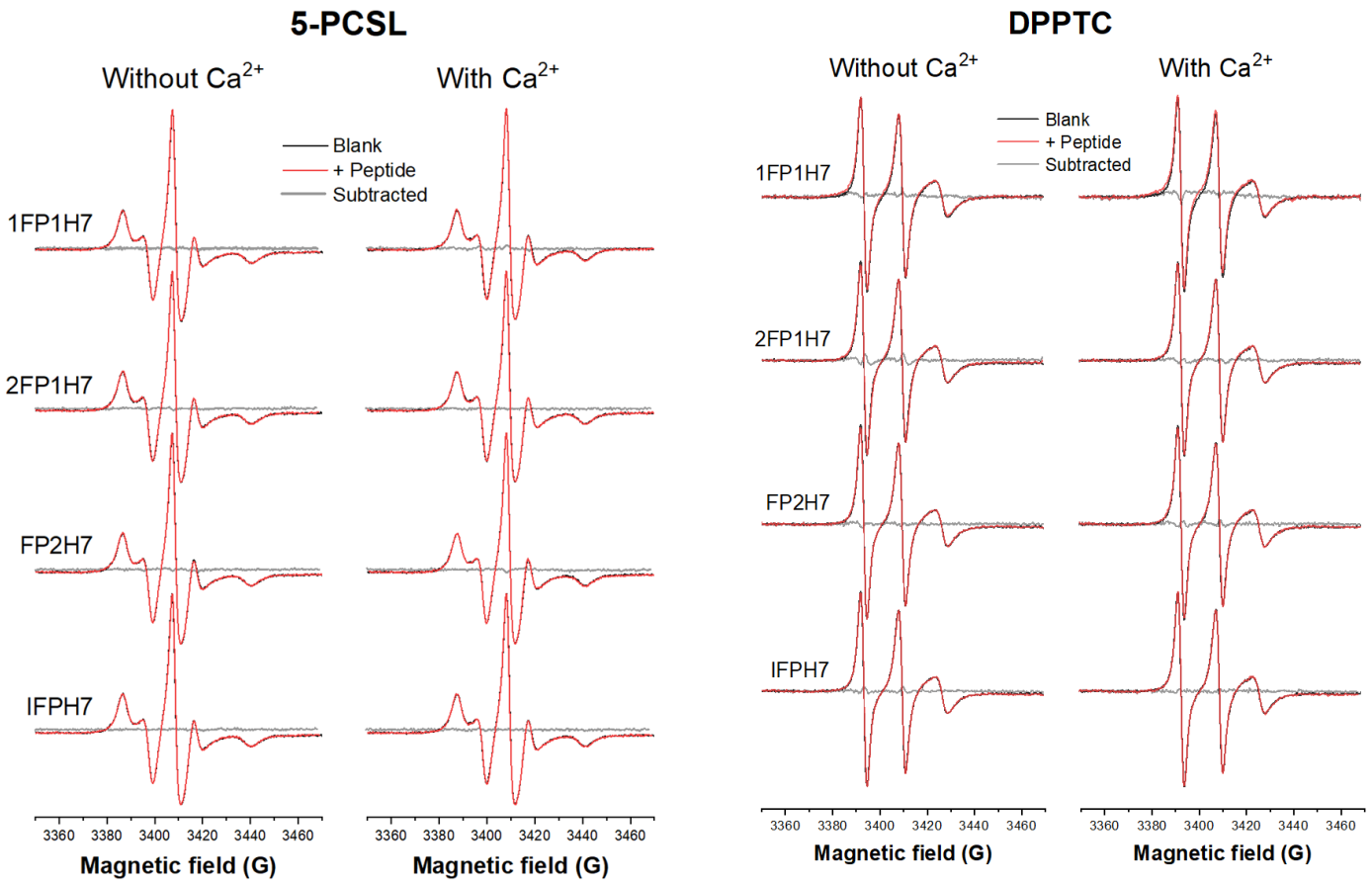

EPR spectra for spin-labeled POPE membranes in the absence and presence of fusion peptides and calcium at pH 5.0. EPR spectra of 5-PCSL (**left**) and DPPTC (**right**) in 5 mg/mL SUVs composed of POPC/POPE/Chol at a 60/20/20 molar ratio in the absence and presence of FPs and calcium. A residual spectrum (gray line), obtained by subtracting the peptide-containing spectrum from the vesicle-only spectrum, is included to facilitate the identification of spectral variations. The lipid-to-peptide ratio was 20:1. $CaCl_2$ was added at a 2 mM concentration. Buffer: 10 mM HEPES/MES, 150 mM NaCl, pH 5.0.

ANNEX 12

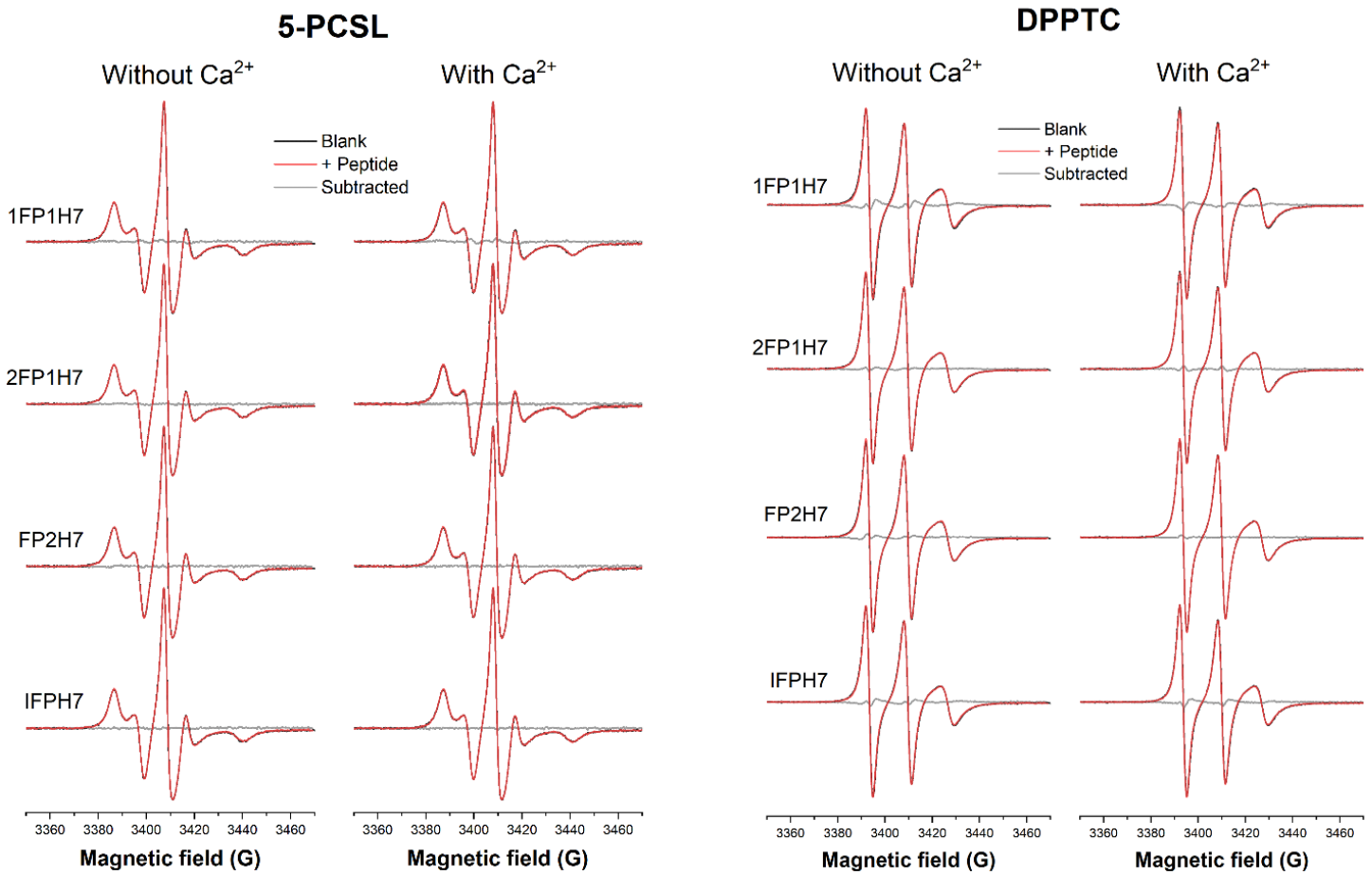

EPR spectra for spin-labeled POPE membranes in the absence and presence of fusion peptides and calcium at pH 7.4. EPR spectra of 5-PCSL (**left**) and DPPTC (**right**) in 5 mg/mL SUVs composed of POPC/POPE/Chol at a 60/20/20 molar ratio in the absence and presence of FPs and calcium. A residual spectrum (gray line), obtained by subtracting the peptide-containing spectrum from the vesicle-only spectrum, is included to facilitate the identification of spectral variations. The lipid-to-peptide ratio was 20:1. $CaCl_2$ was added at a 2 mM concentration. Buffer: 10 mM HEPES/MES, 150 mM NaCl, pH 7.4.

ANNEX 13

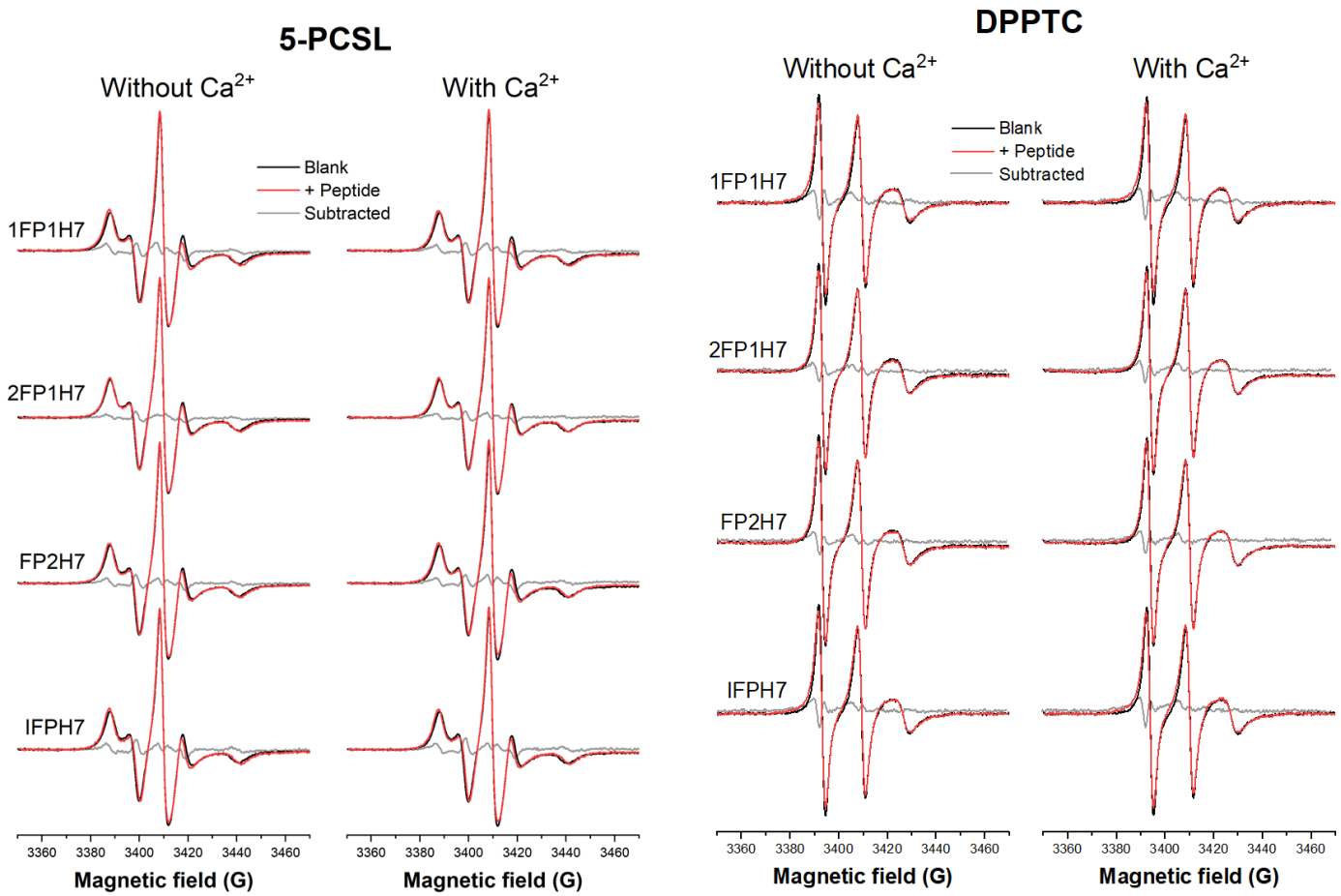

EPR spectra for spin-labeled POPS membranes in the absence and presence of fusion peptides and calcium at pH 7.4. EPR spectra of 5-PCSL (**left**) and DPPTC (**right**) in 5 mg/mL SUVs composed of POPC/POPS/Chol at a 60/20/20 molar ratio in the absence and presence of FPs and calcium. A residual spectrum (gray line), obtained by subtracting the peptide-containing spectrum from the vesicle-only spectrum, is included to facilitate the identification of spectral variations. The lipid-to-peptide ratio was 20:1. $CaCl_2$ was added at a 2 mM concentration. Buffer: 10 mM HEPES/MES, 150 mM NaCl, pH 7.4.

ANNEX 14

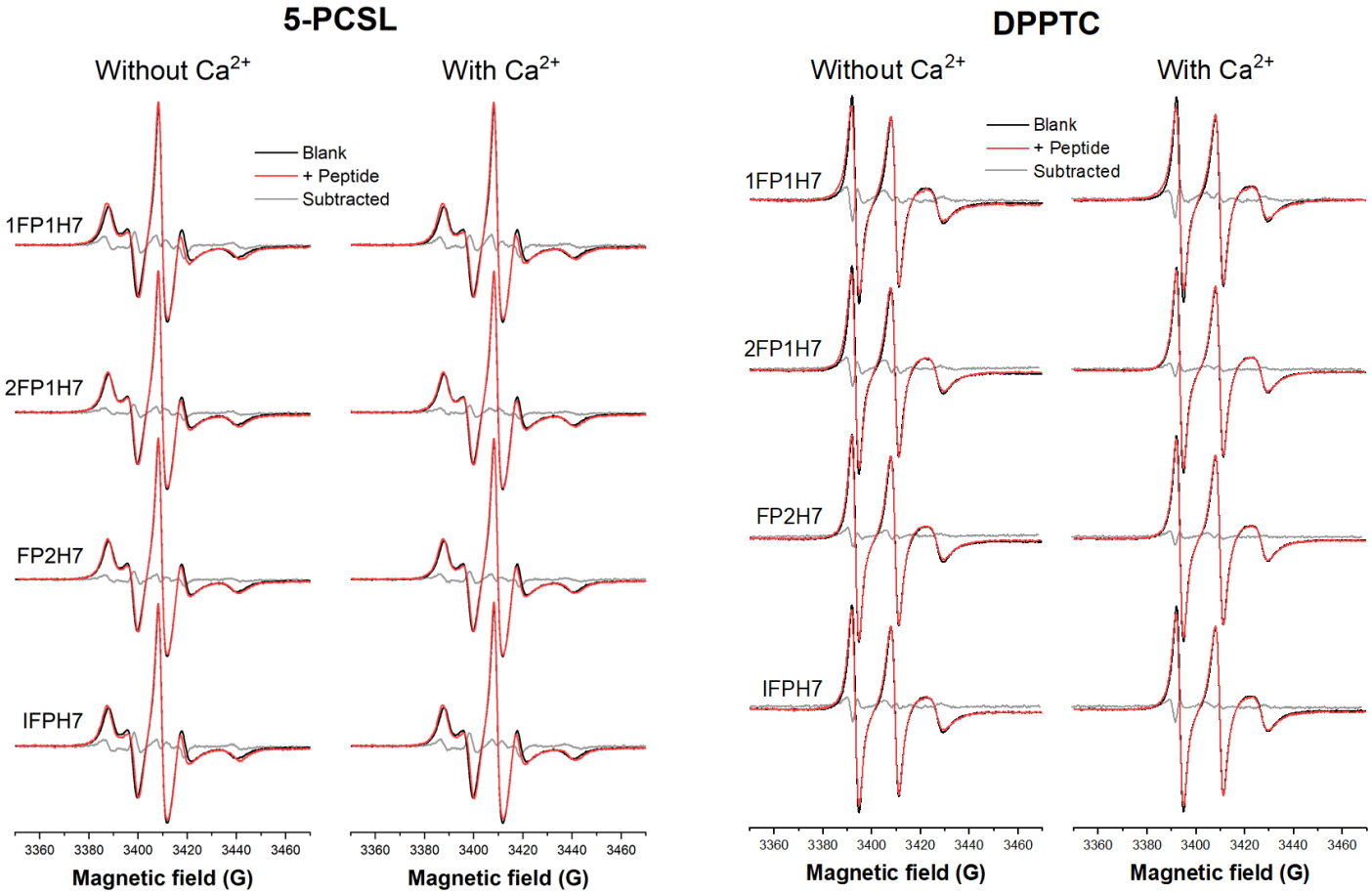

EPR spectra for spin-labeled POPS membranes in the absence and presence of fusion peptides and calcium at pH 7.4. EPR spectra of 5-PCSL (**left**) and DPPTC (**right**) in 5 mg/mL SUVs composed of POPC/POPS/Chol at a 60/20/20 molar ratio in the absence and presence of FPs and calcium. A residual spectrum (gray line), obtained by subtracting the peptide-containing spectrum from the vesicle-only spectrum, is included to facilitate the identification of spectral variations. The lipid-to-peptide ratio was 20:1. $CaCl_2$ was added at a 2 mM concentration. Buffer: 10 mM HEPES/MES, 150 mM NaCl, pH 7.4.

ANNEX 15

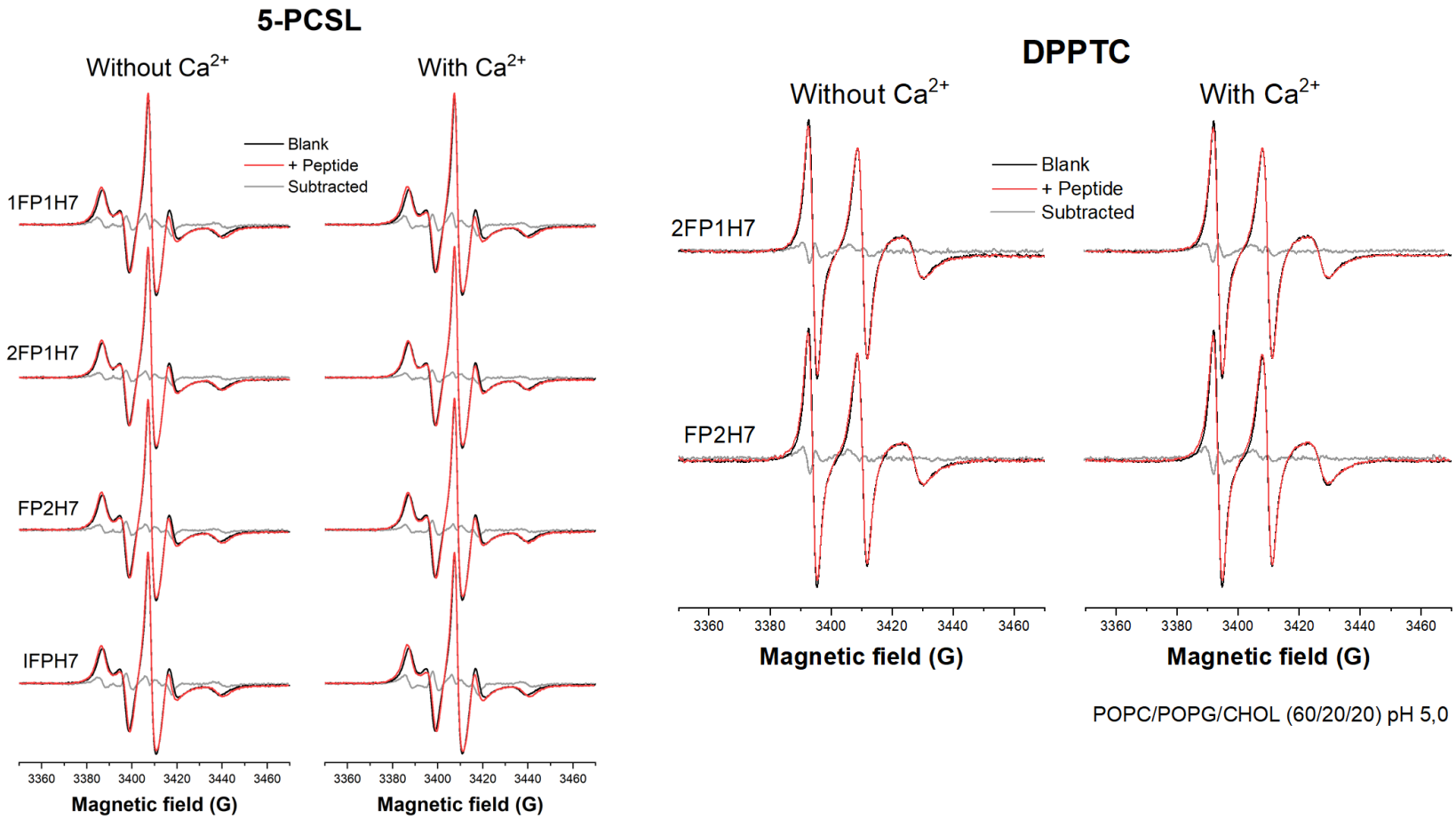

EPR spectra for spin-labeled POPG membranes in the absence and presence of fusion peptides and calcium at pH 5.0. EPR spectra of 5-PCSL (**left**) and DPPTC (**right**) in 5 mg/mL SUVs composed of POPC/POPG/Chol at a 60/20/20 molar ratio in the absence and presence of FPs and calcium. A residual spectrum (gray line), obtained by subtracting the peptide-containing spectrum from the vesicle-only spectrum, is included to facilitate the identification of spectral variations. The lipid-to-peptide ratio was 20:1. $CaCl_2$ was added at a 2 mM concentration. Buffer: 10 mM HEPES/MES, 150 mM NaCl, pH 5.0.

ANNEX 16

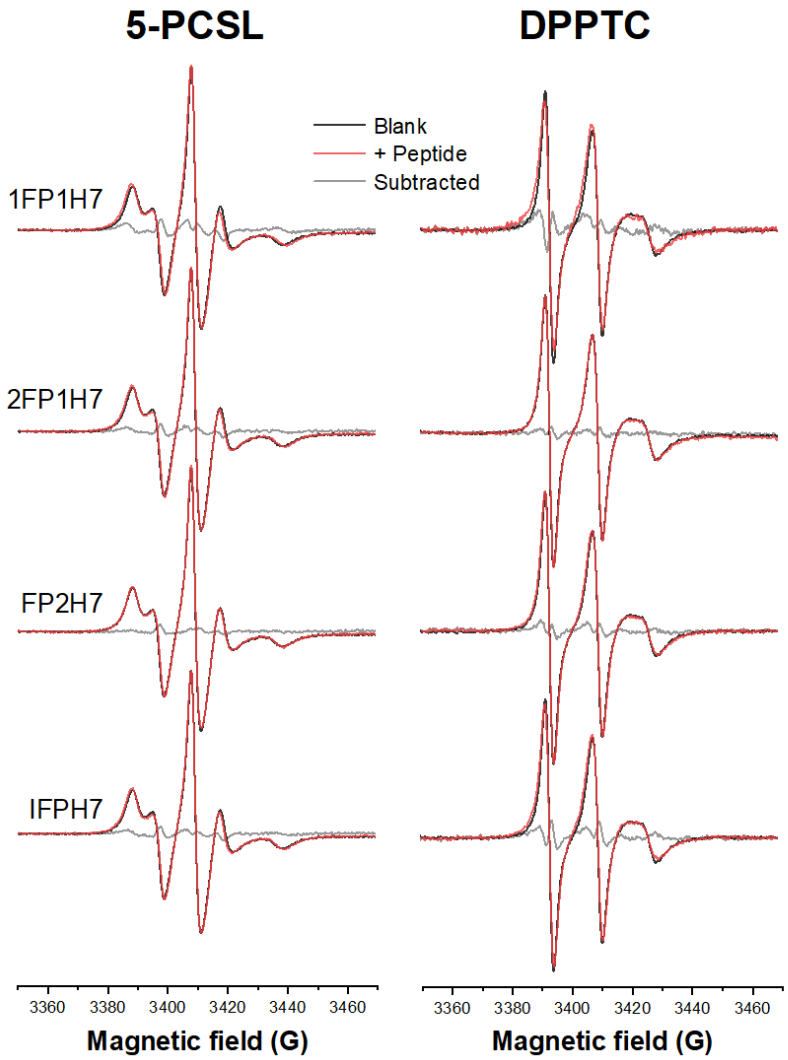

EPR spectra for spin-labeled POPC/POPG in the absence and presence of fusion peptides at pH 5.0. EPR spectra of spin-labeled SUVs composed of POPC/POPG at an 80/20 molar ratio, labeled with 5-PCSL (**left**) and DPPTC (**right**), are shown in the absence and presence of fusion peptides. A subtracted spectrum (gray line), obtained by subtracting the vesicle-only spectrum from the peptide-containing spectrum, is included to facilitate the identification of spectral variations. SUVs were tested at a membrane concentration of 5 mg/mL, with peptides added at a lipid-to-peptide ratio of 20:1. Buffer 10 mM HEPES/MES 150 mM NaCl pH 5.0 was used.

ANNEX 17

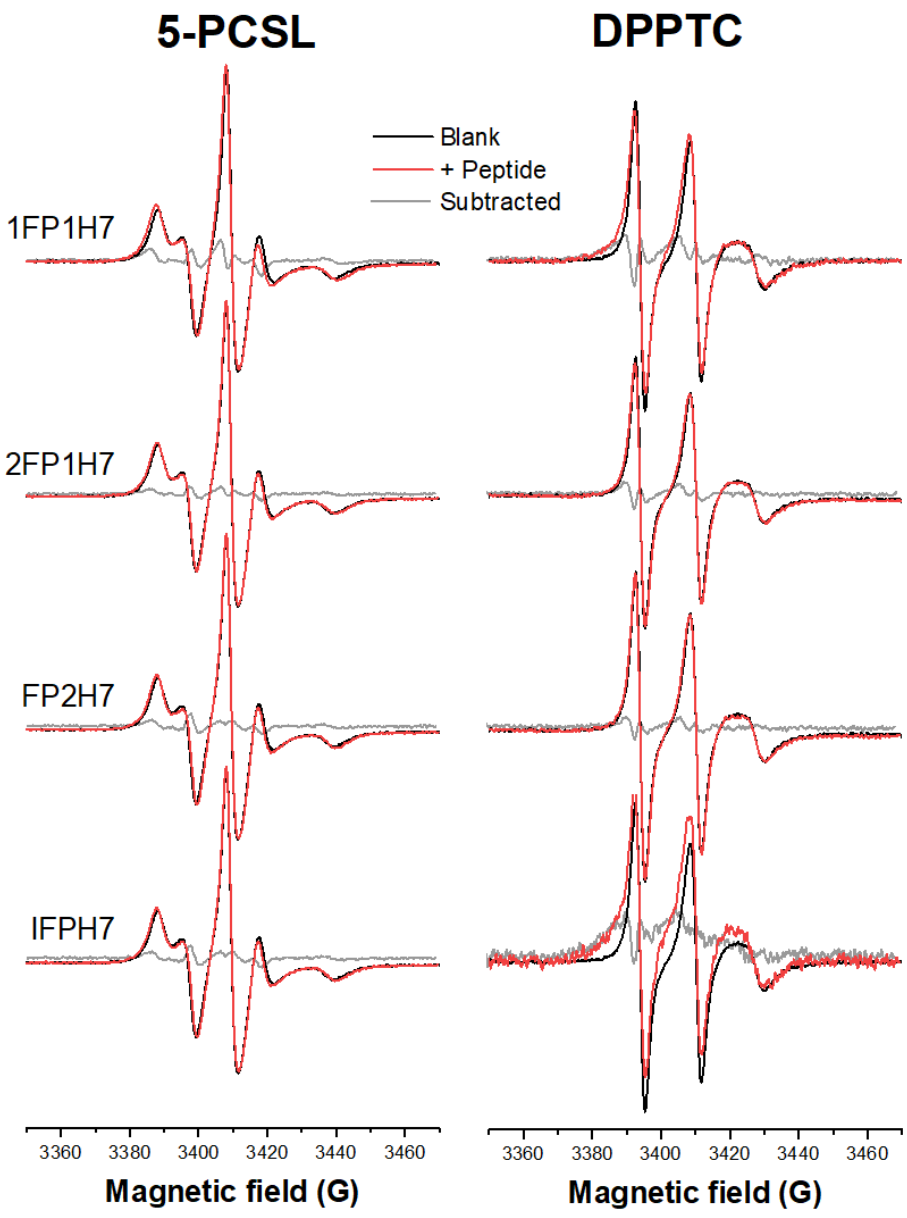

EPR spectra for spin-labeled POPC/POPG/CHOL in the absence and presence of fusion peptides at pH 5.0. EPR spectra of spin-labeled SUVs composed of POPC/POPG/CHOL at an 70/20/10 molar ratio, labeled with 5-PCSL (**left**) and DPPTC (**right**), are shown in the absence and presence of fusion peptides. A subtracted spectrum (gray line), obtained by subtracting the vesicle-only spectrum from the peptide-containing spectrum, is included to facilitate the identification of spectral variations. SUVs were tested at a membrane concentration of 5 mg/mL, with peptides added at a lipid-to-peptide ratio of 20:1. Buffer 10 mM HEPES/MES 150 mM NaCl pH 5.0 was used

ANNEX 18

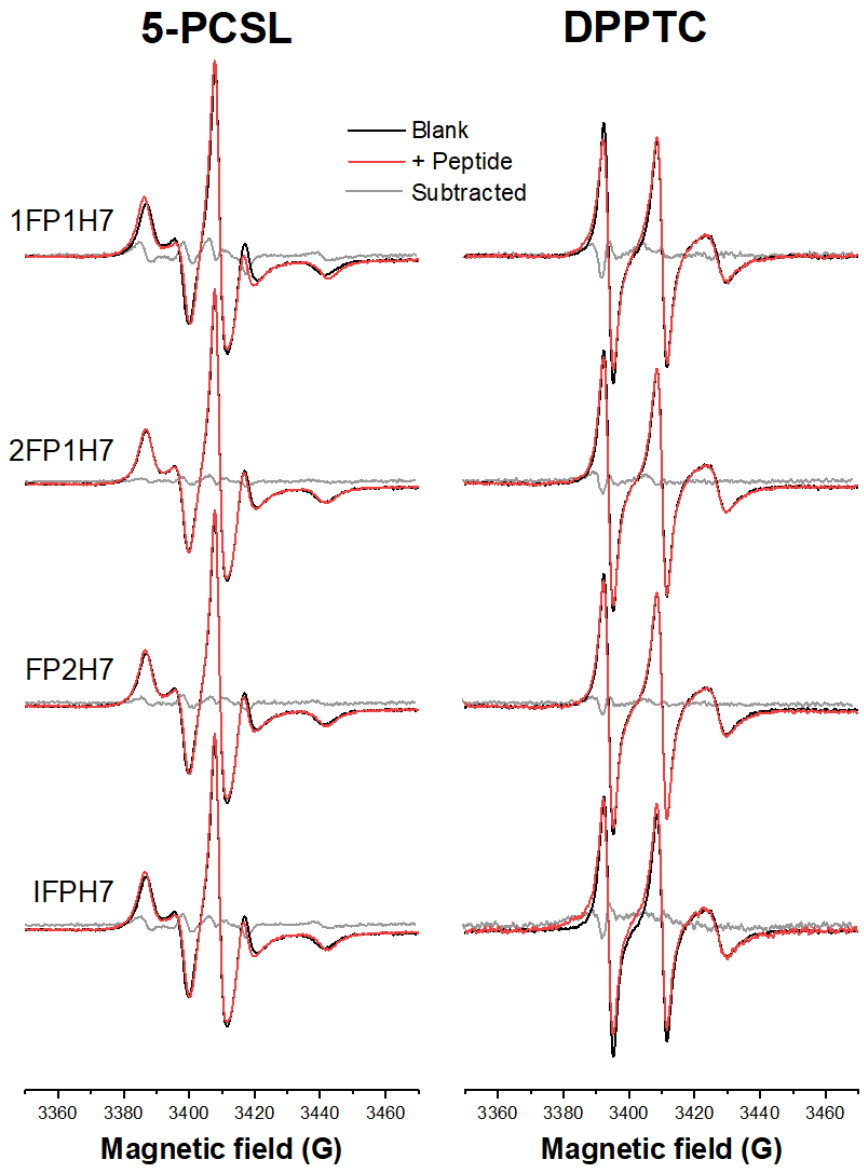

EPR spectra for spin-labeled POPC/POPG/Chol in the absence and presence of fusion peptides at pH 5.0. EPR spectra of spin-labeled SUVs composed of POPC/POPG/Chol at an 50/20/30 molar ratio, labeled with 5-PCSL (**left**) and DPPTC (**right**), are shown in the absence and presence of fusion peptides. A subtracted spectrum (gray line), obtained by subtracting the vesicle-only spectrum from the peptide-containing spectrum, is included to facilitate the identification of spectral variations. SUVs were tested at a membrane concentration of 5 mg/mL, with peptides added at a lipid-to-peptide ratio of 20:1. Buffer 10 mM HEPES/MES 150 mM NaCl pH 5.0 was used.

ANNEX 19

EPR parameters extracted from 5-PCSL and DPPTC spectra of spin-labeled vesicles with different lipid compositions. This table presents parameters for the quantitative characterization of EPR spectral variations in spin-labeled vesicles in the absence and presence of fusion peptides. These parameters provide key insights into spin probe mobility and membrane dynamics within phospholipid bilayers. SUVs with varying compositions containing 20 mol% POPE, POPS, or POPG were evaluated at a concentration of 5 mg/mL, with peptides added at a lipid-to-peptide molar ratio of 20:1. Buffers: 10 mM HEPES/MES, 150 mM NaCl, pH 5.0 and 7.4.

Membrane	Peptide	Calcium	pH 5,0							pH 7,4						
			5-PCSL					DPPTC-SL		5-PCSL					DPPTC-SL	
			$2A_{max}$ (G)	%Δ $2A_{max}$	$2A_{min}$ (G)	S_{zz}	%ΔS_{zz}	h_{+1}/h_0	%Δh_{+1}/h_0	$2A_{max}$ (G)	%Δ $2A_{max}$	$2A_{min}$ (G)	S_{zz}	%ΔS_{zz}	h_{+1}/h_0	%Δh_{+1}/h_0
POPC/POPE/CHOL (60-20-20)	Blank	Without Ca	**53.46**	0.00	**17.18**	**0.651**	0.000	**1.196**	0.000	**53.35**	0.00	**17.35**	**0.643**	0.000	**1.166**	0.000
		With Ca	**52.88**	0.00	**17.29**	**0.640**	0.000	**1.193**	0.000	**53.58**	0.44	**17.35**	**0.646**	0.445	**1.170**	0.355
	1FP1H7	Without Ca	**54.64**	2.19	**17.23**	**0.663**	1.832	**1.181**	-1.229	**53.93**	1.10	**17.29**	**0.653**	1.441	**1.166**	-0.012
		With Ca	**53.58**	1.33	**17.18**	**0.653**	2.024	**1.189**	-0.342	**53.29**	-0.55	**17.12**	**0.651**	0.785	**1.151**	-1.648
	2FP1H7	Without Ca	**54.28**	1.54	**17.18**	**0.661**	1.521	**1.163**	-2.771	**53.46**	0.22	**17.41**	**0.643**	-0.111	**1.172**	0.552
		With Ca	**52.94**	0.11	**17.41**	**0.636**	-0.559	**1.170**	-1.927	**53.52**	-0.11	**17.18**	**0.652**	0.892	**1.166**	-0.286
	FP2H7	Without Ca	**54.17**	1.32	**17.29**	**0.655**	0.642	**1.174**	-1.835	**53.52**	0.33	**17.41**	**0.643**	0.000	**1.182**	1.425
		With Ca	**54.05**	2.22	**17.23**	**0.656**	2.571	**1.167**	-2.183	**54.11**	0.98	**17.12**	**0.661**	2.324	**1.185**	1.315
	IFPH7	Without Ca	**54.28**	1.54	**17.23**	**0.659**	1.189	**1.186**	-0.813	**53.58**	0.44	**17.47**	**0.642**	-0.221	**1.174**	0.677
		With Ca	**54.81**	3.66	**17.23**	**0.665**	3.991	**1.192**	-0.120	**53.93**	0.66	**17.35**	**0.650**	0.659	**1.178**	0.686
POPC/POPS/CHOL (60-20-20)	Blank	Without Ca	**52.94**	0.00	**17.82**	**0.621**	0.000	**1.250**	0.000	**52.53**	0.00	**18.00**	**0.610**	0.000	**1.229**	0.000
		With Ca	**52.76**	0.00	**17.82**	**0.619**	-0.351	**1.234**	0.000	**53.11**	0.00	**18.00**	**0.617**	0.000	**1.214**	-1.181
	1FP1H7	Without Ca	**53.87**	1.77	**17.00**	**0.663**	6.668	**1.131**	-9.547	**53.76**	2.34	**16.82**	**0.668**	9.505	**1.111**	-9.602
		With Ca	**53.52**	1.44	**17.18**	**0.652**	5.300	**1.127**	-8.719	**54.40**	2.43	**16.94**	**0.671**	8.751	**1.079**	-11.191
	2FP1H7	Without Ca	**53.82**	1.66	**17.47**	**0.645**	3.773	**1.178**	-5.723	**52.99**	0.89	**17.41**	**0.637**	4.411	**1.156**	-5.932
		With Ca	**53.05**	0.56	**17.35**	**0.640**	3.327	**1.180**	-4.402	**53.82**	1.32	**17.47**	**0.645**	4.458	**1.173**	-3.374

	FP2H7	Without Ca	**52.94**	0.00	**17.18**	**0.645**	3.775	**1.191**	-4.692	**53.82**	2.46	**17.41**	**0.647**	6.055	**1.208**	-1.695
		With Ca	**53.05**	0.56	**17.12**	**0.648**	4.725	**1.200**	-2.804	**53.11**	0.00	**17.23**	**0.645**	4.460	**1.172**	-3.507
	IFPH7	Without Ca	**54.34**	2.66	**17.06**	**0.666**	7.222	**1.164**	-6.848	**53.82**	2.46	**17.12**	**0.658**	7.823	**1.159**	-5.724
		With Ca	**54.05**	2.44	**17.18**	**0.658**	6.331	**1.165**	-5.603	**53.76**	1.21	**17.00**	**0.661**	7.144	**1.141**	-6.029
POPC/POPG/CHOL (60-20-20)	Blank	Without Ca	**52.23**	0.00	**17.76**	**0.615**	0.000	**1.232**	0.000	**X**	X	**X**	X	X	**X**	X
		With Ca	**52.82**	0.00	**17.76**	**0.622**	1.191	**1.220**	0.000	**X**	X	**X**	X	X	**X**	X
	1FP1H7	Without Ca	**53.82**	3.03	**17.00**	**0.662**	7.712			**X**	X	**X**	X	X	**X**	X
		With Ca	**53.40**	1.11	**17.12**	**0.653**	4.942			**X**	X	**X**	X	X	**X**	X
	2FP1H7	Without Ca	**53.40**	2.24	**17.35**	**0.644**	4.785	**1.180**	-4.159	**X**	X	**X**	X	X	**X**	X
		With Ca	**53.76**	1.78	**17.35**	**0.648**	4.239	**1.168**	-4.220	**X**	X	**X**	X	X	**X**	X
	FP2H7	Without Ca	**52.94**	1.35	**17.23**	**0.643**	4.550	**1.178**	-4.305	**X**	X	**X**	X	X	**X**	X
		With Ca	**53.29**	0.89	**17.29**	**0.645**	3.667	**1.165**	-4.466	**X**	X	**X**	X	X	**X**	X
	IFPH7	Without Ca	**53.64**	2.69	**17.29**	**0.649**	5.599			**X**	X	**X**	X	X	**X**	X
		With Ca	**54.58**	3.33	**17.00**	**0.671**	7.910			**X**	X	**X**	X	X	**X**	X

ANNEX 20

EPR parameters extracted from 5PC-SL and DPPTC spectra of spin-labeled vesicles with varying cholesterol content. This table presents parameters for the quantitative characterization of EPR spectral variations in spin-labeled vesicles in the absence and presence of fusion peptides. These parameters provide key insights into spin probe mobility and membrane dynamics within phospholipid bilayers with varying cholesterol concentration (mol%). SUVs with containing 20 mol% POPG, with a variation in its cholesterol content from 0 mol% to 30 mol% were evaluated at a concentration of 5 mg/mL, with peptides added at a lipid-to-peptide molar ratio of 20:1. Buffers 10 mM HEPES/MES 150 mM pH 5.0 was used.

Membrane	Peptide	pH 5,0						
		5-PCSL					DPPTC	
		2Amax (G)	%Δ 2Amax	2Amin (G)	Szz	%ΔSzz	h+1/h0	%Δh+1/h0
POPC/POPG (80-20)	Blank	**50.77**	0.00	**18.64**	**0.565**	0.000	**1.320**	0.000
	1FP1H7	**51.88**	2.19	**18.00**	**0.602**	6.507	**1.210**	-8.376
	2FP1H7	**51.53**	1.50	**18.41**	**0.583**	3.171	**1.312**	-0.634
	FP2H7	**50.65**	-0.23	**18.41**	**0.572**	1.157	**1.322**	0.116
	IFPH7	**51.35**	1.15	**18.23**	**0.587**	3.854	**1.277**	-3.251
POPC/POPG/CHOL (70-20-10)	Blank	**50.30**	0.00	**18.23**	**0.573**	0.000	**1.295**	0.000
	1FP1H7	**52.47**	4.31	**17.47**	**0.628**	9.607	**1.182**	-8.712
	2FP1H7	**51.70**	2.80	**18.00**	**0.600**	4.621	**1.256**	-3.001
	FP2H7	**51.70**	2.80	**17.76**	**0.608**	6.080	**1.276**	-1.467
	IFPH7	**51.70**	2.80	**17.70**	**0.610**	6.447	**1.218**	-5.900
POPC/POPG/CHOL (60-20-20)	Blank	**52.23**	0.00	**17.76**	**0.615**	0.000	**1.232**	0.000
	1FP1H7	**53.82**	3.03	**17.00**	**0.662**	7.712	**—**	**—**
	2FP1H7	**53.40**	2.24	**17.35**	**0.644**	4.785	**1.180**	-4.159
	FP2H7	**52.94**	1.35	**17.23**	**0.643**	4.550	**1.178**	-4.305
	IFPH7	**53.64**	2.69	**17.29**	**0.649**	5.599	**—**	**—**
POPC/POPG/CHOL (50-20-30)	Blank	**54.58**	0.00	**17.12**	**0.667**	0.000	**1.149**	0.000
	1FP1H7	**56.45**	3.44	**16.30**	**0.720**	7.910	**1.016**	-11.578
	2FP1H7	**55.40**	1.50	**16.82**	**0.687**	3.085	**1.095**	-4.752
	FP2H7	**55.40**	1.50	**16.59**	**0.696**	4.416	**1.092**	-4.985
	IFPH7	**55.11**	0.97	**16.36**	**0.702**	5.254	**1.043**	-9.266